# MATERIALS STRUCTURE

in

Chemistry, Biology, Physics and Technology

STRUKTURA 2022

Kolokvium Krystalografické společnosti

vol. 28, no. 2, 2022

# MATERIALS STRUCTURE
in Chemistry, Biology, Physics and Technology

*Bulletin of the Czech and Slovak Crystallographic Association*

www.xray.cz




## Struktura 2022
### June 20-23


Struktura 2022 is organized fully as in person meeting after three years break due to pandemy. We planned the largest satellite of the IUCr25 congress - School on Electron Crystallography to hotel Dvořák in Tábor where Struktura 2016 took place but we had to postpone it in 2020 and finally cancel it in 2021. Fortunately, the congress itself could be successfully organized in hybrid form in August 2021, in Prague. An article about this congress is included in this issue.
We are returning to this beautiful place and the participation - 90 people is higher than in 2016. One full day is devoted to the meeting of users of neutron scattering, and also of synchrotron radiation with a few guests from large European facilities. Another day, already the 15th student symposium and competition with participation of 20 students is organized. Election of a new board of Krystalografická společnost will be completed during the conference.

Electronic version of the journal can be found at http://www.xray.cz/ms together with the instructions for the authors.

*R. Kužel*


Supported by the Czech Academy of Sciences
Published by the Czech and Slovak Crystallographic Association (CSCA).
Technical editors: Ivana Kutá Smatanová, Radomír Kužel.
Supported by the Czech Academy of Sciences.
Printed by Karel Hájek, designhhstudio.
**ISSN 1211 5894 (print), ISSN 1805-4382 (Online)** volume **28** (June 2022), no. 2 @CSCA

# CT Lab HX Compact X-ray microtomography

The CT Lab HX is a compact and versatile computed tomography system suitable for a wide range of sample types and required measurement conditions. It's ideal for applications in materials and life science R&D, failure analysis, and manufacturing quality control.

CT Lab HX

- Compact Benchtop design
- 130 kV, 39 W high -power X-ray source
- Large field of view (max. 200 mm diameter)
- High-resolution (max. 2.1 µm voxel resolution)
- High speed scan (max. 18 seconds/ scan)
- Easy- to use software


## APPLICATIONS:

| |
|---|
| Non-destructive testing of a variety of samples |
| Scanning with flexible FOVs |
| High-resolution CT scans |
| High energy scans for dense materials |
| Lower energy scans for organic materials |

Please have a look at the video to get a first impression for CT Lab HX applications

Watch Video ▸

SCAN ME

SCAN ME

## SPECIFICATIONS:

- High-speed and **high-resolution** X-ray Computed Tomography (XCT)
- **Wide variety of samples** including electronic devices, batteries, printed circuit boards, aluminum casted parts, pharmaceutical products, medical devices, and bones.
- Compact benchtop design **saves lab space** and **energy consumption**
- Scan time takes **only 18 seconds** at the top speed
- The **pixel size is 2.2 µm** at the highest resolution setting
- **Large field of view** (FOV) can be scanned at **high resolution**

Rigaku

# XRDynamic 500

Automatizovaný víceúčelový práškový rentgenový difraktometr

## Univerzální řešení rentgenové difrakce


Práškový difraktometr XRDynamic 500 je vybaven pokročilou optikou, goniometrem nové generace a nejmodernějšími detektory s širokou škálou aplikací, které pokrývá rozsáhlé portfolio ambientních a neambientních vzorkovacích stupňů, takže vždy najdete optimální systém XRD pro své potřeby.

Velký poloměr goniometru a evakuovaný paprsek pro lepší rozlišení


Až tři geometrie paprsků na jedno kliknutí

Jednoduché automatické vyrovnávání

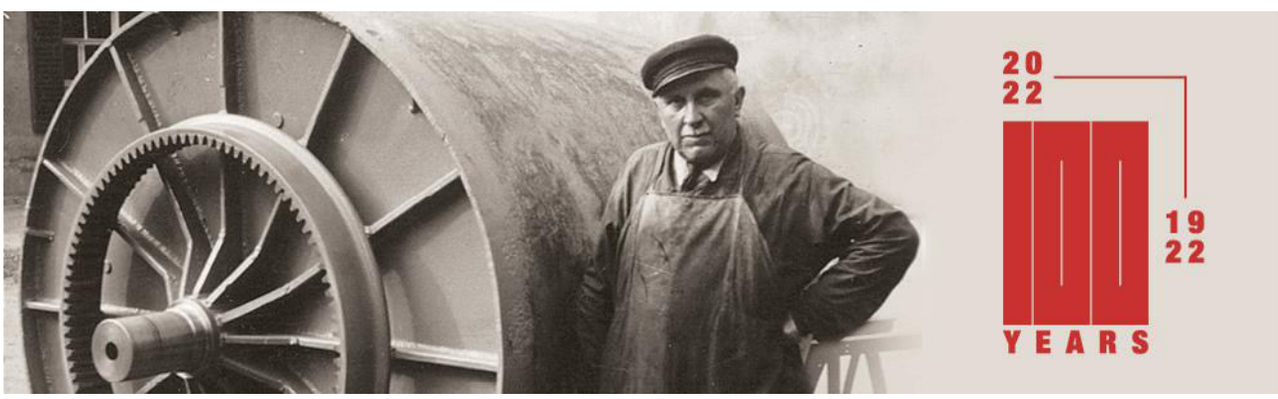

# STRUKTURA 2022

**Tábor, 20. 6. - 23. 6. 2022**

**Session I, Monday, June 20**

**L1**

## FIRST FIFTY YEARS OF POWDER DIFFRACTION: FROM PAUL SCHERRER TO HUGO RIETVELD

**F. Laufek**

*Czech Geological Survey, Geologická 6, 152 00 Praha 5, Czech Republic*
*frantisek.laufek@geology.cz*

In 1912, Max von Laue, Walter Friedrich, and Paul Knipping performed their famous X-ray diffraction experiment and proved for the first time two basic principles in physics: that a single crystal is composed of regular blocks and that X-rays behave as waves with a wavelength in the order of the distances between the building blocks of the crystal. It is interesting to note, that Fridrich and Knipping also carried out first powder X-ray diffraction experiment. They ground a copper sulphate crystal and placed the powder sample in the X-ray beam instead of a single-crystal. They observed small speckles around a central spot. Unfortunately, they used a polychromatic beam and the exposure was too short to observe diffraction rings [1].

The powder X-ray diffraction method was developed independently by Peter Debye and Paul Scherrer (1916) and by Alfred Hull (1917). Debye and Scherer made a 57 mm diameter cylindrical camera, used two films with each forming two half of circle in contact with a camera wall, a primary beam collimator and a light-tight cover. For the sample, they used the finest grain powder of LiF [2]. Debye and Scherrer were surprised to find on the first photographs the sharp lines of first powder diagram, which they correctly interpreted as crystalline diffraction by the randomly oriented micro-crystal of the powder [3]. Approximately at the same time, Alfred Wallace Hull, an employee of General Electric Research Laboratory in USA, became interested in the X-ray diffraction. Hull saw there a challenge and try to find the crystal structure of iron. Since the single-crystals of iron were not available at that time, he used iron fillings, which were rotated continuously in order to provide randomness [3]. He obtained good diffraction patterns and subsequently checked if the *d*-spacings of the diffraction patterns of iron are consistent to the Bragg values for the three cubic crystal systems [1]. Hull also described many of the experimental factors; was first who used a $K\alpha$ ilter and measured the effect of X-ray voltage on the intensity of the Mo$K\beta$ radiation. He described the importance of the particle size in the sample, specimen rotation and the necessity for the random orientation. Debye and Scherrer did not mention the use of the method for phase identification in the paper (1916), however Hull recognized that powder diffraction analysis can be used for phase identification of crystalline compounds, even if they are in mixtures. A major advance of the powder diffraction method began in the early 1950´s with the introduction of the first commercial high-resolution diffractometers which greatly expand the use of the method [3]. In 1967, a next huge step was taken as Hugo Rietveld published his first whole profile pattern fitting analysis of $WO_3$ [4]. In this work, Hugo Rietveld showed that he could refine a crystal structure having powder diffraction pattern with overlapping reflections. He also introduced residual values (*R* factors), allowing the quantitative judgment of the refinement quality.

This contribution illustrates the discovery of powder diffraction in 1916 and further development of the method till the advent of „Rietveld method“ in 1967. The progress in development of instrumentation (including neutron diffraction), powder diffraction databases, and determination of first non-cubic crystal structures will be discussed.

1. M. Etter, R.E. Dinnebier, *Z. Anorg. Allg. Chem*., 640, (2014), 3015.
2. A. Authier, Early *Days of Crystallography*, IUCr, Oxford University Press, Oxford, 2015.
3. W. Parrish, J.I. Langford, Powder and related techniques: X-ray techniques, *International Tables for Crystallography*, volume C, IUCr London, 1999.
4. H. M. Rietveld, *Acta Crystallogr*. **22**, (1967), 151.

L2

# EXPERIENCES WITH PARTICIPATION IN CRYSTAL STRUCTURE PREDICTION TEST - CSP7

**M. Hušák, F. Fňukal**

*University of Chemistry and Technology, Prague, Technická 5, 166 28 Praha 6 – Dejvice*
*husakm@vscht.cz*

## Introduction

Blind crystal structure prediction (CSP) test is a periodic event organized by Cambridge Crystallographic Data Centre. Structure prediction typically consists from 3 phases:

- 1) Building a 3D molecule model from its connectivity information
- 2) Generating a set of suggested structures
- 3) Ranking of the suggested structures

This year, it was optional to participate only in the phase 3). We had participated in ranking of suggested structures of following molecules:

### Methods

Based on preliminary benchmarks we had used for the ranking energy calculation ground on DFT theory. We had used rSCAN functional combined with MBD dispersion correction. The data were prepared in BIOVIA Materials Studio software. Computation was performed on Karolina supercomputer at TU Ostrava. CASTEP 20.11 software was used. The computational power required for the calculations was approximately 2 000 000 core/hours.

### Results

Based on the energy ranking, we had identified following structures from the input data sets as the one probably existing in reality: XXVII_structure_59, XXXI_structure_59, XXXIII_structure_452. The correct results of CSP7 were not disclosed up to now so we can not confirm any success.

During the data processing we were faced with limitation of commercial software used for CIF data transfer to DFT software acceptable format as well as with issues related to manage multiple jobs on a supercomputer. Based on the experiences we had chosen to develop our own software for DFT calculation handling.

### Development of the CheckCIF-DFT code

The CheckCIF-DFT code is software targeted primary for transformation of CIF files to format acceptable by DFT software. The code just supports CASTEP and Quantum Espresso formats. The program can manage external DFT software run as well as analyze results. It can manage computation of multiple structures collection suitable for structure prediction. Calculation setup can be defined in a form of user-editable templates. The code was tested on structure ranking of the XXXI CSP7 target. Calculations on an 8 core PC (PBE functional with Grimme dispersion correction, Quantum Espresso) take 5 months. The results suggested the same structure (XXXI_structure_59) as the previous calculation. The code can be utilized for crystal structure solution verification, low-quality structure solution improvement as well as for light atom position clarification.

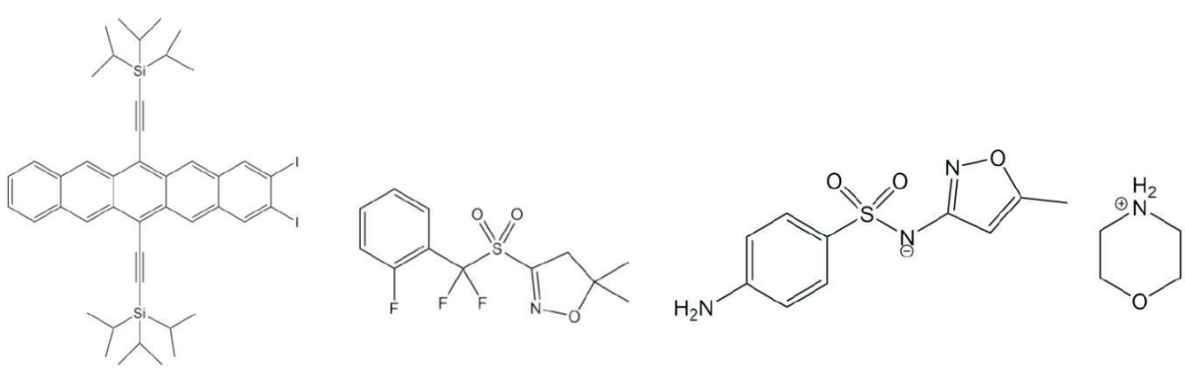


**Figure 1**. Structures from CSP7 test, XXVII (100 suggestions), XXXI (100 suggestions), XXXIII (500 suggestions)

L3

# STRUCTURE OF HALLOYSITE NANOTUBE WITH IRINOTECAN SOLVED BY MOLECULAR SIMULATION METHODS

**M. Pospíšil[1], M. Pšenička[1], E. Gianni[2] , D. Papoulis[2], K. Avgoustakis[3]**

*[1]Charles University, Faculty of Mathematics and Physics, Prague, CZ*
*[2]Department of Geology, University of Patras, Rio, 26504, Patras, Greece*
*[3]Department of Pharmacy, University of Patras, Rio, 26504, Patras, Greece*
*miroslav.pospisil@mff.cuni.cz*

Halloysite is a clay mineral derived from kaolinite with proven spiral-shape tubular crystal morphology and moreover biocompatible with the human body. It determines halloysite for possible use as drug delivery nanocarrier because it allows the encapsulation of various bioactive molecules. Halloysite nanotubes have been investigated as a potential drug delivery system of irinotecan for colon cancer treatment administered by the oral route [1]. To allow releasing of irinotecan in an intestinal environment the whole halloysite nanotubes loaded with irinotecan were coated with EudragitS100 to protect releasing of irinotecan in stomach pH. The loading efficiency of the halloysite nanotube for irinotecan was very high, reaching 84.42 ± 3.10 %. Experimental measurements like transmission electron microscopy showed that the irinotecan molecule is just on the surface of nanotubes and X-ray diffraction patterns proved that there was no intercalation of irinotecan among individual layers. Based on thermogravimetric analysis and tests with various weight ratios between halloysite and polymer was shown that drug release rate from the polymer-coated nanotubes was minimal (0.7 % in 2 h) at stomach pH (pH 1.2) and high at intestinal pH 7.4 conditions (when the pH was increased to 7.4, drug release increased by approx. 70 % in 2 h) [1]. Based on experimental results, methods of molecular simulations were used to determine mutual positions and arrangements of irinotecan molecules on the halloysite nanotube surface, which means the most probably structural model. Results of calculations showed that the most appropriate amount of irinotecan molecules for a given size of halloysite nanotube with a length of 25.359 Å is 6. This amount is in a good agreement with the molar weight ratio of the compounds determined from the real samples. Calculated models showed that the energetically preferred positions of the irinotecan molecules remain closed to the outer part of the halloysite nanotubes and longitudinal axes of irinotecan and the nanotube are parallel.

1. E. Gianni, K. Avgoustakis, M. Pšenička, M. Pospíšil, D. Papoulis, *Journal of Drug Delivery Science and Technology*, **52**, (2019), pp. 568-576.

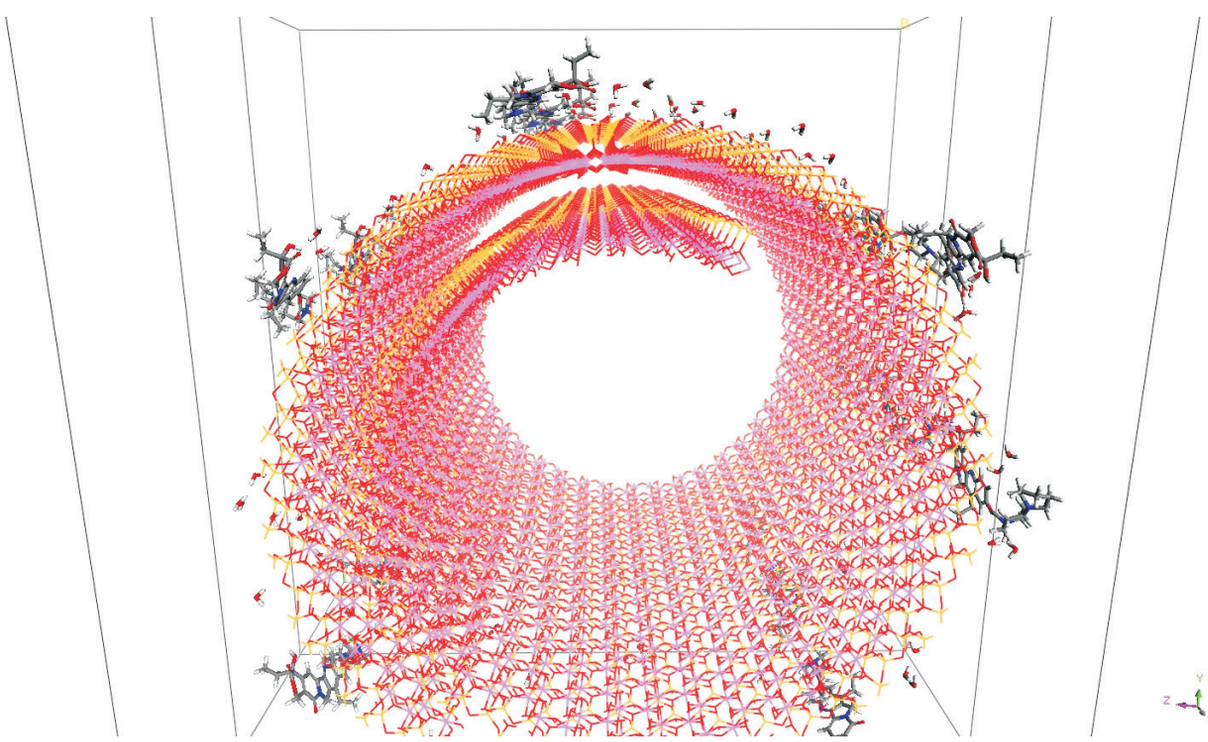

**Figure 1**. View along longitudinal axe for the optimized structure of the halloysite tube with 6 drug molecules.

L4

# FIBRE TEXTURES OF CRONSTEDTITE

**J. Hybler**

*Institute of Physics, Czech Academy of Sciences, Na Slovance 2, 182 21 Praha 8, Czech Republic*
*hybler@fzu.cz*

**Keywords: cronstedtite; 1:1 layer silicates; fibre textures**

The layered 1:1 silicate cronstedtite $(Fe^{2+}_{3-x}Fe^{3+}_{x})(Si_{2-x}Fe^{3+}_{x})O_5(OH)_4$, ($0.5< x< 0.85$) belongs to the serpentine-kaoline group. It forms relatively numerous polytypes generated by stacking 1:1 structure building layers – equivalents of OD packets with the trigonal protocell $a$ = 5.5, $c$ = 7.1 Å. Polytypes are subdivided into four OD subfamilies, or Bailey's groups A, B, C, D according to different stacking rules. Cronstedtite occurs rarely in low temperature hydrothermal deposits [1], in certain meteorites (CM chondrites) [2], and presumably on asteroids. Synthetic micron-size crystals were prepared by Pignatelli and her co-workers [1,3].

The data collected by four circle single-crystal X-ray diffractometer with area detector processed by an appropriate software provide precession-like reciprocal space sections (RS sections in the following). Similar RS sections are obtained by electron diffraction tomography (EDT), for micron-size crystals [1]. Distributions of so called subfamily reflections along the reciprocal lattice rows $[2\bar{1}l]$* / $[11l]$* / $[\bar{1}2l]$* in $(2h\bar{h}l_{hex})$* / $(hhl_{hex})$* / $(\bar{h}2hl_{hex})$* RS planes is used for subfamily determination. Similarly, distributions of characteristic reflections along $[10l]$* / $[01l]$* / $[\bar{1}1l]$* rows in $(h0l_{hex})$* / $(0kl_{hex})$* / $(\bar{h}hl_{hex})$ planes allow determination of particular polytypes. For this purpose, graphical identification diagrams simulating distribution of reflections along named rows are used [1]. Modern diffractometers allow checking of many specimens and quick generation of RS sections. These techniques allow identification of various polytypes, twins, as well as allotwins – oriented crystal associations of more polytypes.

Lot of specimens of cronstedtite from various terrestrial localities and synthetic run products were studied by the author [1, 4, 5, 6]. RS sections were recorded, and selected ones were published and interpreted.

Recently cronstedtite from the new locality in Morocco was studied [6]. The sample was originally collected in 2017 by local people digging for mineral specimens from the hydrothermal veins with pyrite and calcite hosted in a skarn body situated at the base of the El Hammam hill (Djebel el Hammam), close to the Wadi (Ouedi) Beht (Beht river). It is located near the El Hammam fluorite deposit, ~45 km SW of Meknès in the northeastern part of the Variscan Moroccan Central Massif in northern Morocco. The sample was purchased from Fabre Minerals by M. Števko for the National Museum, Prague, where is now stored (catalogue No. P1N 114314).

The specimens separated from the sample provided a relatively high number of common as well as unusual (non-standard) polytypes of subfamilies A and D. Many crystals were identified as twins and/or allotwins of more polytypes (up to six). In many cases, the particular polytypes were mechanicaly separated by cleaving of allotwinned crystals. Some polytypes found were not known to date [6].

Several specimens separated from the central part of the sample appeared to be polycrystalline aggregates with a strong fibre texture – (001) preferred orientation and azimuthally misoriented (100) and (010) directions of domains or crystallites. The $(2h\bar{h}l_{hex})$*/ $(hhl_{hex})$*/ $(\bar{h}2hl_{hex})$* and $(h0l_{hex})$*/ $(0kl_{hex})$* / $(\bar{h}hl_{hex})$* RS sections indicating the subfamily D and $2H_2$ polytype were superimposed (Fig. 1a). In order to further examine this peculiar kind of intergrowths, the series of RS sections $(hk0_{hex})$*, $(hk1_{hex})$*, $(hk2_{hex})$*, $(hk2_{hex})$*, $(hk4_{hex})$*, etc., perpendicular to $\mathbf{c}_{hex}$ was generated. In these sections, concentric rings around $\mathbf{c}_{hex}$ were recorded instead of discrete reflections. The apparent reflections visible in $(2h\bar{h}l_{hex})$*/ $(hhl_{hex})$*/ $(\bar{h}2hl_{hex})$* and $(h0l_{hex})$*/ $(0kl_{hex})$* / $(\bar{h}hl_{hex})$* RS sections represented in fact intersections of named planes with these rings rather than discrete points. The nature of rings varied from sample to sample, from coarse-grained to quite smooth (Figs. 1b-d). However, in addition of $[00l]$* row with discrete maxima, some reflections and/or denser maxima on rings were usually present in the reciprocal space, so that indexing of diffraction patterns and generation of RS section became possible. For few crystals, however, the indexing procedure failed, possibly due to 'too perfect' rings in the reciprocal space.

The back-scattering electrons (BSE) photograph of one of these specimens revealed existence of domains elongated in the **c** direction, probably azimuthally misoriented. (Fig. 2a). For comparison, a BSE image of an ordinary single crystal of the subfamily D is added (Fig. 2b). The electron microprobe analysis revealed partial substitution of Mn and Mg for Fe (0.09-0.10 and 0.19-0.25 a.p.f.u., respectively).

1. J. Hybler, M. Klementová, M. Jarošová, I. Pignatelli, R. Mosser-Ruck, S. Ďurovič, *Clay. Clay Miner.,* **66**, (2018), 379–402, DOI: 10.1346/CCMN.2018.064106.
2. I. Pignatelli, E. Mugnaioli, Y. Marrocchi, *Eur. J. Mineral.,* **30**, (2018), 349-354, DOI: 10.1127/ejm/2018/0030-2713.
3. I. Pignatelli, E. Mugnaioli, J. Hybler, R. Mosser-Ruck, M. Cathelineau, N. Michau, *Clay. Clay Miner.,* **61**, (2013), 277-289, DOI: 10.1346/CCMN.2013.0610408.
4. J. Hybler, J. Sejkora, V. Venclík, *Eur. J. Mineral.,* **28**, (2016), 765-775, DOI: 10.1127/ejm/2016/0028-2532
5. J. Hybler, *Eur. J. Mineral.,* **28**, (2016), 777-788, DOI: 10.1127/ejm/2016/0028-2541
6. J. Hybler, J. Sejkora, Z. Dolníček, M. Števko, *Clay. Clay Miner.,* **69**, (2016), 702-734, DOI: 10.1007/s42860-021-00157-2

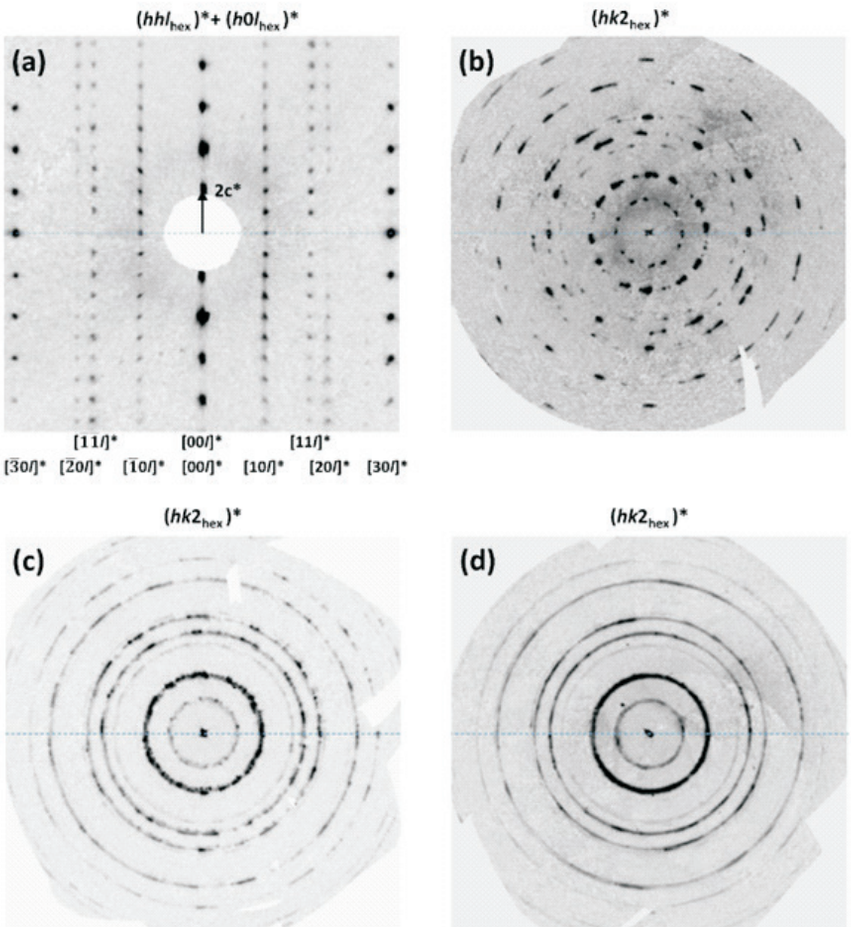


**Figure 1**. Examples of RS sections of strongly textured polycrystalline samples. **a** The apparent superposition of ($hhl_{hex}$)* and ($h0l_{hex}$)* sections of the well-ordered $2H_2$ polytype of the subfamily D. **b-d** Examples of diffraction rings at the level of ($hk2_{hex}$)* RS section of several specimens varying from coarse-grained to almost smooth.

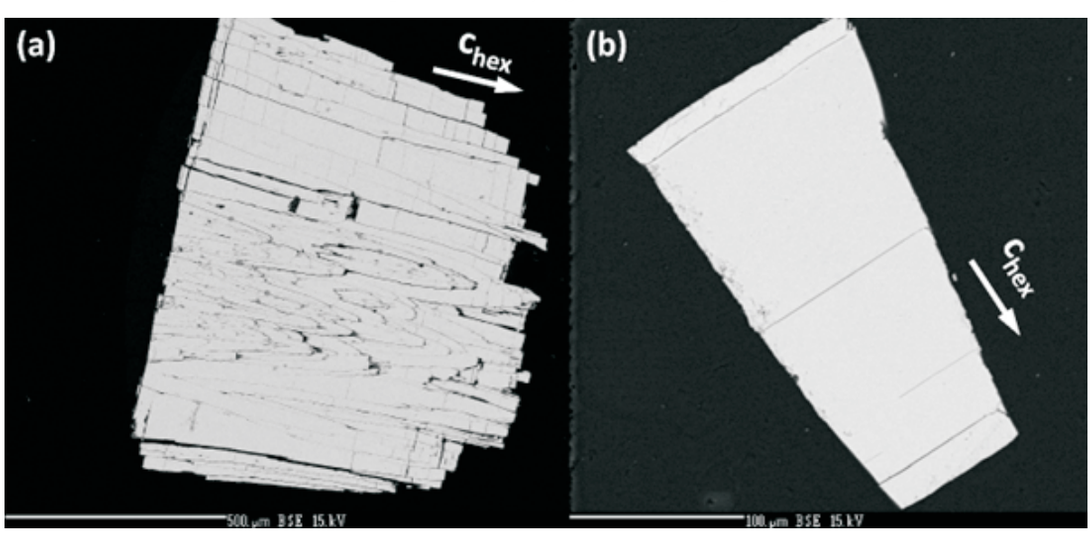


**Figure 2**. **a** The BSE image of the polycrystalline aggregate with fibre texture. Crystals are elongated about $\mathbf{c}_{hex}$, and are parallel to the section in clusters above and below the centre of the image. In the central cluster, the orientation of crystals is somewhat inclined, so that they are cut obliquely. Borders of individual crystals are recognizable. **b** The BSE image of the common single crystal of the subfamily D. Note the same degree of grey throughout the surfaces of both specimens due to the homogeneity of chemical composition. Photo Z. Dolníček.

*The research was supported by project 18-10504S of the Czech Science Foundation, and by project CZ.02.1.01/0.0/0.0/16_019/0000760 Solid 21 under the Ministry of Education, Youth and Sports. Author also thanks National Museum for allowing of taking of specimens for the study.*

L5

# "PŘÍRODNÍ SLITINY" Z HLUBOKOMOŘSKÝCH KONKRECÍ

**J. Kopeček[1,*], F. Laufek[2], L. Klimša[1], A. Michalcová, L. Šulcová[3], A. Tsepeleva[3], K. Borkovcová[3], D. Nováček[3], Hong N. Vu[3], P. Dvořák[3], P. Novák[3]**

*[1]Department of Materials Analysis, Institute of Physics of the CAS, Prague, Czech Republic*
*[2]Czech Geological Survey, Prague, Czech Republic*
*[3]Department of Metals and Corrosion Engineering, University of Chemistry and Technology Prague, Prague, Czech Republic*
*[*]kopecek@fzu.cz*

Kritický nedostatek barevných kovů spojený s tranzicí ekonomiky vede k hledání méně obvyklých zdrojů, jako jsou například hlubokomořské konkrece. Zatímco konvenční těžba je ekologicky závadná nebo probíhá v nedostatečně přátelských teritoriích, zóny hlubokomořského dna jsou volně dostupné nebo předmětem mezinárodních smluv, které je činí právně přístupné (např. společný claim několika post-socialistických zemí v zóně Clarion-Clipperton v Tichém oceánu). Odhlédneme-li od realizačních obtíží či vysokých vstupních nákladů, jedná se o zajímavý technologický i strukturní problém. Tradiční přístup ke konkrecím vycházel z postupné separace a následného čištění jednotlivých obsažených prvků a v hledání těch, které jsou finančně náležitě zajímavé pro těžbu. Projekt, jehož výsledky jsou prezentovány vychází z revoluční myšlenky „přírodních slitin", tedy v redukci nikoli na čisté kovy, ale na čistou směs kovů, která bude následně využita jako funkční příměs například do hliníkové matrice. Konkrece byly redukovány aluminotermicky a titanotermicky se stechiometrickým a zvýšeným obsahem redukujícího kovu (obvykle 0, 10, 20 a 100 % přebytku).

Struktura takto získaných slitin byla následně studována strukturně (kombinace XRD, LOM, SEM), mechanicky i korozně. Získané výsledky jsou překvapivě komplexní – struktura je složitá, pozorované fáze jsou nestechiometrické, případně jsou prvky ve strukturách substituovány. Slitina bez přebytku hliníku při aluminotermii obsahuje majoritní fázi β- $Mn_{0.66}Ni_{0.2}Si_{0.16}$ a tři minoritní fáze; slitina s 10 % přebytku obsahuje sedm fází, z nichž tři mají přes 10 hm. %; slitina s 10 % přebytku obsahuje 9 fází, z nichž pět je minoritních. Majoritní fáze ve všech vzorcích je odlišná. Mechanické vlastnosti jsou poplatné majoritnímu podílu manganu – připravené vzorky jsou tvrdé a extrémně křehké [1], avšak korozní vlastnosti jsou dobré [2]. Materiály připravené titanotermicky nechávají extrémní množství materiálu ve strusce, avšak výsledné složení není tak komplexní jako v případě aluminotermických materiálů. Ostatně výchozí fázové složené samotných konkrecí je také složité: obsahují birnessit, todorokit a křemen a další minoritní fáze.

Metodologicky byla práce postavena na součinnosti metod XRD (Bruker D8 Advance) a SEM (Tescan FERA 3) včetně analyzátorů EDS a EBSD (EDAX Octane Super 60 $mm^2$ a DigiView V). Bylo dosaženo dobré shody v obsahu fází stanovaných pomocí XRD a EBSD/EDS. Některé zcela minoritní fáze byly potvrzeny pomocí EDS/EBSD, protože stejnou krystalografickou strukturu v materiálu mají i jiné, více zastoupené fáze (případ MnS). V aluminotermických slitinách byly potvrzeny Heuslerovy fáze $Mn_2FeAl$ a $Mn_2FeSi$ vlastně dříve než byl publikován jejich objev v čistých ternárních systémech.

1. Novák P, Nguyen H V, Šulcová L, Kopeček J, Laufek F, Tsepeleva A, Dvořák P, Michalcová A 2021, Materials 14 561.

2. Msallamová Š, Novák P, Miossec P, Kopeček J, Tsepeleva A, Rudomilová D, Fojt J 2021 Materials 14 5211.

*Výzkum je podporován GA ČR z projektu 20-15217S a strukturními projekty MŠMT CzechNanoLab (LM 2018110) a SOLID21 (CZ.02.1.01/0.0/0.0/16_019/ 0000760).*

L6

# STRUCTURE AND MICROSTRUCTURE IN (111) AND (111)+(001) ScN/MgO THIN FILMS

**E. de Prado, J. More Chevalier, S. Cichoň, L. Fekete. J. Lančok**

*Institute of Physics of the Czech Academy of Sciences, Na Slovance 2, 18221 Praha 8, Czechia*
*prado@fzu.cz*

ScN is an emerging semiconductor that exhibits rock-salt (cubic) crystalline structure . It is of high interest in material science due to its physical properties such as high melting point and high electron mobility. To improve the mobility and other electronic properties, it is necessary to produce single crystal ScN thin films with low density of defects. It has been demonstrated that the presence of point defects and impurities affects thermoelectric properties . Planar defects such as twins have been also explored for (111) and (001) ScN thin films grown on different substrates . The presence of twins for bi-oriented (111)+(001) ScN films on MgO (001) has been reported but its origin is not fully understood yet. In this work we pay special attention to the system (111)+(001) ScN/MgO (001) and we compare our results with single oriented (111) ScN films. To it, several ScN films were deposited on MgO (001) substrate by DC reactive magnetron sputtering at different temperatures. The morphology of the films has been explored by Atomic Force Microscopy (AFM) and the presence of twins has been analyzed by X-Ray Diffraction through 2theta scans, and 002, 022, and 111 pole figures.

For the bi-oriented kind of films a very complex system of twins is obtained (Figure 1), which can be separated in the contribution of two, one coming from the (001) ScN oriented crystals and the other one coming from the (111) crystals. A deep study of the structure and microstructure of such a system could provide a better understanding of the role of twins in the final film orientation.

**Keywords: ScN; twins; pole figure; epitaxial layer**

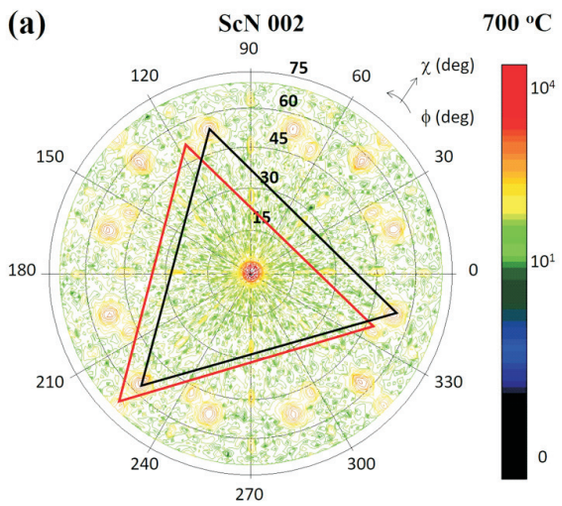


a)

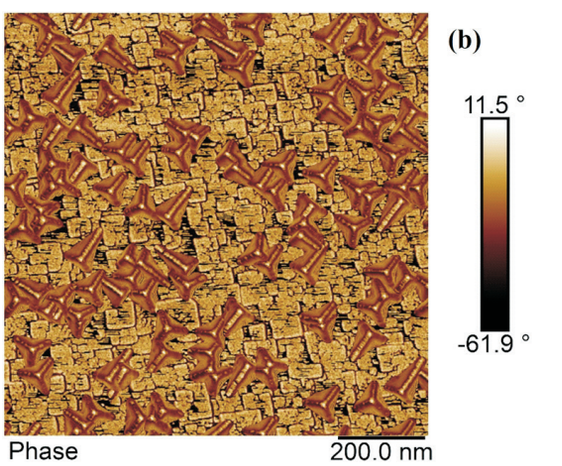


b)

**Figure 1.** Results for bi-oriented ScN films. (a) 002 Pole figure and (b) AFM image with phase contrast.

1. M. A. Moram, T. B. Joyce, P. R. Chalker, Z. H. Barber, and C. J. Humphreys, "Microstructure of epitaxial scandium nitride films grown on silicon," *Appl. Surf. Sci.*, vol. 252, pp. 8385–8387, 2006.
2. S. Kerdsongpanya, B. Alling, and P. Eklund, "Effect of point defects on the electronic density of states of ScN studied by first-principles calculations and implications for thermoelectric properties," *Phys. Rev. B - Condens. Matter Mater. Phys.*, vol. 86, no. 19, pp. 1–7, 2012.
3. S. Acharya *et al.*, "Twinned growth of ScN thin films on lattice-matched GaN substrates," *Mater. Res. Bull.*, vol. 143, no. January, p. 111443, 2021.
4. E. de Prado, J. More-Chevalier, S. Cichoň, and J. Lančok, "Twin domains of ScN (001) films on MgO (001)," *Acta Crystallogr. Sect. A Found. Adv.*, vol. 77, no. a2, pp. C835–C835, 2021.
5. S. Chowdhury *et al.*, "Synthesis and study of ScN thin films," pp. 1–13, 2021.
6. J. More-chevalier *et al.*, "Applied Surface Science Correlation between crystallization and oxidation process of ScN films exposed to air," *Appl. Surf. Sci.*, vol. 515, no. December 2019, p. 145968, 2020.

**Session II, Monday, June 20**

**L7**

# LINE PROFILE ANALYSIS AND ROCKING CURVE EVALUATION OF 3D DIFFRACTION DATA

**Gergely Farkas[1], Jishnu Bhattacharyya[2], Gyula Zilahi[3], Kristián Máthis[4], Sean R. Agnew[5]**

*[1]Nuclear Physics Institute of the CAS, Řež, Czech Republic*
*[2]University of Virginia, Charlottesville, USA*
*[3]D UK Atomic Energy Authority, Oxfordshire, United Kingdom*
*[4]Department of Physics of Materials, Charles University, Prague, Czech Republic*
*afarkas@ujf.cas.cz*

Diffraction patterns from ~100 individual grains of a solutionized and quenched metastable β-Ti alloy were obtained by high energy synchrotron diffraction during in-situ tensile deformation experiments. The diffraction patterns of select grains were analyzed per an established single-crystal line profile analysis technique to assess the dislocation density evolution on individual slip systems. Further, a new technique to estimate the geometrically necessary dislocation (GND) density from rocking curves is introduced. The results provide a powerful complement to previously published comparisons between measured and crystal plasticity simulated internal elastic strains (and stresses). In particular, they reveal there is no preference for 1/2 <111> Burgers vector dislocations to reside on a particular glide plane, since they have similar densities on {110} and {112} planes. In addition, an explanation for the observation of strain softening in some of the grains is hypothesized as form of "plastic buckling". A select number of strain softening grains exhibit higher lattice curvature (GND density) than other grains, indicating that the grains have "broken up" into smaller domains which are deforming in distinct ways from one another, and more easily than they would have together.

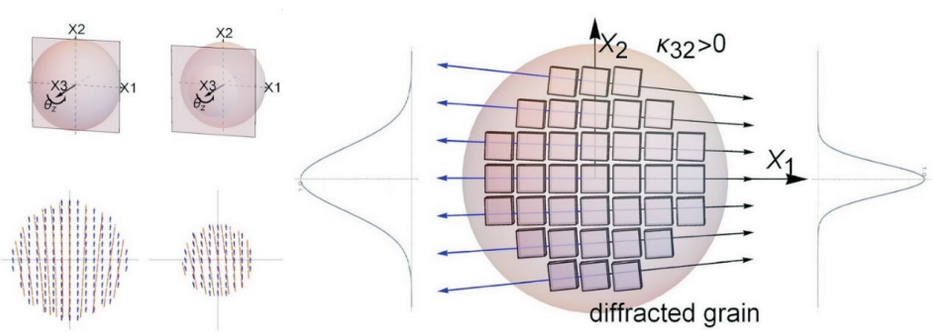


**Figure 1.** Rocking curve broadening vs grain curvature

L8

# LABORATORY AND SYNCHROTRON ROCKING CURVE IMAGING FOR CRYSTAL LATTICE MISORIENTATION MAPPING

**P. Mikulík, M. Meduňa, O. Caha**

*Department of Condensed Matter Physics, Faculty of Science, Masaryk University, Brno, Czech Republic*

X-ray diffraction topography (diffractometry) is a traditional method of visualising crystal structure perfectness on a film with a high spatial resolution. However, angular misorientation inspection requires multiple exposures for several diffraction angles around the Bragg peak by means of a manual film exchange, which is a bit cumbersome. This limitation has been overcome by utilisation of digital 2D detectors which were available at synchrotron imaging beamlines with high flux and parallel beam, thus the rocking curve imaging (RCI) technique has been developed. Recently, RCI was transferred from synchrotron to laboratory set-ups.

Nowadays, RCI is an X-ray diffraction technique which combines full-field X-ray digital topography and Bragg-diffraction rocking curve recording. A large (almost) parallel monochromatic beam irradiates a crystalline sample with a misorientation distribution characterized by local tilt angles. Series of digital topographs are measured by a two-dimensional detector at different sample orientations from which peak characteristics of millions of local Bragg peaks from each series are extracted. The field of view and lateral resolution is given by the camera size, its pixel size and the Bragg angle, while the angular resolution is given by the rocking curve width being typically much smaller than the misorientation angles of the studied crystal. Simultaneous high spatial resolution provided by the two-dimensional detector and high angular resolution (0.001°) allows to quantify crystalline structure perfectness over large sample area which scales with the area of the detector. Therefore the rocking curve imaging is an imaging method with faster recording compared to usual laboratory scanning area diffractometry which requests measurement of the rocking curve at each surface point.

Synchrotron RCI [1,2] profits from large parallel beam, high flux and small detector pixel size down to one micrometre. For small misorientations of the crystal lattice, detector can have any distance from the sample, while larger misorientations due to inherent focusing and defocusing of the diffracted (micro)beams require a dedicated reconstruction procedure.

Laboratory RCI [3] with a slightly diverging beam requires small misorientation angles and very small sample to detector distance, thus a home-made extension for a commercial diffractometer is necessary. Current two-dimensional detectors available at laboratory diffractometers have typical spatial resolution downto 0.1 mm which make it possible to analyze a large sample area at once.

On several examples, we will demonstrate the RCI technique for a characterisation of several large-area semiconductor wafers, such as silicon, silicon carbide, gallium nitride or overgrown silicon-germanium microstructures.

1. P. Mikulík, D. Lübbert, D. Korytár, P. Pernot, T. Baumbach, *Journal of Physics D: Appl. Phys.* **36**, 2003, A74.
2. D. Lübbert, C. Ferrari, P. Mikulík, P. Pernot, L. Helfen, N. Verdi, D. Korytár, T. Baumbach, *Journal of Applied Crystallography* **38**, 2005, 91.
3. M. Meduňa, O. Caha, E. Choumas, F. Bressan, H. von Känel, *Journal of Applied Crystallography* **54**, 2021, 1071.

L9

# RADON TRANSFORMATION IN RECIPROCAL SPACE

**M. Meduňa[1], F. Isa[2], F. Bressan[3], H. von Känel[2,3]**

*[1]Department of Condensed Matter Physics, Masaryk University, Brno, Czech Republic*
*[2]Laboratory for Solid State Physics, ETH-Zürich, Zürich, Switzerland*
*[3]G-ray Switzerland SA Hauterive Switzerland*
*mjme@physics.muni.cz*

Mapping intensity in reciprocal space around certain reciprocal lattice points is mostly realized in two-dimensions within the ($Q_xQ_z$) plane which is usually sufficient for any analysis of crystal lattice strain, mosaicity, structural quality, internal defect distribution or surface morphology and structure, depending on the scattering technique used. Nevertheless, in certain cases mapping of the scattered intensity in 3D space, out of the scattering plane e.g. along the $Q_y$ axis, is more and more demanded as well. Scanning reciprocal space in 3D however requires a well collimated X-ray beam in all directions, so that such experiments are realized mainly at synchrotron sources in order to have a sufficiently intense and parallel beam. Practically any 2D pixel detector is also extremely suitable for timely effective collection of reciprocal space maps (RSMs).

In this work we realize a collection of 3D RSMs using standard laboratory equipment with only a partially-collimated beam using a typical linear focus X-ray tube. We use a Rigaku SmartLab diffractometer equipped with a 2D HyPix area pixel detector for recording series of symmetric diffraction RSMs on microstructured semiconductor samples. The 2D detector is used in a linear mode for fast collection of typical 2D $Q_xQ_z$ RSMs where the sample is scanned at many different azimuths with respect to the diffraction vector as an axis of rotation. The 3D intensity distribution in reciprocal space is then reconstructed by means of a Radon transform procedure, typically used for many decades in real space computer tomography (CT) [1]. The details of the technique used here in reciprocal space and experimental details realized can be found in recently presented work [2], including the details of the samples.

The method of applying the Radon transform for the reconstruction of RSMs is presented on Ge, GaAs and SiGe microcrystals epitaxially grown on patterned Si substrates [3]. Series of synchrotron experiments using a nanofocused beam, where 3D RSMs have already been measured on many samples, were previously presented in several of our publications [4,5,6], however in this study we compare similar laboratory measurements with the previously performed synchrotron experiments [2].

The $Q_xQ_z$ RSMs obtained at various azimuths φ are first decomposed into sinograms for all $Q_z$ positions, see an example for fixed $Q_z$ in the left panel of figure 1. This example is built from RSMs where certain (004) lateral diffraction satellites appear and their $Q_x$ position changes as the sample is rotated along φ. After application of the inverse Radon transformation on this sinogam map, we can obtain the spatial distribution of these maxima within the $Q_xQ_y$ plane perpendicular to the axis of rotation which shows four-fold symmetry, see the right panel of figure 1. Let us note that these satellites originate from a superlattice covering the faceted SiGe microcrystals. Comparing the new laboratory data [2] with previous synchrotron measurements [6], we get a very good agreement of the 3D spatial distribution of intensity.

1. P. Suetens, in Fundamentals of Medical Imaging, Cambridge University Press, 2009, pp. 35–41.

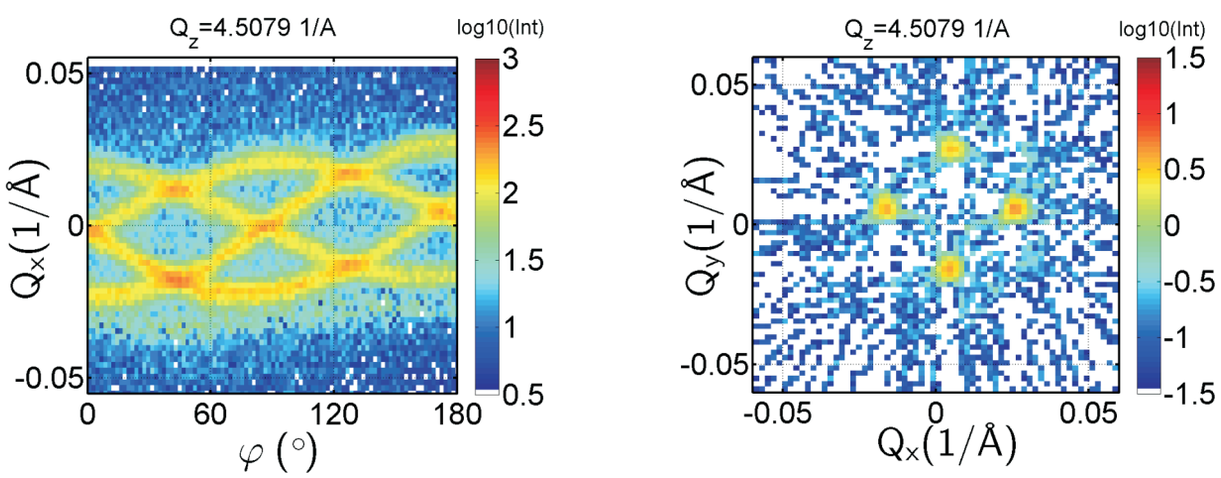


**Figure 1.** (left) Sinogram built from slices of typical $Q_xQ_z$ RSMs for fixed $Q_z$ position close to SiGe (004) recorded at a series of azimuthal rotations of the sample containing four-fold symmetric diffraction superlattice satellites. (right) Reconstruction of the $Q_xQ_y$ map in reciprocal space using the inverse Radon transform applied on the sinogram in the left panel can be understood as a given slice for fixed $Q_z$ through the 3D RSM. The four-fold structure of the four maxima is evident.

2. M. Meduňa, F. Isa, F. Brennan, H. von Känel, J. Appl. Cryst. 55, (2022) in print.
3. C.V. Falub, H. von Känel, F. Isa, R. Bergamaschini, A. Marzegalli, D. Chrastina, G. Isella, E. Müller, P. Niedermann, L. Miglio, Science, 335, (2012), 1330.
4. C. V. Falub, M. Meduňa, D. Chrastina, F. Isa, A. Marzegalli, T. Kreiliger, A.G. Taboada, G. Isella, L. Miglio, A. Dommann, and H. von Känel, Scientific Reports 3 (2013), 2276.
5. M. Meduňa, C.V. Falub, F. Isa, A. Marzegalli, D. Chrastina, G. Isella, L. Miglio, A. Dommann, and H. von Känel, J. Appl. Cryst, 49, (2016), 976.
6. M. Meduňa, C.V. Falub, F. Isa, D. Chrastina, T. Kreiliger, G. Isella, H. von Känel, J. Appl. Cryst., 47, (2014), 2030.

*We acknowledge the staff of the ID01 beamline at the ESRF, Grenoble.*

**L10**

# IMAGE CORRECTIONS FOR POWDER DIFFRACTION WITH THICK SENSOR DETECTORS

**S. Selleck, C. López Jurado, M. Ramakrishnan, C. Weninger, J. Just, Z. Matěj**

*MAX IV Laboratory, Lund University, Sweden*
*zdenek.matej@maxiv.lu.se*

Flat hybrid pixel detectors present the most common instruments for recording X-ray intensities in scattering experiments at photon light facilities as well as in X-ray laboratories. This holds in particular for conventional crystallographic experiments. In order to optimize quantum efficiency of the detection process the ratio of detector sensor thickness and pixel size is often set quite high. A narrow X-ray beam entering such a detector at an oblique angle is absorbed in multiple consecutive pixels. This is causing an effective shift of the detected signal known as the "parallax" effect [1, 2]. Beside this the absorption of X-ray beam in the detector sensor is more complete. The latter is called an "oblique incidence effect" [2]. Appropriate corrections are well established in software for single crystal diffraction data processing [1]. Marlton et al. [2] introduced the parallax effect correction for pair distribution function measurements. The idea is used to improve effective camera resolution in synchrotron and medical imaging [3]. In case of diffraction experiments with a flat powder sample in parallel beam geometry angular resolution is dominated by geometrical effects. In addition, for samples with crystallite size >1 um grain statistics is often not-ideal and azimuthally integrated diffraction profiles are not well defined. Diffraction spots may present blurred signal due to the parallax and oblique incidence effects as shown in Figure 1. Point spread function (PSF) over the detector area was estimated by ray-tracing the detector and the know PSF is deconvoluted from the measured signal in the next step. Results of such diffraction image processing are presented (Figure 1). Different methods for positionally variant deblurring with known PSF were used: direct inversion with regularization, Richardson-Lucy deconvolution [4, 5]

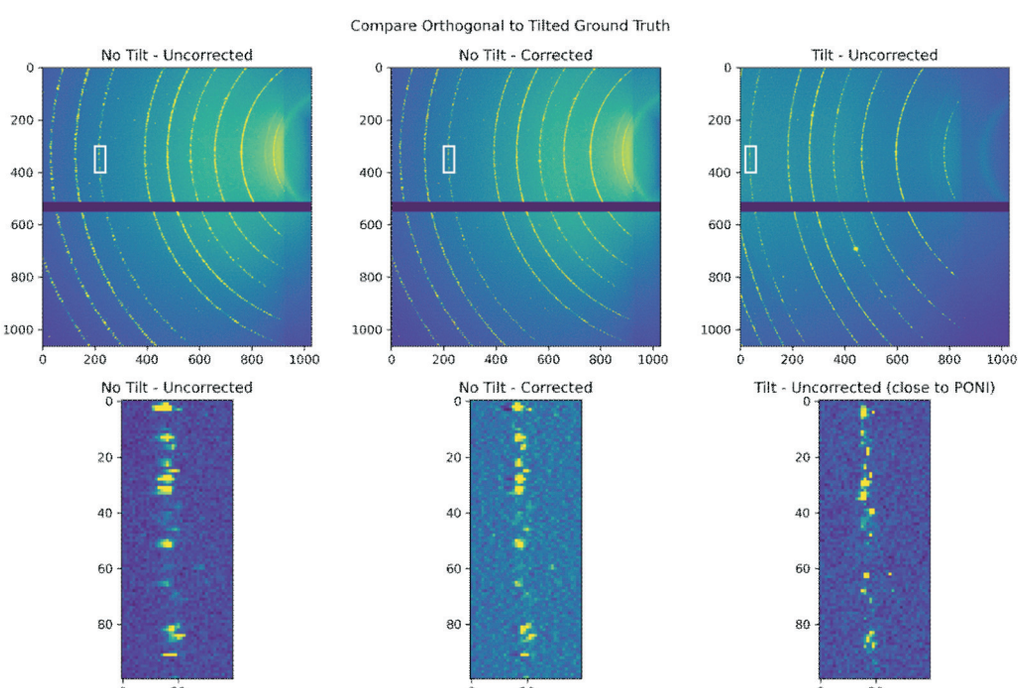


**Figure 1**. Positionally variant deblurring of X-ray diffraction images with known detector PSF.

ant deblurring with known PSF were used: direct inversion with regularization, Richardson-Lucy deconvolution [4, 5] and Deep learning approach [6]. Pros and cons of different methods are described, and applicability of the method is briefly discussed.

1. W. Kabsch, *X-ray Detector Software, XDS version: March 15,* (2007), https://xds.mr.mpg.de/html_doc/Release_Notes.html (visited May 20, 2022)
2. F. Marlton, O. Ivashko, M.V. Zimmerman, O. Gutowski, A.C. Dippel, M.R.V. Jørgensen, *J. ApplCryst.*, **52**, (2019), 1072-1076. doi: 10.1107/S1600576719011580
3. P. Shikhaliev, O. Fox, N. Tartoni, *IEEE Nuclear Science Symposium and Medical Imaging Conference (NSS/MIC)*, (2020), 1-3. doi: 10.1109/NSS/MIC42677.2020.9507906
4. W. Richardson, *J. Opt. Soc. Am.*, **62**, (1972), 55-59. doi: 10.1364/JOSA.62.000055
5. L.B. Lucy, *Astronomical Journal*, **79**, (1974), 745. doi: 10.1086/111605
6. J. Mustaniemi, J. Kannala, S. Särkkä, J. Matas. J. Heikkila, *IEEE Winter Conference on Applications of Computer Vision (WACV)*, (2019), 1914-1922. doi: 10.1109/WACV.2019.00208

**L11**

## 25TH ASSEMBLY AND CONGRESS OF THE IUCr IN PRAGUE, HISTORY, EXPERIENCE, STATISTICS

**Radomír Kužel**

**Faculty of Mathematics and Physics, Charles University, Prague**

see p. 144

# Session III - Neutron scattering, Tuesday, June 21

## L12

## OPPORTUNITIES AND PERSPECTIVES AT THE INSTITUT LAUE LANGEVIN: THE ENDURANCE UPGRADE PROGRAMME

**M. Johnson**

*Institut Laue Langevin, Grenoble, France*
*johnson@ill.eu*

The Endurance upgrade programme covers the period 2016 – 2023 with a budget of 60 M€. About 30 projects have been delivered or are nearing completion. They include neutron guide systems, new and upgraded instruments, sample environment and data and software services. The upgrade programme as a whole ensures that research capability at the ILL will continue to be world leading for the next decade, offering new opportunities and perspectives for excellent science, both for academia and industry. The Endurance programme will be presented, including specific examples and initial results, and set in the context of future reactor operation, given the recent agreement by the ILL Associates to fund the Institute for the period 2024 – 2033.

## L13

## NEUTRON DIFFRACTION TO STUDY THE STRUCTURE OF MATERIALS

**Thomas C. Hansen**

*Institut Laue-Langevin, 71 avenue des Martyrs, 38000 Grenoble, France*
*hansen@ill.fr*

For the inspection of processes involving condensed matter, *in situ* neutron powder diffraction proves itself to be a versatile tool, giving insight into processes of technological pertinence. Only a few high-intensity powder diffractometers at intense neutron sources allow for this. D20 at Institut Laue-Langevin provides the highest available intensity in constant wavelength neutron powder diffraction. A stationary, curved linear position sensitive detector allows for in-situ diffraction studies down to a second and encourages the use of complex sample environments with inherently small sample sizes. D20 adapts to various levels of crystallographic complexity and rapidity of an observed phenomenon.

The portable electronics market, as well as non-polluting ground transportation, need portable energy storage solutions with improved characteristics. Li-ion batteries with solid electrolytes overcome issues of liquid electrolytes in battery safety and high-voltage operation. Neutron diffraction determines the Li diffusion pathway in solid-state Li-ion conductors. Development of better electrode materials in terms of gravimetric and volumetric energy density, temperature operation range and cycling stability needs understanding of lithium (de)intercalation phenomena. Operando diffraction techniques are well suited here. Electrochemical cells based on a neutron-transparent (Ti,Zr) alloy combine good electrochemical properties and the ability to collect neutron diffraction patterns with reasonable statistics and no other Bragg peaks than those of the electrode material. This allows detailed structural determination of electrode materials by Rietveld refinement during operation.

Solid-oxide fuel cells convert chemical energy into electricity at higher efficiency than conventional methods, with less pollution. The anode (fuel electrode) must not alter at high temperature (thermal stability), not form nonconductive phases at interfaces (chemical stability) and not degrade upon reduction and oxidation cycles (redox stability). The state-of-the-art "cermet" of Ni and yttria-stabilized zirconia ceramic loses performance upon usage as its porosity is reduced by Ni agglomeration and as oxidation of Ni causes redox instability. Cermet deactivates through carbon coking and sulfur poisoning, making it unsuited for hydrocarbon fuels. Single-phase mixed ionic and electronic conductors provide microstructural stability and increase the electrode fraction accessible to oxide ions. Many of those oxides have been investigated successfully in operando at high temperature under oxidizing and reducing gas flow by neutron diffraction, following the crystal chemistry of oxide ions during the process.

Classical *in situ* work (thermo-diffractometry) has been done on the photovoltaic materials, $MaPbI_3$ and derivates, and neutron diffraction turned out to be a perfect tool to screen the crystal chemistry of light organic atoms beside the heavy metal atoms over a wide range of temperatures.

Hydrogen is an attractive energy carrier for renewable energy sources due to its high energy density. Solid-state hydrogen storage provides higher storage capacities than compressed or liquefied hydrogen. Complex metal hydrides have high hydrogen storage capacities but suffer from poor kinetic and thermodynamic properties. Tuning the thermodynamics for dehydrogenation, to reduce the temperature at which hydrogen is evolved is achieved

through the addition of a second phase, which will lead to the formation of a more stable product upon decomposition and thereby reducing the enthalpy for dehydrogenation. Neutron powder diffraction screens the crystal chemistry of the different phases *in situ*.

Finally, the work on the structure and the formation and decomposition of gas hydrates and related ice phases will be presented, as well as the prospects of work at very high pressures up to 25 GPa at low temperatures down to 1.6 K.

**L14**

## SOFT MATTER SEEN BY SMALL-ANGLE NEUTRON SCATTERING, NEUTRON REFLECTOMETRY, AND COMPLEMENTARY TECHNIQUES

**Leonardo Chiappisi**

*Institut Laue-Langevin, Large Scale Structure Group, Grenoble, France*

Soft. Condensed. Matter. Soft matter systems are defined as those which are structurally altered when external force of the magnitude of thermal fluctuation is applied. This definition, despite being scientifically accurate, does not do justice to the complexity and diversity of soft matter mattery systems.

Soft. Condensed. Matter. It includes biomaterials, polymers, nanoparticles, emulsions, surfactants, and many other building blocks. Understanding and controlling soft matter systems, is key for technological progress and for the transition to a sustainable society: detergents, food additives, lubricants, foams, coatings, are examples of soft matter systems.

Soft. Condensed. Matter. The low energy required to trigger structural, and thereby functional changes in soft matter systems makes them the most suited ingredients for many responsive systems. These systems are characterized by a complex energetic landscape, and often by ill-defined structures.

In this contribution, through a series of examples, the use and potential of neutron scattering, and reflectometry is illustrated. The examples aim at covering the broad domain of soft matter science probed at the Institut Laue-Langevin.

**L15**

## INELASTIC NEUTRON SCATTERING - FROM STRUCTURE TO DYNAMICS OF FUNCTIONAL MATERIALS

**Paul Steffens**

*Institut Laue-Langevin, Grenoble, France*
*steffens@ill.fr*

The first part of this presentation will give an overview about the capabilities of the ILL to perform inelastic neutron scattering measurements. Depending on the use case (energy range, resolution, type of sample etc.), different classes of instruments are available: time-of-flight, triple axis, and more specialized techniques (spin-echo, backscattering). Most of the instruments at the ILL have undergone significant up-grade in the recent years. Thanks to these recent developments, long-standing questions in materials such as unconventional superconductors can now be addressed, as well as, for instance, the study of new quantum magnetic effects. The current state of the experimental possibilities, together with typical applications, will be discussed.

A particularly powerful technique for the study of magnetism are polarized neutrons. This technique allows separating different types of nuclear and magnetic processes from each other precisely; however, intensity issues sometimes limit its application in inelastic neutron scattering, which is why in only few places worldwide such experiments can be performed. We will present an example of inelastic scattering from the skyrmion phase of manganese silicide, a model system for complex magnetic order and its potential applications (spintronics etc.). The excitation spectrum of this particular magnetic order is extremely complex and has recently been measured in unprecedented detail thanks to the use of polarization analysis. In excellent agreement with theory, these works provide a comprehensive understanding of fundamental magnetic excitations of the magnetic skyrmion phase.

# Session IV - Neutron scattering, Tuesday, June 21

## L16

## FIRST SCIENCE ON THE ESS INSTRUMENT SUITE

**Andreas Schreyer**

*ESS Lund, Sweden*

The European Spallation Source currently under construction in Lund, Sweden is designed to become the world's most powerful neutron spallation source, opening up new scientific opportunities.

An overview of the progress of the construction project will be given, the time to starting user operation will be discussed and new scientific opportunities will be highlighted.

## L17

## EUROPEAN SPALLATION SOURCE - CONTRIBUTION OF THE CZECH REPUBLIC

**J. Šaroun[1], P. Lukáš[1], P. Beran[1,2]**

*[1]Nuclear Physics Institute, CAS, Hlavní 130, 25068 Řež, Czech Republic*
*[2]European Spallation Source ERIC, Box 176, SE-221 00, Lund, Sweden*
*saroun@ujf.cas.cz*

European Spallation Source (ESS) is the world's most powerful neutron source under construction in Lund (Sweden), which will offer about 4000 beam days annually to scientists from Europe when built to its planned capacity of 22 instruments. Even with just the 15 instruments to be built within the ESS construction scope, ESS will greatly increase the capacity of the European network of neutron sources by opening new opportunities for breakthrough research with neutrons thanks to the unprecedented neutron beam brightness accompanied by world-class instrumentation and novel experimental methods developed for the long-pulse neutron source.

The Czech Republic became one of the 13 founding members of the ESS ERIC consortium in 2015 with the planned 2% contribution to the ESS construction, which should ensure a proportional share of beam capacity for Czech users after ESS is put into operation. This step is of great importance for the Czech user community when considering the fading capacity of neutron sources in Europe: several research reactors which used to serve our user community were shut down recently, while others are approaching the end of their lifetime, including the research reactor LVR-15 in Řež and ILL Grenoble.

In-kind contributions make a significant part of the ESS construction. The Nuclear Physics Institute, CAS (NPI) in Řež has the task of implementing several of these contributions:

The supply of systems for the ESS target station includes the helium cooling loop, water cooling of the target and HVAC (Heating, Ventilation, Air Conditioning) of the target station building. These technologies have already been delivered, and their installation is being finalized.

NPI, together with Helmholtz Zentrum Hereon in Geesthacht, develops and builds one of the neutron scattering instruments – the Beamline for European Materials Engineering Research (BEER). According to the current schedule, BEER is supposed to be ready for hot commissioning in early 2024 and enter into the user regime during the ESS operation ramp-up between 2025 and 2027. BEER has been developed in cooperation with neutron users from the material research and engineering areas. On the Czech side, teams from the Faculty of Mathematics and Physics of the Charles University and the Institute of Physics, CAS, largely contributed to the instrument concept and actively participated in the development of a sample environment for in-situ measurements and novel methods to be tested during early operation. Such a collaboration is vitally important for a successful start of the user program at BEER, and neutron users are encouraged to collaborate with the instrument team on the preparation of the early operation program.

*The contribution of the Czech Republic to the ESS construction has been supported by the Czech Ministry of Education, Youth and Sports through the project of large infrastructure ESS Scandinavia-CZ (project LM2018111) and by EU Structural Funds (Reg. No. CZ.02.1.01/0.0/0.0/16_013/0001794).*

L18

# BEER - SCIENCE CASE AND STATUS

**Beran P.[*,1,3], Šaroun J.[1], Lukáš P.[1], Fenske J.[2], Nowak G.[2], Siemers D.J.[2], Kiehn R.[2], Burmester J.[2], Müller M.[2], Woracek R.[3]**

[1]*Nuclear Physics Institute CAS, Hlavni 130, 25068 Rez, Czech Republic*
[2]*Helmholtz-Zentrum Hereon, Max-Planck-Straße, 21502 Geesthacht, Germany*
[3]*European Spallation Source ERIC, P.O. Box 176, 22100 Lund, Sweden*
[*]*premysl.beran@ess.eu*

The time-of-flight engineering diffractometer BEER [1] (Beamline for European Materials Engineering Research), which is under construction at the European Spallation Source (ESS), will offer new opportunities for investigations of microstructures, residual stress evolutions and in-situ phase transformations under near-processing conditions. The layout of the instrument is depicted in Figure 1 and the basic parameters are listed in Table 1.

The construction of the instrument is divided into two stages called *Day-1* (coloured parts in Figure 1) and *Full-scope* (white parts in Fig. 1). The *Day-1* instrument will provide reduced capabilities mainly in the detector coverage, SANS option and variability of chopper cascade but will be fully operational and comparable with the current engineering instruments worldwide.

BEER combines the high brilliance of the ESS source with large instrument flexibility. The diffractometer includes a novel beam-shaping technique, the so-called modulation technique (see Figure 2) [2]. By a time-encoded extraction of several short pulses from the long ESS pulse, a substantial intensity gain of up to an order of magnitude compared to a pulse shaping method (one pulse extraction) for high-crystal-symmetry materials can be achieved without compromising the resolution. More complex crystal symmetries or multi-phase materials can be investigated by the standard pulse shaping method. The variable chopper set-ups and advanced extracting techniques [3] offer broad intensity/resolution ranges that can be adjusted for the experiment's needs. This flexibility opens up new possibilities for in-situ experiments studying materials processing and performance under operating conditions.

**Table 1** - Basic facts about the BEER instrument

| | |
|---|---|
| Instrument Class | Engineering Diffraction |
| Moderator | Bispectral |
| Primary Flightpath | 158 m |
| Secondary Flightpath | 2 m |
| Wavelength Range | 0.8 – 6 Å |
| Bandwidth | 1.7 Å |
| d-spacing Range | 0.6 – 7 Å |
| **Pulse-Shaping Mode** | |
| Resolution Δd/d | 0.15 – 0.6 % |
| Flux at Sample at 2MW | 0.18 – 1.4•$10^8$ n $s^{-1}$ $cm^{-2}$ |
| **Modulation Mode** | |
| Resolution Δd/d | 0.1 – 0.3 % |
| Flux at Sample at 2MW | 0.18 – 0.87•$10^8$ n $s^{-1}$ $cm^{-2}$ |

Advanced sample environments dedicated to thermo-mechanical processing are foreseen to fulfil this

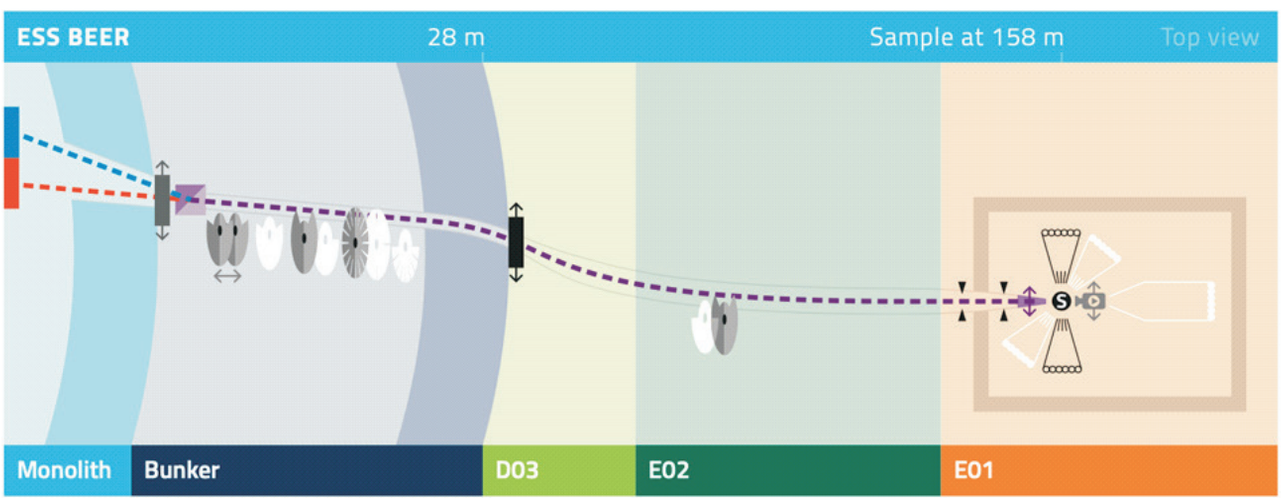


**Figure 1.** The BEER instrument schematic layout

task, e.g. a quenching and deformation dilatometer, and various deformation rigs.

1. K.H. Andersen, et al., The instrument suite of the European Spallation Source, *Nuclear Instruments and Methods in Physics Research Section A.* **957**, (2020), 163402.
2. M. Rouijaa, R. Kampmann, J. Šaroun, J. Fenske, P. Beran, M. Müller, P. Lukáš, A. Schreyer, Beam modulation: A novel ToF-technique for high resolution diffraction at the Beamline for European Materials Engineering Research (BEER), *Nuclear Instruments and Methods in Physics Research, Section A.* **889**, (2018), 7–15.
3. J. Šaroun, J. Fenske, M. Rouijaa, P. Beran, J. Navrátil, P. Lukáš, A. Schreyer, M. Strobl, Neutron optics concept for the materials engineering diffractometer at the ESS, *J. Phys.: Conf. Ser.* **746**, (2016), 012011.

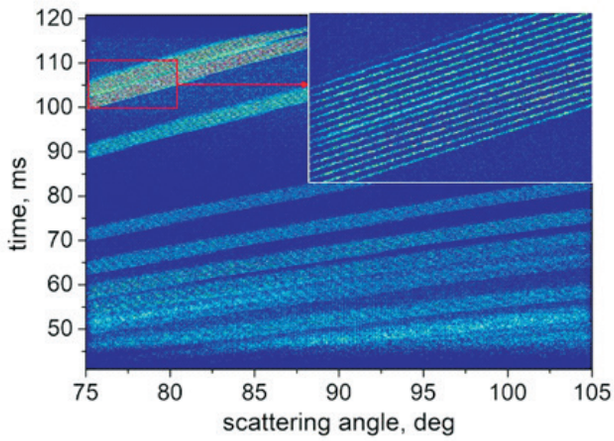


**Figure 2.** Simulated time-of-flight diffraction pattern of a duplex-steel for +90° detector showing the splitting of the Bragg reflections when modulation technique is used [2].

## Session V - Neutron scattering, Tuesday, June 21

**L19**

# SANS INVESTIGATION OF MICROSTRUCTURE EVOLUTION IN SINGLE CRYSTAL Ti-15Mo METASTABLE β-Ti ALLOY AT ELEVATED TEMPERATURES

**P. Strunz[1], V. Ryukhtin[1], P. Zháňal[2,3], P. Harcuba[2], J. Šmilauerová[2], U. Keiderling[4]**

*[1]Nuclear Physics Institute v.v.i. of the CAS, Department of Neutron Physics, 25068 Řež, Czech Republic*
*[2]Charles University, Mathematics and Physics Faculty, Department of Physics of Materials, Ke Karlovu 5, 12116 Prague, Czech Republic*
*[2]Research Centre Řež, Hlavní 130, 250 68 Řež, Czech Republic*
*[4]Helmholtz Zentrum Berlin for Materials and Energy, D-14109 Berlin, Germany*
*strunz@ujf.cas.cz*

Titanium alloys have a plenty of applications in industry and medicine [1] due to unique combination of high strength, low density and excellent biocompatibility. Ti-15Mo alloy is a metastable β-Ti alloy containing ω (hexagonal) and α (hcp) precipitates in β-phase matrix. Particular microstructure resulting from the heat treatment has a large impact on mechanical properties and thermal stability of the alloy. One of the techniques able to deliver bulk information on the precipitate evolution directly at elevated temperatures is Small-Angle Neutron Scattering (SANS). V4 SANS facility of HZB Berlin [2] was used for investigation of Ti-15Mo (wt.%) alloy. SANS data were acquired in-situ up to 600°C at three orientations of the single crystal sample – with <111>, <110> and <100> directions of β-phase parallel to the neutron beam. The rate of 1 K/min was used for the in-situ heating during SANS measurement. The orientation of the crystal in this case was <110> direction of the β-phase matrix parallel to the neutron beam.

Strongly anisotropic scattering pattern, moreover evolving with temperature increase, was detected. Observed 2D intensity distribution at temperatures 400-530 °C originated from isothermal prolate-spheroidal ω precipitates arranged on a simple cubic-like grid. When heating above 400 °C, the mean size and interparticle distance of ω particles gradually increased. Initially, volume fraction times scattering contrast of ω-phase increases up to 443 °C, and it then gradually decreases up to 530 °C.

In the temperature range 531-538 °C, both ω-phase ordered spheroids and a population of α plates is needed to fit the observed SANS patterns well. Fig. 1 (left side) shows an example with already well visible α-phase streaks (near the edge of the detector), but with still present major part of the scattering (including interparticle-interference maxima near the detector centre) originating from the ω spheroids.

Above 538 °C, no more scattering from ω particles exists; nevertheless, the scattering coming from the population of α plates remains. Moreover, a second type of streaks appears, which has orientation clearly distinguished from the first ones caused by α plates. The two types of streaks in the scattering pattern can be seen in Fig. 1, right side. The cause of the second type of streaks can be a formation of a second population of α plates which has orientation clearly distinguished from the first population of α plates. The data were evaluated and interpreted using this hypothesis.

In the initial stage after their appearance, the scattering intensity from both α-phase populations gradually increases on temperature increase. Both α phase populations

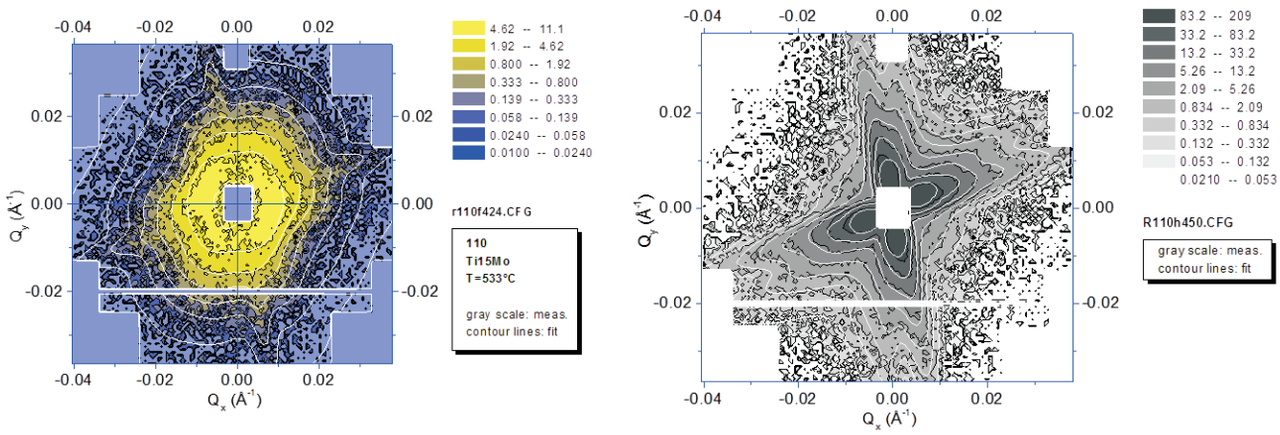


**Figure 1**. Left: SANS pattern measured in ω–α phases transition region (T = 533 °C). Right: SANS pattern in α-phase region (T = 559 °C). For both cases $[110]_\beta$, is perpendicular to the figure plane. Color or gray scale depicts measured data, white contour lines show the fit to the data.

remain present up to the highest measured temperature of 608 °C.

It was also found that the observed orientation of both populations of α plates do not fit the standard orientation [3]. The streaks in SANS patterns are oriented parallel to $[\bar{4}45]_\beta$ or $[\bar{3}34]_\beta$ crystallographic directions for the first population of α plates, and to $[\bar{4}43]_\beta$ or $[554]_\beta$ for the second population of α plates, or in an orientation very similar to these crystallographic directions. Microstructure of α precipitates was not changed during cooling down from 608 °C to the room temperature.

Morphology (size and distance) of ω particles and their evolution were also deduced from the SANS data using 3D modelling and fitting of the 2D SANS data by NOC software [4].

1. J. Disegi, Implant Materials. Wrought Titanium –15% Molybdenum (Synthes, 2009).
2. U. Keiderling, C. Jafta, *Journal of large-scale research facilities* **2**, 97 (2016), 97.
3. G. Lütjering and J.C. Williams. Titanium (Engineering Materials and Processes). Berlin, Heidelberg: Springer-Verlag, 2007, p.31.
4. P. Strunz, J.Šmilauerová, M. Janeček, J. Stráský, P. Harcuba, J. Pospíšil, J. Veselý, P. Lindner, L. Karge, *Philosophical Magazine* **98** (2018) 3086-3108, https://doi.org/10.1080/14786435.2018.1520403.

*V. Ryukhtin and P. Strunz acknowledge partial support from the long-term conceptual development project RVO 61389005 of the Nuclear Physics Institute of the Czech Academy of Sciences and from the Czech Academy of Sciences in the frame of the program "Strategie AV21, No. 23".*

L20

# STUDIES OF PRECIPITATION IN ENGINEERING MATERIALS USING SMALL-ANGLE NEUTRON SCATTERING

**V. Ryukhtin[1], P. Strunz[1], A. B. Yildiz[2], P. Beran[1,3], S. Bakardjieva[4]**

[1]*Nuclear Physics Institute ASCR, v.v.i., Řež, Czech Republic*
[2]*Dep. of Materials Science and Eng., KTH Royal Institute of Technology, SE-100 44 Stockholm, Sweden*
[3]*ESS ERIC, Lund, Sweden*
[4]*Institute of Inorganic Chemistry CAS, 250 68 Husinec-Řež, Czech Republic*
*ryukhtin@ujf.cas.cz*

Precipitations microstructure in alloys is strongly connected with their physical properties such as hardness or ductility. Usually, conventional methods of electron microscopy are used for assessing the morphological characteristics of the precipitates. Nevertheless, in some cases, the small-angle neutron scattering (SANS) technique can be more efficient due to its unique abilities. Here, we would like to demonstrate few examples.

Influence of copper on precipitations during aging was studied in medium carbon spring steel [1]. It was found that alloying by copper significantly improves material characteristics (increases yield stress, increases corrosion resistance, causes "self-healing" of ultrafine cracks). Magnetic SANS (MSANS) was used for accurate characterization of nanosized copper particles nucleated by tempering at 400-500°C. In this case, MSANS was very effective and, potentially, it can be used for in-situ study of Cu precipitation kinetics in similar alloys.

Another example is investigation of sintering of composite tungsten (W) grains in cobalt (Co) binder. In vanadium-doped tungsten carbide (WC) - Co composite material system, in-situ and ex-situ SANS and ultra-small-angle neutron scattering (USANS) experiments helped to explain how additions of vanadium (V) affect the nano- and microstructure during sintering, and result in smaller WC grains [2]. Whereas SANS quantified the nano-scale interfacial layers responsible of grain coarsening inhibition, USANS was applied to study microstructural refinement.

SANS was also applied for the investigation of the Sc-doped $TiO_2$ anatase as material for photocatalysis [3]. Growth of Sc precipitations was observed with increasing aging temperature due to its expelling from anatase crystallites. It was showed by SANS with agreement of jointly refined neutron and X-rays diffraction data, that entire scandium content at aging temperature above 800°C was driven out of grains and formed particles at $TiO_2$ grain boundaries.

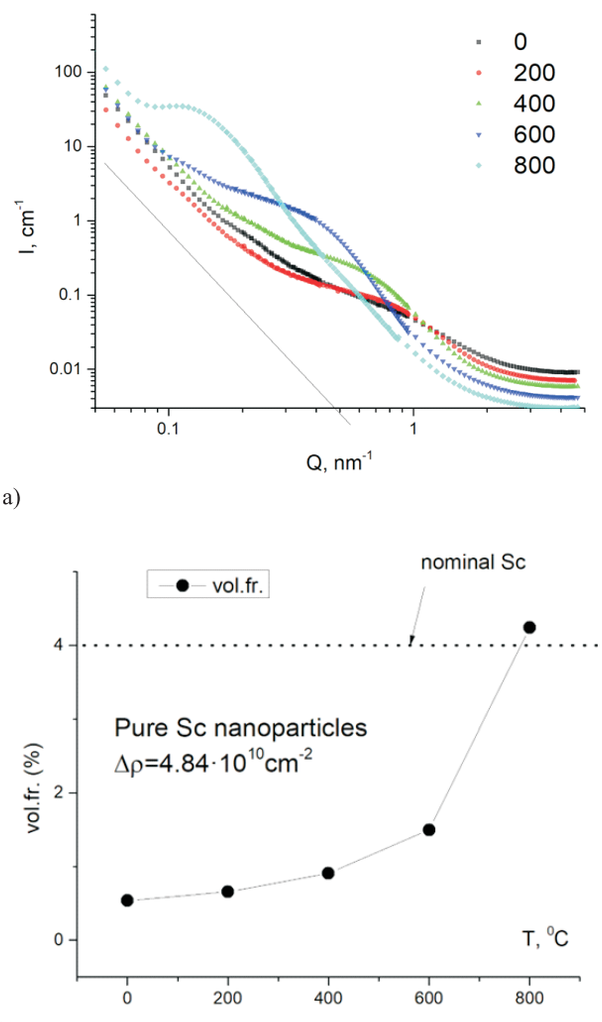


**Figure 1**. SANS data of Sc-doped $TiO_2$ aged at temperatures (a) and fitted volume fraction of Sc precipitates from corresponded SANS data (b)

1. A. Gokhman, Z. Nový, P. Salvetr, V. Ryukhtin, P. Strunz, P. Motyčka, J. Zmeko, J. Kotous, *Materials,* **14**, (2001) 1445.
2. A. B. Yildiz, J. Weidow, V. Ryukhtin, S. Norgrend, G. Wahnström, P. Hedström, *Scripta Mat.* **173**, (2019) 106-109.
3. S. Bakardjieva, J. Mares, E. Koci, J. Tolasz, R. Fajgar, V. Ryukhtin, M. Klementova, Š. Michna, H. Bibova, R. Holmestad, R. Titorenkova, M. Caplovicova, *Nanomaterials*, **12**, (2022) 750.

*V. Ryukhtin and P. Strunz acknowledge partial support from the long-term conceptual development project RVO 61389005 of the Nuclear Physics Institute of the Czech Academy of Sciences and from the Czech Academy of Sciences in the frame of the program "Strategie AV21, No. 23". USANS measurements were conducted at CANAM infrastructure supported by MŠMT projects LM2015056 and LM2018120. V. Ryukhtin acknowledges beamtime at V4 SANS facility granted by HZB.*

L21

# ALSA – AUTOMATIC LAUE SAMPLE ALIGNER

**Petr Čermák[1], Damián Wałoszek[1], Kryštof Višňák[1], Ivo Gold[1,2]**

*[1]Charles University (MGML, Dep. Condensed Matter Physics), 12116 Prague 2, Czechia*
*[2]Institute of Physics of the Czech Academy of Science, 182 21 Prague 8, Czechia*
*petr.cermak@matfyz.cuni.cz*

While the evolution of the synchrotron brightness still follows exponential Moore's law [1], the time-integrated flux of the neutron sources reached its maximum 50 years ago at ILL, and it will be only slightly surpassed by the upcoming ESS [2]. Therefore, scientists have been trying for decades to optimize optics, measurement strategies or build multi-detector systems to take advantage of every possible neutron to measure weaker fluctuations on smaller samples.

Another approach is to increase the sample size for inelastic neutron experiments by co-aligning more single crystals. This process is very time-consuming and often not very precise (e.g. [3]). The goal of ALSA (Fig. 1) is to change it. It will automatize the co-alignment process by using a state-of-the-art X-Ray Laue diffractometer (*Photonic Science*), robotized manipulators (*Mecademic Meca500*), real-time camera recognition (*Basler*), and bespoke neural network software for crystal placing and Laue pattern solving. The device ALSA will be a true game-changer in the field of inelastic neutron scattering because it will drastically speed up sample preparation.

To glue small crystals as close to each other as possible, we have developed an online algorithm for irregular polygon stacking; a series of benchmarking tests proved, that it is the most efficient online algorithm available. In this presentation, we will focus on the hardware and software design of the device, and we will discuss possibilities of using neutral networks for Laue patterns solving.

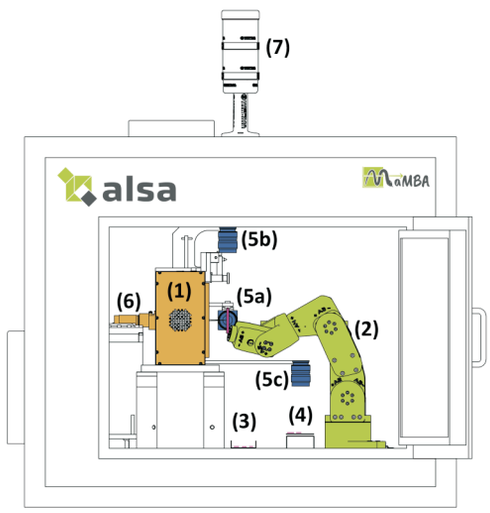


**Figure 1**. Sideview of the ALSA device. (1) Photonic Science CCD back reflection Laue X-ray Detector, (2) Mecademic Meca500 six-axis industrial robot arm, (3) Samples waiting for alignment, (4) Aluminium plate with aligned samples, (5a, b, c) CCD cameras for sample shape determination and alignment, (6) High brilliance X-ray generator, (7) Signalling for X-Ray source.

1. Assoufid, L. and Graafsma, H. *MRS Bulletin* **42**, (2017), 418-423. doi:10.1557/mrs.2017.118.
2. Rønnow H.M. et al. Swiss Academies Reports 16, (2021), 7. doi:10.5281/zenodo.4637660.
3. Duan, C. Et al. Nature 600, (2021), 636–640. doi:10.1038/s41586-021-04151-5.

L22

# NEUTRON DIFFRACTION STUDY OF RESIDUAL STRESSES IN ENGINEERING COMPONENTS FORMED VIA ADDITIVE MANUFACTURING

**G. Németh[1], R. Kocich[2], M. Benč[2]**

*[1]Nuclear Physics Institute, 25068 Řež near Prague, Czech Republic*
*[2]Faculty of Materials Science and Technology, VŠB-Technical University of Ostrava, 708 00 Ostrava, Czech Republic*

Additive manufacturing (AM) technique enables us to build three-dimensional complex engineering parts without the use of expensive tools such as casting molds, dies or punches. However, large thermal gradients appear during the process [1] which may give rise to anisotropy of the structure and consequently to residual stresses (RS). Neutron diffraction (ND) strain scanning is a powerful technique to study the distribution of RS non-destructively. Two samples from ASI 316 steel, prepared by AM, were subjected to linear ND strain scans with three mutually perpendicular orientations of the diffraction vector. In the case of the complex shape-sample 1 (CS) (Figure 1.), the tip was scanned. In the case of a cylinder-sample 2 (with diameter 10.25 mm after additional swaging), four scan-lines mutually rotated by 45°, lying in the cross section of the cylinder, were applied (Figure 2.).

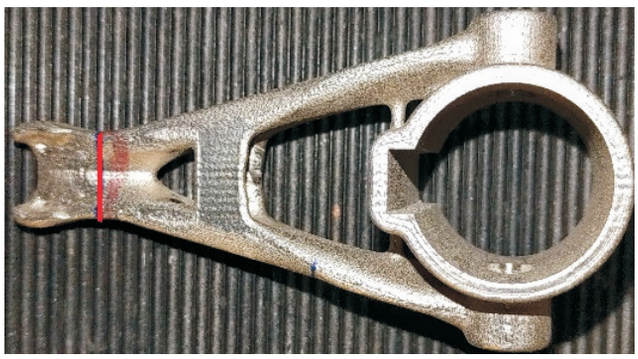

**Figure 1.** Complex shape sample 1 and Figure 2. Cylinder and the scanned line (red).

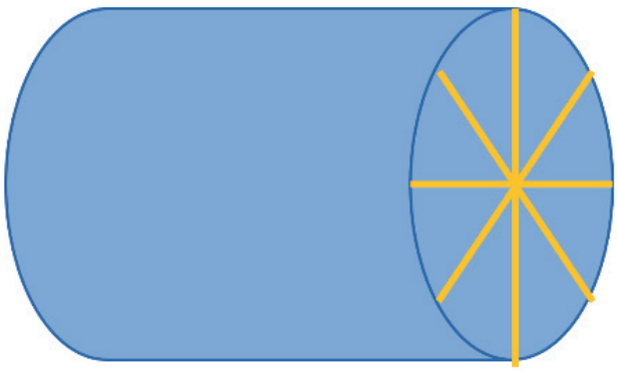

**Figure 2.** Cylinder and the scanned lines

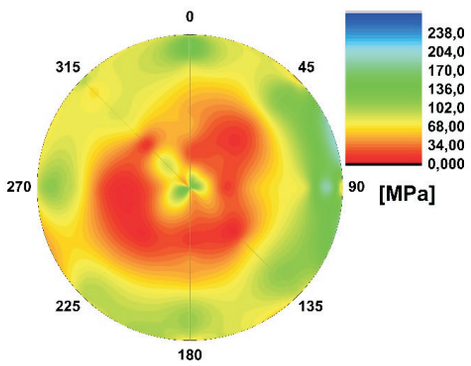


**Figure 3.** VM stress distribution in the cross section of cylinder-sample 2

However, the measured data had to be corrected due to pseudo-strains caused by beam attenuation and by partial immersion of sampling volume in the sample near the edges [2]. Since the stress-free reference was unavailable, the absolute stress differences and then the Von Mises (VM) equivalent stresses were evaluated from the reconstructed two theta distributions [3]. The VM stresses provide valuable information about the overall RS state of the measured regions. According to this, the tip of the CS sample exhibits the largest RS 3-5 mm beyond the edges, where the arms connect to the tip. The maximum VM stress in these regions were 100-120 MPa. In the case of sample 2, RS distribution maxima are mainly located near surface regions (Figure 3.) however, the center region also shows larger RS. The distribution roughly maintains the axial symmetry of sample 2. Areas with increased VM stresses are closer to the yield point.

1. T. D. Ngo, A. Kashani, G. Imbalzano, K. T. Q. Nguyen, D. Hui, *Composites Part B-Engineering* 143 (2018) 172-196.

2. J. Šaroun, J. Rebelo-Kornmeier, J. Gibmeier, M. Hofmann, *Physica B: Condensed Matter* 551 (2018) 468-471.

3. P. Strunz, R. Kocich, D. Canelo-Yubero, A. Macháčková, P. Beran, L. Krátká, *Materials* 13(12) (2020) 2869.

L23

## EFFICIENT MODELING OF SINGLE CRYSTAL DIFFUSE SCATTERING

**J. Kulda**

*Institut Laue-Langevin, BP 156, 380042 Grenoble Cedex, France*
*kulda@ill.fr*

Many modern materials exhibit a considerable portion of structural disorder, playing a key role in their functionalities. Routine crystallographic structure solutions based on positions and integrated intensities of Bragg peaks only reveal their average structure. In order to access the details of local atomic arrangements and their short-range correlations one has to study the shape of the Bragg lines and the diffuse scattering below and between them.

Unfortunately there does not exist any direct procedure permitting to extract such information from the observed diffuse intensities. The only way is to compare modelbased calculated intensities with the observed ones. The progress in computing techniques in last decades permits to produce realistic models of crystalline lattices on nanometer scale by a variety of approaches ranging from ab initio DFT methods via molecular dynamics (MD) to phase-field models based on classical phenomenology (Landau formalism). Alternatively, one may approach the problem by reverse Monte-Carlo (RMC) modelling the displacement pattern in a supercell without making any assumptions on its origin.

With this progress in place the bottleneck has shifted from calculating supercell models with adequate displacement patterns to generating the corresponding diffuse scattering distributions in reciprocal space. The principal issue being the fact that scattering amplitudes from a lattice with displaced atoms cannot be summed up using fast Fourier transform algorithms (FFT) because of the displacement phase factor exp(-i$\boldsymbol{QR}$) being $\boldsymbol{Q}$-dependent. For this reason many efforts in recent years have been restricted to simple models on small supercells, which made the direct (naive) summation of the Fourier series viable [1,2], or to more involved models and RMC analysis of the pair distribution functions (PDF) [3-5], where the summation problém is reduced to a single dimension.

In this presentation we will introduce a novel approach [6] permitting to address this problem and to generate diffracted intensities from model supercells containing $10^6$ atoms on seconds time scale. Even the computation of dynamic scattering functions S($\boldsymbol{Q}$, ω) necessitating to handle "movie" sequences of thousands of frames for the frequency transform can be addressed in an interactive manner.

1. Welberry T.R., Butler B.: J. Appl. Cryst. 27 (1994) 205-231.
2. Neder R.B., Proffen Th.: Diffuse Scattering and Defect Structure Simulations: A cook book using the program DISCUS, Oxford, 2008; DOI:10.1093/acprof:oso/9780199233694.001.0001.
3. McGreevy R.L., J. Phys.: Condens. Matter 13 (2001) R877–R913.
4. Proffen Th. et al., Z. Kristallogr. 218 (2003) 132–143.
5. Eremenko M. et al., Nature Comm. 10 (2019) 2728.
6. Kulda J., Acta Cryst. A (2022) in preparation.

# Session VI - Synchrotron radiation, Tuesday, June 21

L24

## MICRO- AND NANO-SCALE 3D IMAGING AT SYNCHROTRONS

**R. Mokso[1,2]**

*[1]Technical University of Denmark, 2800 Lyngby, Denmark*
*[2]MAX IV Laboratory, Fotonngatan 1, Lund, Sweden*
*rajmo@dtu.dk*

Shortly after the first diffraction limited synchrotron source was built in Sweden, the ESRF upgrade took place and with this the second modern storage ring entered operation in Europe. The next one being the Swiss Light Source in 2025 we can ask the question what are the implications of the new technology for X-ray imaging. I will approach this question from various viewpoints including a discussion about the opportunities offered by the higher spatial coherence for nano and microtomography methods development. Through selected science cases I will attempt to indicate current trends in imaging methods development. Beside these trends in novel acquisition and reconstruction methods the weakest element in the workflow remains multidimensional image analysis, therefore I will conclude with commenting on this aspect of synchrotron imaging.

L25

# MHZ MICROSCOPY AT EUROPEAN XFEL

**P. Vagovič[1, 2], Pablo Villanueva Perez[3], T. Sato[2], V. Bellucci[2], S. Birsteinova[2], H. J. Kirkwood[2], G. Giovanetti[2], M. Stupar[2], N. Jardon[2], J. Szuba[2], K. Wrona[2], R. Bean[2], R. Letrun[2], J. Koliyadu[2], R. Graceffa[2], Antonio Bonucci[2], L. Adriano[2], M.C. Zdora[4], J. Uličný[5], P. F. Garcia-Moreno[6,7], S. Hall[3], C.D. Ohl[8], W. Yashiro[9], A. Korsunsky[10], H. Soyama[11], A. P. Mancuso[2,12], A. Meents[1] , H. Chapman[1]**

*[1]Center for Free-Electron Laser Science (CFEL), DESY, Hamburg, Germany, [2]European XFEL GmbH, Hamburg, Germany, [3] Lund University, Sweden, [4]Paul Scherrer Institute, 5232 Villigen PSI, Switzerland, [5] Faculty of Science, Department of Biophysics, P. J. Šafárik University,Slovakia, [6]Department of Chemistry and Physics, Institute of Applied Materials, Helmholtz Centre Berlin, Hahn-Meitner-Platz 1, Berlin 14109, Germany, [7]Institute of Materials Science and Technologies, Technical University Berlin, Hardenbergstr. 60, Berlin 10623, Germany, [8]Faculty of Natural Sciences, Institute for Physics, Otto-von-Guericke-University Magdeburg, Universitätsplatz 2, 39016 Magdeburg, Germany,[9]International Center for Synchrotron Radiation Innovation Smart (SRIS), Tohoku University, [10]Department of Engineering Science, University of Oxford, Parks Road, Oxford, Oxfordshire, OX1 3PJ, United Kingdom, [11]Finemechanics Department, Tohoku University, 6-6-01 Aoba, Aramaki, Aoba-ku, Sendai 980-8579, Japan, [12]La Trobe Institute for Molecular Science, La Trobe University, Melbourne, Victoria 3086, Australia*
**patrik.vagovic@cfel.de*

First MHz rate fourth generation hard X-ray XFEL source European XFEL [1] provide unique opportunity for characterisation of stochastic dynamics occurring in various systems either naturally or response is stimulated by an external force. High repetition rate of pulses (up to 4.5 MHz) together with high flux per pulse allow to record projected X-ray radiograms of dynamic samples and image more then million frames per second with high spatio-temporal resolution. Each such frame is illuminated using ultrashort exposure (fs scale) given by the X-ray pulse duration providing "frozen in time" snapshots of stochastic phenomena. This enable to film fast stochastic processes individual realisations in slow smooth motion. Experimental configuration of projection X-ray radiography is shown on Fig.1. Moreover, EuXFEL SASE1 undulator generate X-ray pulses with three orders higher number of photons per pulse ($10^{12}$ photons) as compared to synchrotrons reaching hard X-ray range up to 24keV with ~20eV bandwidth. This unique performance allows for implementation of X-ray beam splitting schemes of multiprotection microscopy to obtain 3D snapshots per single pulse of dynamic objects sampled at MHz rate. We will present applications of recently developed MHz XFEL projection X-ray microscopy [2] applied for study of industrially relevant fluidic system behaving stochastically and we will present experimental results from recent characterisation of multi-projection MHz X-ray which is being developed under EIC-Pathfinder MHz-Tomoscopy project at SPB/SFX instrument [3].

1. W. Decking *et al.*, Nature Photonics **14**, 391–397 (2020).
2. P. Vagovič, et al., Optica 6, 1106-1109 (2019).
3. A. P. Mancuso *et al.*, J. Synchrotron Rad., **26**, 660–676 (2019).

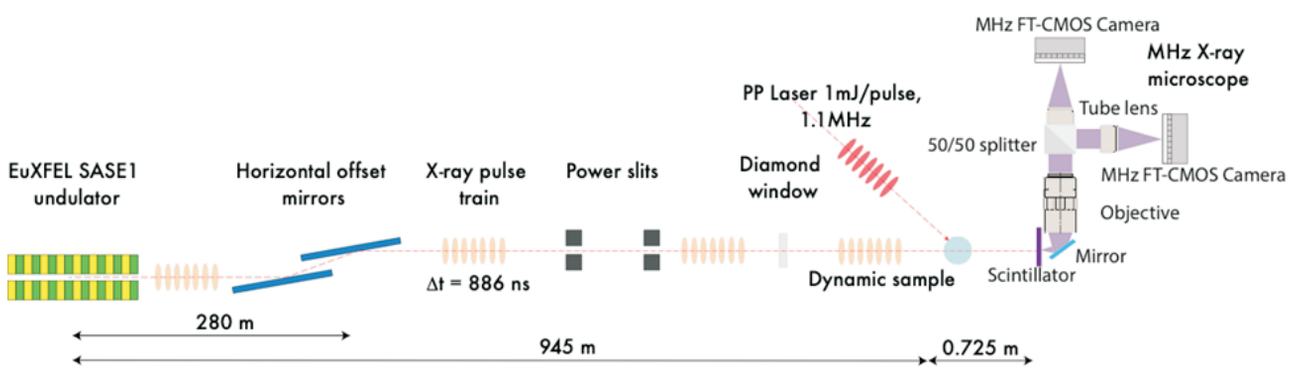


**Figure 1.** Experimental arrangement of MHz X-ray projection Microscopy at European XFEL SPB/SFX instrument.

L26

# STRAIN MAPPING USING HIGH-ENERGY X-RAY DIFFRACTION

**J. Bednarčík[1,2]**

[1]*Institute of Experimental Physics, Slovak Academy of Science, Watsonova 47, 040 01 Košice, SR*
[2]*P.J. Šafárik University in Košice, Institute of Physics, Park Angelinum 9, 041 54 Košice, SR*
*jozef.bednarcik@upjs.sk*

Zr-based bulk metallic glasses (BMGs) exhibit extremely interesting mechanical properties such as superior strength (~2 GPa), high elastic strain limit (~2%), relatively low Young's modulus (50–100 GPa), high impact and fracture toughness, high corrosion resistance, excellent formability in the supercooled liquid region, wear resistance and biocompatibility [1]. Because of these unique properties Zr-based BMGs are emerging as a new class of metallic materials for biomedical, structural, and functional use.

Indentation techniques are used in many scientific fields ranging from biology to materials science and nowadays, they are at the heart of material nanoscience. In recent years the use of synchrotron radiation (SR) was increasing, and many diffraction techniques appears to be more desirable [2]. High-energy X-ray diffraction provides an effective method to observe the changes at the atomic level caused by mechanical treatment. Therefore, high-energy X-ray diffraction can be used to map the strain fields around an indent. Correlating the mechanical properties with the structure on the atomic and mesoscopic scale is a topic that promises a deeper understanding of the relevant processes during deformation. While the physics in crystalline materials is understood by large, the situation in case of amorphous solids is not advanced yet. Therefore, the connection of an indentation and diffraction gives a powerful tool for the delineation of composition-structure-property relationships and hence for material discovery and optimization.

In this contribution we present mapping of strain fields of indented Zr-based BMG using high-energy micro-diffraction technique. High-resolution spatially resolved scans in the vicinity of indents were done both ex-situ and in-situ.

1. Q. Chen, L. Liu, S. M. Zhang, *Front. Mater. Sci China*, **4**, (2010), 34.
2. M. K. Khan, M. E. Fitzpatrick, S. V. Hainsworth, A. D. Evans, L. Edwards, *Acta Mater.*, **59**, (2011), 7508.

**Information**

**Peter Oberta**

ESRF

**Petr Mikulík**

ESUO

## Session VII - Wednesday, June 22

**Obituaries**

**Radomír Kužel**
Vzpomínka na Václava Janovce
Obituary - Václav Janovec

**Pavlína Řezáčová**
Vzpomínka na Juraje Sedláčka
Obituary - Juraj Sedláček

**Commercial presentations**

Petr Marvan
(*Panalytical*)
Panalytical 2022

Boris Míč
(*MTM*)
Bruker 2022

# Session VIII - Thursday, June 23

## L27

### PAIRED REFINEMENT AND CRYSTAL ANISOTROPY

**P. Kolenko[1,2], P. Mikulecký[2], P.N. Pham[2], M. Malý[1,2], B. Schneider[2]**

*[1]Czech Technical University in Prague, Břehová 7, 115 19 Prague*
*[2]Institute of Biotechnology CAS, v.v.i., Průmyslová 595, 252 50 Vestec*
*petr.kolenko@fjfi.cvut.cz*

Anisotropy in diffraction qualities of crystals may represent a serious threat to the structure determination process. When the differences in various directions of the reciprocal space exceed the range of 0.5Å resolution, problems with phasing may arise, and the structure refinement process is frequently unstable. Such difficulties also appear for structures with high resolution. Although a limited number of tools for the data analysis is available, the current praxis is not standardized and needs thorough revision.

We analyzed diffraction data from a crystal of an engineered protein binder with a promising application as a protein therapeutics [1]. The protein crystallized in space group $I4_122$. The initial diffraction data quality indicators of the data processed the standard way suggested the high-resolution diffraction limit at 2.9 Å. However, a combination of data processed with *STARANISO* [2] and paired refinement with *PAIREF* [3] showed a possible extension of the diffraction limit to 2.6 Å in the direction along the $l$ axis. Calculated electron density display moderate improvement and easier interpretation for some side chains.

1. P. N. Pham, M. Huličiak, L. Biedermannová, J. Černý, T. Charnavets, G. Fuertes, Š. Herynek, L. Kolářová, P. Kolenko, J. Pavlíček, J. Zahradník, P. Mikulecký, B. Schneider, *Viruses*, **13**, (2021), 190.
2. I. J. Tickle, C. Flensburg, P. Keller, W. Paciorek, A. Sharff, C. Vonrhein, G. Bricogne. (2018). STARANISO (http://staraniso.globalphasing.org/cgi-bin/staraniso.cgi). Cambridge, United Kingdom: Global Phasing Ltd.
3. M. Malý, K. Diederichs, J. Dohnálek, P. Kolenko, *IUCrJ*, **7**, (2020), 681-692.

*This work was supported by MEYS CR (projects CAAS – CZ.02.1.01/0.0/0.0/16_019/0000778) from the ERDF fund and by the GA CTU in Prague (SGS22/114/OHK4/2T/14).*

## L28

### STRUCTURE DATABASE OF ORGANIC POLYMERS AND THEIR INTERACTIONS WITH BIOMACROMOLECULES

**J. Hašek[1], M. Steinhart[2], T. Koval[1], P. Kolenko[1,3], T. Skálová[1], J. Brus[2], J. Dohnálek[1]**

*[1]Institute of Biotechnology, Academy of Sciences, Průmyslová 595, Vestec*
*[2]Institute of Macromolecular Chemistry, Academy of Sciences, Heyrovského nám.2, Praha 6*
*[3]Faculty of Nuclear Sciences and Physical Engineering CTU, Břehová 7, Praha 1*
*hasekjh@seznam.cz*

***The Cambridge Structure Database of Organic and Organo-Metalic Compounds (CSD*) [1]** in its 2022 version) can be searched by the keyword "polymer". It results in a large number of *organo-metalic polymers*, i.e. the crystalline structures in which organic molecules are inter-connected by metal bridges to form the "infinite" 1D, 2D, or 3D networks passing through the whole crystalline blocks. These crystals are typically regular and the corresponding clear diffraction pattern allows reliable and precise structure determination required for deposition into the CSD.

However, in the case of the *classical organic polymers*, the preparation of the high quality crystalline samples is extremely difficult namely because of polydispersity and extremely long times required to achieve the equilibrium state. Diffraction quality is thus often very low. The experimental structures are often inaccurate and require theoretical re-modelling. Roughly, a half of the structure determinations do not satisfy requirement for deposition in the CSD. Some synthetic or natural polymers can be found also in the ***Crystallography Open Database [2]***. However, about half of the published structures are not present in these databases**.** This is the reason why the ***Polymer Structure Database (POLYBASE-2011)*** collecting all available organic polymers **[3]** was prepared. The new ***POLYBASE-2022*** version will be completely re-cured now.

Hydrophilic polymers are often used as precipitants for crystallization of bio-macromolecules. It is the reason why the ***Database of Protein-Polymer Interactions (DPPI-2011)*** **[3]** was formed. The contemporary ***DPPI-2022 version*** contains 3667 PDB structures of bio-macromolecules (proteins and nucleic acids). The structures collected from the ***RCSB server*** **[4]** experimentally confirm complexation of poly(ethyleneglycol) chains (at least four monomers in length) at the protein surface.

Because many of these proteins are complexed with more polymer chains, the ***DPPI-2022*** contains several thousand experimentally verified interactions of hydrophilic organic polymers bound directly on the surface of protein molecules. Visual inspection of the ***DPPI-2022*** provides surprisingly high number of various types of protein-polymer interactions. Classification of these interactions is a useful background for explaining the success of poly(ethyleneglycol)-type polymers in many economically important applications in the industry, science, medicine and pharmaceutics.

The ***Polymer Structure Database (POLYBASE)*** and the ***Database of Protein-Polymer Interactions (DPPI)*** are presently updated and will be available on request in their new versions by the end of 2022.

*The research was supported by the project CZ.02.1.01/0.0/0.0/15_003/0000447 from the ERDF.*

1. Groom, C. R., Bruno, I. J., Lightfoot M. P. and. Ward, S. C. *Acta Cryst.* (2016) **B72**, 171-179. *DOI: 10.1107/S2052520616003954*
2. Quirós, M., Graţulis, S., Girdzijauskaitë, S., Merkys, A. & Vaitkus, A. *Journal of Cheminformatics,* (2018) ***10*** (23), 1-17. *DOI:* 10.1186/s13321-018-0279-6
3. Hašek, J., *Z. Kristallogr.* (2011) **28**, 475-480. *DOI: 10.1524/9783486991321-077.*
4. wwPDB consortium Protein Data Bank: *Nucleic Acids Research, (2018) **47**, D520-D528. DOI:* 10.1093/nar/gky949.

**L29**

# THE UNIQUE STRUCTURE OF THE CELL WALL BINDING DOMAIN OF PHAGE ENDOLYSIN

**Ľubica Urbániková[1], Martina Gerová[1], Jiří Brynda[2], Július Košťan[3], Nora Halgašová[1] and Gabriela Bukovská[1]**

*[1]Institute of Molecular Biology SAS, Dubravska cesta 21, Bratislava, Slovak Republic*
*[2]Institute of Organic Chemistry and Biochemistry CAS, Flemmingovo namesti 542/2, Prague, c*
*[3]Max F. Perutz Laboratories, University of Vienna, Vienna, Austria*
*lubica.urbanikova@savba.sk*

Bacteriophage-encoded endolysins, enzymes showing bacteriolytic activity, are of growing interest for their applications as enzybiotics in veterinary and/or human medicines and various field of biotechnology, e.g. food safety. Bacteriophage BFK20 is a lytic phage of *Brevibacterium flavum* CCM 251 (gram positive corynebacteria), industrial producer of L-lysine. The genome of the bacteriophage BFK20 has been sequenced and analyzed (EMBL accession no. AJ278322) [1]. The gene product of ORF24´ was identified as endolysin gp24´ (UniProt ID Q9MBI0), an enzyme necessary for cell lysis and release of mature phage particles from the infected bacterial cells. The protein is composed of two domains, a catalytic domain exhibiting N-acetylmuramoyl-L-alanine amidase activity, and a cell wall binding domain (gp24BD), which are connected by a proline-rich linker. The individual domains were cloned separately and the cell wall binding capability of the C-terminal region (81 aa) was proved experimentally [2]. The whole protein as well as individual domains were crystallized, but only crystals of individual gp24BD were obtained. Needle shaped crystals belonging to hexagonal space group P622 were grown overnight. Crystals diffracted to 3.2Å resolution using synchrotron source of radiation, but were twinned and not suitable for structure determination. Later, the crystals recrystallized directly in the crystallization drop. The newly obtained crystals diffracted to 1.4Å resolution using home diffractometer. They belonged to tetragonal space group $P42_12$. The same protein samples stored for several weeks at 4 °C crystallized directly in the form of tetragonal crystals. Tetragonal crystals were dissolved and the protein analysis showed random proteolysis and protein shortening by 8 amino acid residues.

The 1.4Å resolution data set was used for structure solution by the direct method using the program ARCIMBOLDO-LITE [3]. The overall structure revealed very loose bundle of three α-helices. The asymmetric unit contains one protein molecule. The crystal symmetry gives four molecules in the unit cell forming very compact tetramer. Based on the PISA prediction the tetramer is stable also in solution. The oligomers have also been experimentally detected, thus one can speculate about the oligomeric state as biologically active unit. Closer inspection revealed the amphipathic nature of the helices and the tetrameric coiled-coil structure. An electron density was found in the tetramer cavity to which metal and chlorine ions were modelled. The coiled-coil structure is interrupted by a loop (one from each molecule). Between each two neighbour molecules a molecule of glycerol was identified sitting mostly at the loop. Molecular docking experiments performed using a rhamnose molecule supported the idea that glycerol maps the binding site which may be large enough to accommodate a substrate composed of several monomers. The gp24BD is unrelated to any of the known cell wall binding domains of phage endolysins by the amino acid sequence and also by the structure; this is the first evidence of the endolysin binding domain showing the coiled-coil structure. BFK20 phage endolysin binds to the cell walls of corynebacteria in a highly specific manner, unfortunately, the specific composition and structure of their cell walls and the exact peptidoglycan substrate of gp24BD have not yet been determined. To answer the questions concerning the functioning of the binding do-

main and the whole endolysin, further work is needed, especially the structure of the whole molecule and the complexes with possible ligands should be solved.

1. G. Bukovska, L. Klucar, C. Vlcek, J. Adamovic, J. Turna, J. Timko, *Virology*, **348**, (2006), 57-71.
2. M. Gerova, N. Halgasova, J. Ugorcakova, G. Bukovska, FEMS *Microbiol Lett.*, **321**, (2011), 83-91.
3. D. Rodríguez, M. Sammito, K. Meindl, I. M. de Ilarduya, M. Potratz, G. M. Sheldrick and I. Usón, *Acta Crystallogr. D*, **D68**, (2012), 336-343.

## Session IX - Thursday, June 23

### L30

## XRPD AS A POWERFUL TOOL FOR STUDY OF PAINTED ARTWORKS

**Silvie Švarcová[1], Petr Bezdička[1], Eva Kočí[1], Janka Hradilová[2], David Hradil[1,2]**

[1]*Institute of Inorganic Chemistry of the Czech Academy of Sciences, ALMA Laboratory, Husinec-Řež 1001, 250 68 Husinec-Řež*
[2]*Academy of Fine Arts in Prague, ALMA Laboratory, U Akademie 4, 170 22 Prague 7 Czech Republic*

Laboratory X-ray powder diffraction is a very effective and non-destructive method for direct phase analysis of paint layers usually consisting of complicated mixtures of pigments, binders, dyes, fillers and/or degradation products. While a conventional Bragg-Brentano set-up allows direct non-invasive analysis of smaller painted objects, e.g. miniature portraits, a micro-diffraction mode plays a substantial role in the analysis of samples (usually smaller than 1 mm) taken from paintings. The application of mineralogical analysis for study of provenance and technology of late Gothic/early Renaissance painting materials as well as examples of uncovered degradation products will be presented. The methodological pros and cons will be also discussed.

### L31

## DETERMINATION OF STRUCTURE OF SMALL PARTICLES

**P. Roupcová[1,2], O. Schneeweiss[1], T. Sojková[1], N. Pizurová[1]**

[1]*Institute of Physics of Material ASCR, Zizkova 22, Brno 61662, Czech Republic*
[2]*CEITEC Brno University of Technology, Purkyňova 123, Brno 612 00, Czech Republic*
*roupcova@ipm.cz*

We are producing and studying Magnetic Nanoparticles (MNPs) due its applications in biomedicine. The suitable size have to be comparable to biological entities (cells, proteins, and genes), controllable transport of MNPs in human body (drug delivery). The purpose of our study is produce particles for their ability to generate heat when an AC magnetic field is applied (magnetic hyperthermia). In particular, magnetic hyperthermia therapy is based on the fact that some types of cancer cells are more sensitive at temperature 41-45 °C than the healthy cells and that the required heat can be produced by MNPs. Nowadays majority in-field investigations are based on *in vitro* or *in vivo* animal model, but also, in the case of iron oxide based MNPs, this approach is used at the clinical level [1]. The heating ability of MNPs is dependent on morphology, microstructural and magnetic properties of MNPs, but also related to the amplitude and frequency of an applied magnetic field. In that sense, during the last years the synthesis methods have been intensively developed in order to control particle size distribution, surface effects and the degree of interparticle interactions, so that magnetic properties favourable for particular application could be successfully tailored. Although the tons of studies was published, there is huge confusion and misunderstanding in terms such as particle, crystalline and grain size, which influenced the main characteristic – the magnetic properties. The confusion is originated by very wrong understanding of analytical method which are applied. For our purpose of magnetic hyperthermia, we are looking for magnetite $Fe_3O_4$ and maghemite $\gamma$-$Fe_2O_3$.

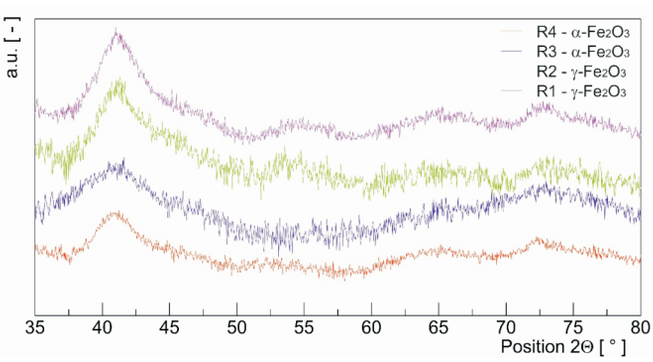


**Figure 1**. X-ray pattern of tiny particles.

The standard method of determination of phase composition by X-ray powder diffraction (XRD) is not very helpful (see Fig. 1) in our case it produced results on the range in between nano/amorphous which could be interpreted in any way or it could not be interpreted at all.

As well as the chemical composition obtain by EDS do not lead us to the correct results because the presence of S was overlooked in the samples R1 a R2. Eventually, the real structure and the chemical bound was determined by X-ray photoemission and Mössbauer spectroscopy which show as the presence of S and omit the existence $Fe^{2+}$ type of bound for all samples. The measurement of magnetic properties by PPMS was much more helpful. It distinguish Neél temperatures and Morine transition of hematite (R3 and R4) at 940K and at 250K and the same temperatures when maghemite transform to hematite (R1 and R2) [2,3].

This more advanced technique helps us to determine the phase composition as maghemite and hematite instead of magnetite and maghemite, we are expecting.

1. M.R. Horsman, J. Overgaard, *Clinical Oncology,* **19**, (2007) 418.
2. Cornell, R. M., Schwertmann, *The Iron Oxides*, Weinheim, Germany, WileyVCH, 2003, 664.
3. MORIN, F., *Physical Review*, **78** , (1950) 819.

*We acknowledge CzechNanoLab Research Infrastructure supported by MEYS CR (LM2018110).*

**L32**

# RTG TOMOGRAFIE – PRVNÍ ZKUšENOSTI

**J. Drahokoupil, A. Školáková, J. Pinc**

*Fyzikální ústav, Akademie věd České Republiky, Na Slovance 2, 182 21 Praha 8, Česká Republika*
*draho@fzu.cz*

Začátkem letošního roku byl ve Fyzikálním ústavu uveden do provozu rentgenový tomograf ZEISS Xradia 610 Versa, viz obr. 1. V příspěvku bych se rád věnoval mým prvním zkušenostem nejenom s tímto tomografem, ale i z tomografií obecně.

Princip měření je na tomto tomografu založen na kombinaci několika stovek až tisíců snímků s různou orientací vzorku kolem vertikální osy. Jako zdroj záření je zde použita wolframová anoda s volbou urychlovacího napětí od 30 do 160 kV. Čím je větší napětí tím má spektrum vlnových délek větší část v tvrdší části spektra, a tedy dochází obecně k menší absorpci záření ve vzorku. Pro modifikaci spektra je možné použít i sadu absorpčních filtrů které se umísťují na zdroj záření. Pro představu lze říci, že např. hořčíkové vzorky lze měřit až o tloušťce několika málo centimetrů, zatímco u vysokoentropických slitin obsahující těžší kovy narážíme na problémy u vzorků o tloušťce několika málo milimetrů. Náš tomograf je vybaven objektivy se zvětšením 4x a 20x a v ideálním případě dosahuje rozlišení až 200 nm na voxel. Dosažitelné rozlišení je dáno také velkostí a tvarem vzorku (vzdálenosti mezi studovanou oblastí na vzorku a zdrojem záření) a jeho absorpčními vlastnostmi, protože s větším

**Obrázek 2**. Řez vnitřní strukturou vlašského ořechu.

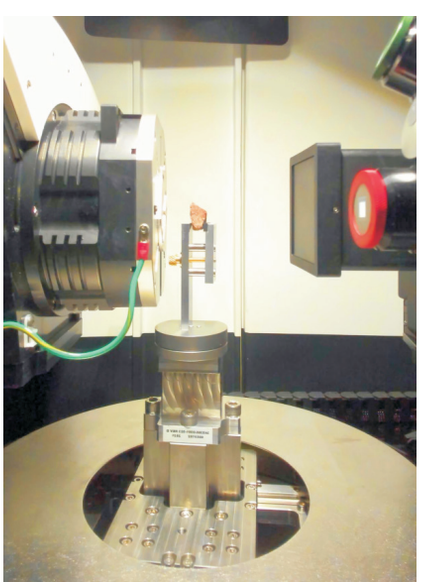

**Obrázek. 1**. Vnitřek tomografu Xradia 610 Versa.

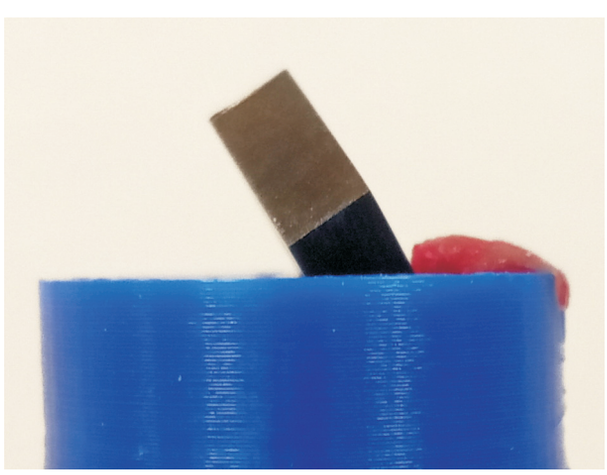

**Obrázek 3**. Držáček vzorku a vzorek vysokoentropické slitiny o rozměrech 5x5x3 mm.

zvětšením objektivu se na detektoru používá tenčí detekční vrstva a tvrdší složky záření se hůře detekují.

Z principu metody je zřejmé že velmi dobře pozorovatelné jsou póry, či kontrast mezi vzduchem a materiálem. Jako ilustrativní příklad zde uvádím řez strukturou vlašského ořechu, obr.2. Zajímavější je již pohled na mikrostrukturu vzorku obsahujícím fáze s menším absorpčním kontrastem, viz. např. dendritická mikrostruktura v lité vysokoentropické slitině na obr 4.

Praktické zkušenosti ukazují, že pokud umístíme vzorek velkými plochami rovnoběžně či kolmo na osu otáčení dochází k nežádoucím artefaktům ve výsledném 3D obraze. Je proto vhodné umístit vzorek pod úhlem. Jako dobrý nástroj se ukázala 3D tiskárna, na které si celkem snadno můžete vytvořit držáček na míru, viz obr 3. Další výhodou umístění běžného vzorku ve tvaru kvádru tak aby byl špičkou nahoru a v ose otáčení je ten, že můžete studovat silně absorbují vzorky bez nutnosti jejich řezání. Což je v duchu rtg tomografie jako nedestruktivní metody, která nám umožňuje nahlédnout do vnitřní struktury materiálu.

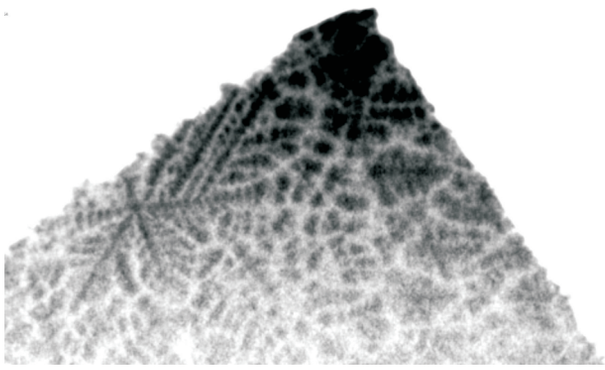

**Obrázek 4**. Řez špičkou vzorku z obr. 3. Velikost pixelu cca 1.5 μm.

**L33**

## PHASE TRANSFORMATIONS IN ZIRCONIUM AND TITANIUM ALLOYS

**Petr Doležal, Kristina Bartha, Anna Veverková, Josef Stráský**

*Faculty of Mathematics and Physics, Charles University, Ke Karlovu 5, 121 16 Praha 2*

The application potential of zirconium and titanium alloys can be seen in automobile, aircraft industry and in medicine as well. Thus, they are intensively studied mainly for their mechanical properties such as corrosion resistance, biocompatibility and specific strength. The mechanical properties are strongly influenced by the microstructure and phase composition of these alloys. Both pure zirconium and titanium can exist in two distinct crystal structures - alpha and beta phase. The beta phase is stable only at high temperatures above 700 °C (so-called beta-transus temperature), however the stability and coexistence of phases are strongly influenced by adding beta-stabilizing elements (stabilizes the beta phase) to the alloy, such as Mo or Nb. A higher content of the beta-stabilizers results in stable beta phase even at room temperature. The beta phase has a cubic body-centred unit cell. The alpha phase has a slightly distorted hexagonal close packed (hcp) structure where the most densely packed planes {110} of beta become the basal planes {0001} of alpha. In alloys with higher amount of the beta-stabilizing elements (~ 10-15 wt.%) a so-called omega phase may form. The omega phase has a hexagonal structure which is a result of a collapse of two-thirds of the {111} beta layers into one layer. The omega phase causes a brittleness of the material – its presence is undesirable. However, it forms in the alloys via martensitic transformation upon quenching from temperatures above beta-transus temperature and disappears upon heating to higher temperatures ~ 500 °C. Therefore, a complete understanding of phase transformations occurring upon heating in the alloys is necessary in order to choose an appropriate thermomechanical treatment to achieve the desired mechanical properties of the materials.

The presented study is focused on the investigation of phase content and stability in Zr12Nb, Zr15Nb and Ti15Mo alloys in temperature interval 30 – 800 °C. The high energy X-ray diffraction measurements were performed on polycrystalline bulk samples. In all three alloys the formation of the omega phase is observable which completely disappears above 500 °C and is followed by the formation of alpha phase. Although the sequence of the formation of phases is the same in both type of alloys, the mechanism and way of the formation of the omega phase is different.

L34

# METASTABLE ALUMINAS IN PLASMA SPRAYED COATINGS

**F. Lukáč[1,2], R. Mušálek[1], T. Tesař[1], Jan Medřický[1], Jonáš Dudík[1,3]**

[1]*Institute of Plasma Physics of the Czech Academy of Sciences, Za Slovankou 3, 182 00 Prague 8, Czech Republic*

[2]*Faculty of Mathematics and Physics, Charles University in Prague, V Holešovičkách 2, 180 00 Prague 8, Czech Republic*

[3]*Faculty of Nuclear Sciences and Physical Engineering, Czech Technical University in Prague, Trojanova 13, 120 01 Prague, Czech Republic*

*lukac@ipp.cas.cz*

Plasma sprayed coatings are materials with history of extreme thermal conditions. Very fine ceramic powder particles are carried by gas into high enthalpy plasma stream generated by plasma torch and molten droplets are projected onto cooled substrate. Solidified splats of added material are being layered and become a heat-sink for next incoming overheated liquid droplets. Therefore, interesting chemical compounds may be formed on the interface between splats despite high cooling rate. Moreover, recent advances in plasma technology enable injection of secondary material into the plasma torch by feeding of liquid suspension or solution. Using ethanol or water carriers influences already harsh conditions and new parameters of freedom for tailoring of coatings are available. Recently, we utilized hybrid plasma spraying process by simultaneously feeding the plasma stream with both powder and liquid feedstocks [1]. Very fine splats formed from liquid precursors may act as a cohesion improving agent for better durability of coatings.

Figure 1 shows an example of hybrid coating sprayed from $Al_2O_3$ powder and a water based $TiO_2$ suspension. At the interface of splats between alumina and titania, the newly formed $Al_2TiO_5$ phase was identified. However, only on the upper interfaces where the large alumina droplet interacted with already deposited miniature $TiO_2$ and the interdiffusion happened. Figure 2 shows the X-ray diffractogram of such coating. Major part of peaks intensity is in metastable phases δ and γ-$Al_2O_3$ whose defected spinel structure is still not well describable by Rietveld refinement fitting. Therefore, combination of standards of powder deposited coatings with XRF method is necessary to achieve accurate phase ratios

1. R. Musalek, T. Tesar, J. Dudik, J. Medricky, J. Cech, F. Lukac, *J Therm Spray Tech* (2022).

*Authors would like to acknowledge the financial support from the Grant Agency of Czech Republic by project 22-21478S.*

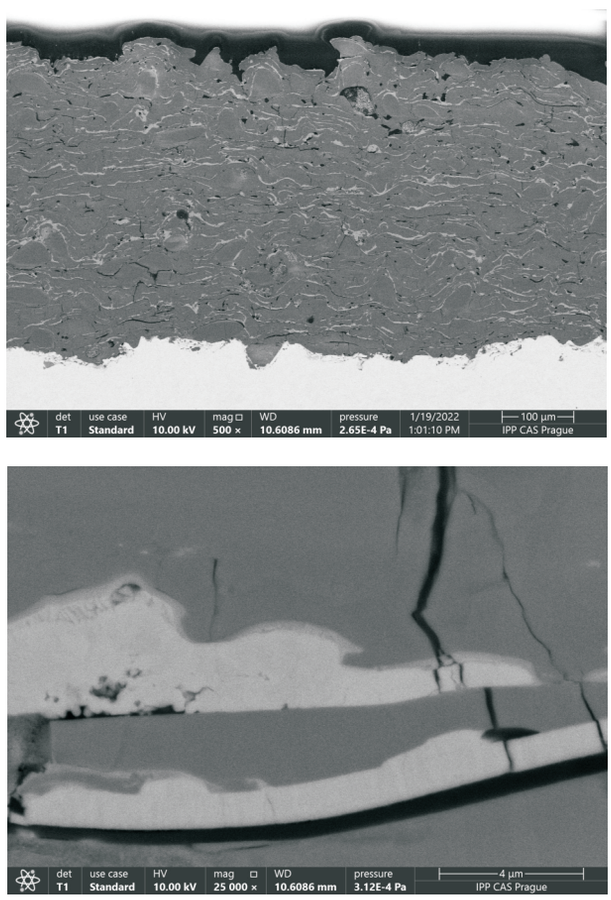


**Figure 1**. Micrographs of plasma sprayed coating of $Al_2O_3$ fed as a powder (dark) and $TiO_2$ fed as a liquid suspension (white). Interface between splats shows formed $Al_2TiO_5$ phase formed during cooling process.

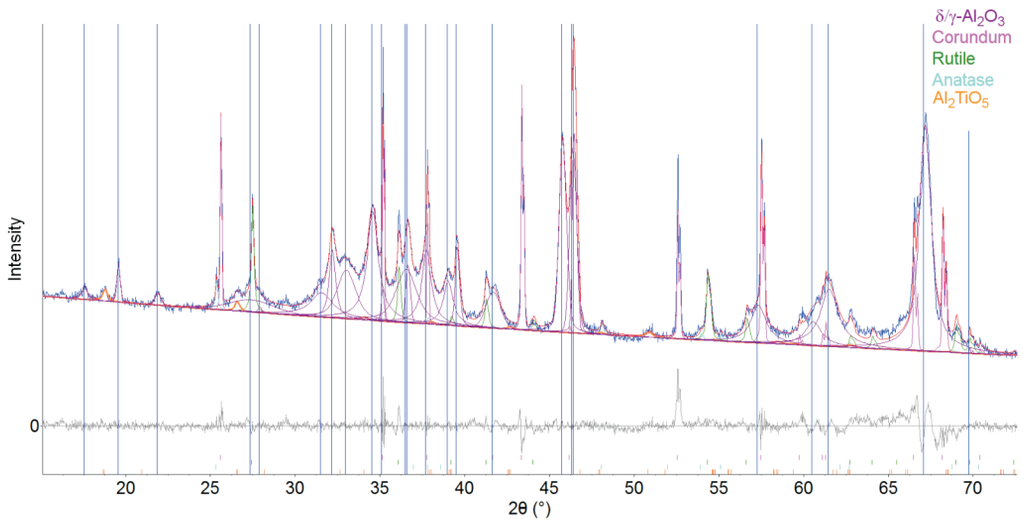


**Figure 2**. Micrographs of plasma sprayed coating of $Al_2O_3$ fed as a powder (dark) and $TiO_2$ fed as a liquid suspension (wihte). Interface between splats shows formed $Al_2TiO_5$ phase formed during cooling process.

L35

## IN-SITU X-RAY DIFFRACTION DURING TENSION ON OFF-STOICHIOMETRIC $Ni_2MnGa$ SINGLE CRYSTAL

**Petr Cejpek, Kristián Mathis, Daria Drozdenko, Ross Colman, Oleg Heczko, Ladislav Straka**

*Faculty of Mathematics and Physics, Charles University, Ke Karlovu , 121 16 Praha 2*

$Ni_2MnGa$ is a broadly studied system because of its properties related to the magnetic shape memory. The compounds based on Ni-Mn-Ga system have also an interesting application potential as the micropumps or the sensors [1, 2]. Their shape memory properties are connected to the martensitic transformation, during which the high-temperature cubic phase (austenite) undergoes a transformation to the low-temperature phase with a lower symmetry (martensite) [3]. Because of a large magnetic anisotropy and a high mobility of the internal regions (so called twin variants/twinned domains)
induced reorientation could be achieved - it is more energetically preferable to reorient the whole unit cell than to rotate magnetic moments. A similar structural reorientation could be achieved by the application of an external mechanical force in tension or compression.

The high-resolution reciprocal space mapping with X-ray diffraction proved itself as a good tool to study the structure in $Ni_2MnGa$ specimens [3, 4], which could contain several twin variants due to the shape memory effects. The reciprocal space mapping helps to distinguish between the Bragg reflections corresponding to individual twins. Moreover, reciprocal space mapping allows the precise study of the lattice parameters and a possible modulation in the structure. Our goal was to study the structure during the reorientation by X-ray diffraction in-situ in the applied tension.

For this purpose, we mounted the tensile stage (possible load up to 4 kN) inside the diffractometer. The studied specimen was $Ni_{50}Mn_{28}Ga_{22}$ with martensitic structure at the room temperature. The diffraction measurements revealed the strain in the direction of applied tension about approximately 3 % at 20 MPa leading to an exceptionally small Young modulus below 1 GPa. The structural modulation propagated along [1 1 0] is affected depending on the direction of applied tension. The modulation amplitude decreases when the applied tension is parallel to the basal plane (0 0 1). When the tension is applied perpendicularly to (0 0 1), the amplitude remains almost constant. The length of modulation vector remains the same within the range of errorbars regardless on the tension direction. The results also differ in dependence on the way how the sample is hold inside the stage. Holding directly with clamps allows almost full structural reorientation at approximately 10 MPa, but the sample cracks when the twin boundary reached the place on the sample hold by the clamps. Holding by a glue prevented the reorientation and the full reorientation did not occur up to 20 MPa.

1. A. R. Smith, et al., Microfluidic. Nanofluidics, 18 (2005), p. 1255, doi: 10.1007/s10404-014-1524-6.
2. A. Hobza, et al., Sensor. Actuator. A, 269 (2018), p. 137, doi: 10.1016/j.sna.2017.11.002.
3. O. Heczko, et al., Acta Mater., 115 (2016), pp. 250-258, doi: 10.1016/j.actamat.2016.05.047.
4. P. Cejpek, et al., J. Alloys Compd., 855 (2021) 157327, doi: 10.1016/j.jallcom.2020.157327.

*This work was supported by CSF grant No. 19-09882S and by Operational Programme Research, Development and Education financed by the European Structural and Investment Funds and the Czech Ministry of Education, Youth and Sports, project MATFUN CZ.02.1.01/0.0/0.0/15_003/0000487.*

# Student Symposium

**Wednesday, June 22**

## Session I

### SL1

## MICROSTRUCTURE OF THIN LAYERS OF GOLD AND GOLD NANOPARTICLES

**T. Košutová[1], Z. Krtouš[1], J. Kousal[1], O. Kylián[1], J. Hanuš[1], L. Martínez[2], Y. Huttel[2], D. Nikitin[1], H. Biederman[1], P. Pleskunov[1], L. Horák[1], M. Dopita[1]**

*[1]Charles University in Prague, Faculty of Mathematica and Physics, Czech Republic*
*[2]Instituto de Cienciade Materialesde Madrid (ICMM-CSIC), Madrid, Spain*

In the presented study, we investigated differences in the microstructure of thin gold layers and layers of gold nanoparticles with a focus on their thermal development. Thin films composed of nanoparticles are interesting for applications because of their inherent high porosity, which is essential for gas sensing, efficient batteries, catalysis or hydrogen storage applications. The thermal stability of nanoparticle layers depends on chemical and phase composition, the configuration of nanoparticles or the atmosphere in which they are heated up and it is critical for multiple applications of gold nanoparticles.

The homogeneous gold nanoparticles in our study were prepared by magnetron sputtering from pure metal targets followed by aggregation of fragments to the metallic clusters, by so-called gas aggregation cluster sources. The gold thin films for comparison were prepared by evaporation and by sputtering. A Series of samples with various thicknesses deposited on silicon substrates were characterized after preparation and also under annealing up to 1000 °C in the air atmosphere.

Size distribution and morphology of nanoparticles were determined by small angle X-ray scattering (SAXS), atomic force microscopy (AFM) and confirmed by scanning electron microscopy measurements (SEM) for ex-situ annealed samples. In-situ measurements of X-ray diffraction were used to characterize the thermal evolution of lattice parameters, microstructural defects and sizes of crystallites.

The as-deposited gold nanoparticles contain a large amount of stacking faults (up to 6 %) and also significant microstrain in the crystal structure. During annealing, ordering of the structure is observed together with the step-like increase of the sizes of crystallites following the increase of the sizes of whole nanoparticles. The occurrence of the holes in the substrates after heating to the highest temperatures was successfully explained.

### SL2

## STRUCTURAL DEFECTS IN SIC AND GE MICROCRYSTALS

**M. Podhorský, M. Meduňa**

*Department of Condensed Matter Physics, Masaryk University, Brno, Czech Republic*
*martinpodhorskyj@gmail.com*

Reciprocal space mapping (RSM) is a method of X-ray analysis which can provide us with useful structural information about studied samples, such as mismatch, strain, relaxation and defects of epitaxial grown layers on a substrate [1].

The studied samples consisted of large array of Ge and SiC microcrystals grown by Low-energy plasma-enhanced chemical vapor deposition (LEPECVD) technique [2]. This method enables fast, low-temperature epitaxial growth of crystals onto micrometer-scale tall pillars etched into Si(001). The method was developed at ETH Zürich, where the samples were also prepared in the group from H. von Känel [3]. It enables to grow relatively thick layers with different lattice parameters of high structural quality [3, 4]. The samples were subjected to X-ray study in order to obtain structural information.

In our experiment we used Rigaku SmartLab diffractometer, which uses X-ray source with characteristic wavelength of 0.154 nm and a hybrid multi-dimensional pixel detector HyPix-3000. The data acquisition by the detector can be done in 0D, 1D and 2D regime. For our analysis we opted for the linear regime. We placed the sample on a goniometric table and put a series of linear slits and monochromators between the source, sample and the detector. First we measured QxQz reciprocal space maps (RSMs) around symmetric and asymmetric diffractions of the samples at two different azimuths (0° and 90°), particularly (004) and (224) for Ge and (004) and (113) for SiC, from which we obtained the lattice parameter, strain and relaxation of the array of microcrystals.

The next part of our measurement was aimed to obtain RSMs of the samples in the plane parallel to sample surface

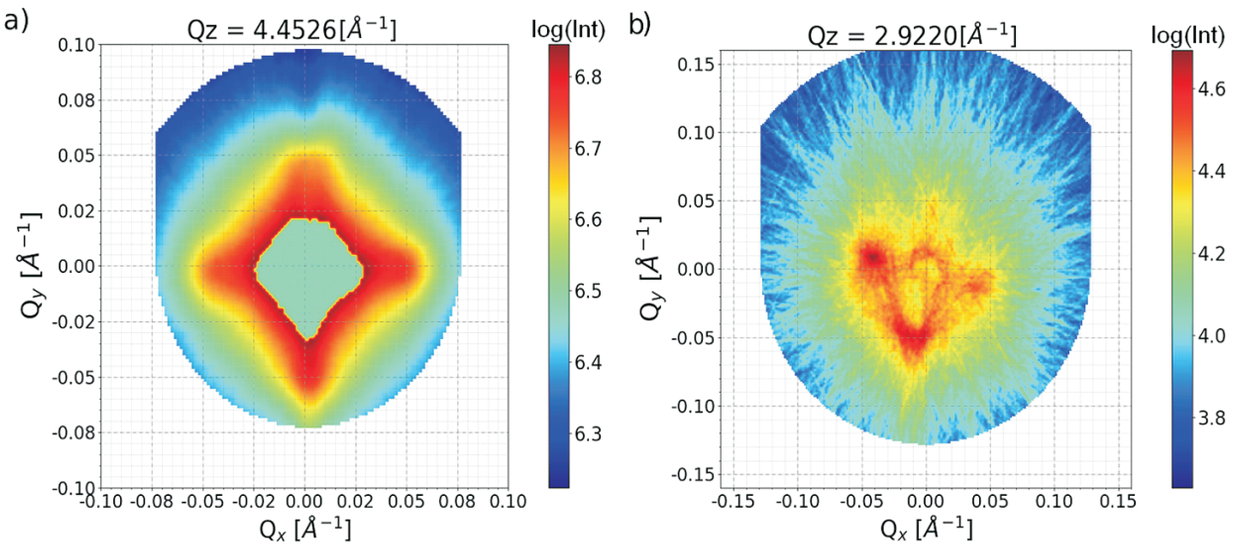


**Figure 1**. QxQy RSMs for a) Ge and b) SiC samples. In a) the maximum was cut out in order to showcase the satellite maxima. The maxima originate from crystal lattice bending and they copy a four-fold symmetry of microcrystal geometry. The satellite maxima in b) correspond to cuts through streaks {111} originating from defects (stacking faults) in the SiC microcrystal layer [7].

(QxQy). This is impossible to do with standard laboratory set-up, which enables us to measure only the QxQz plane of the reciprocal space. One way of obtaining the QxQy RSM for certain Qz is to measure multiple QxQz RSMs at different azimuthal rotations and transforming them using Radon transform [5]. Radon transform is a mathematical method used to construct 3D intensity images from 2D slices, commonly used in computer tomography [6].

We measured RSM of one diffraction maximum, particularly (004) and (002) for Ge and SiC respectively, at different azimuths ranging from 0° up to 180° with a 2° step. The QxQz RSMs measured at different azimuthal angles were transformed into a series of sinograms, from which it was possible to obtain series of QxQy RSMs for the measured range of Qz positions. Examples of reconstructed QxQy RSMs are shown in Figure 1.

The obtained QxQy RSMs for different Qz form set of slices through the reciprocal space which can generally built a 3D RSM. The distribution of scattered intensity in 3D reciprocal space can then provide another view on analysis of structural defects such as local lattice strain, misfit dislocations or stacking faults present in the studied samples.

1. U. Pietsch, V. Holý, T. Baumbach, *High-Resolution X-Ray Scattering*, Springer New York, NY, 2004.
2. C. Rosenblad, H.R. Deller, T. Graf, E. Müller, H. von Känel, *Journal of Crystal Growth* **188**, (1998), 125.
3. C.V. Falub, H. von Känel, F. Isa, R. Bergamaschini, A. Marzegalli, D. Chrastina, G. Isella, E. Müller, P. Niedermann, L. Miglio, *Science*, **335**, (2012), 1330.
4. H. von Känel, L. Miglio, D. Crippa, T. Kreiliger, M. Mauceri, M. Puglisi, F. Mancarella, R. Anzalone, N. Piluso, F. La Via, *Materials Science Forum* **821–823**, (2015), 193.
5. M. Meduňa, F. Isa, F. Brennan, H. von Känel, J. Appl. Cryst. **55**, (2022) in print.
6. P. Suetens, *Fundamentals of Medical Imaging*, Cambridge University Press, 2009.
7. M. Meduňa, T. Kreiliger, M. Mauceri, M. Puglisi, F. Mancarella, F. La Via, D. Crippa, L. Miglio, H. von Känel, *Journal of Crystal Growth* **507**, (2019), 70.

*We acknowledge Claudiu V. Falub and Hans von Känel for providing the SiC and SiGe microcrystal samples.*

SL3

# SIZE DEPENDENCE OF SURFACE SPIN DISORDER IN FERRITE NANOPARTICLES

**M. Gerina[1], M. S. Angotzi[2], V. Gajdošová[3], M. Dopita[4], D. Zákutná[1*]**

[1]*Faculty of Science, Charles University, Prague, Czech Republic*
[2]*Faculty of Chemical and Geological Science, University of Cagliari, Monserrato, Italy*
[3]*Polymer Morphology, Institute of Macromolecular Chemistry CAS, Prague, Czech Republic*
[4]*Faculty of Mathematics and Physics, Charles University, Prague, Czech Republic*

Surface spin disorder or canting arises from the breaking of exchange bonds and the breaking symmetry of the lattice, and thus crucially determines the performance of magnetic nanoparticles (NPs) and their potential technological and biomedical applications [1, 2]. Despite an enormous interest and technological relevance of magnetic NPs, there is still a lack of knowledge on the magnetic NPs spin structure. Due to the surface-to-volume ratio, surface effects will be closely related to the particle and coherent domain size. However, it is difficult to isolate the surface contribution from the bulk effects using macroscopic magnetization techniques, such as magnetization measurements, ferromagnetic resonance, Mössbauer spectroscopy [3], X-ray magnetic circular dichroism [4], and electron energy loss spectroscopy [5]. A spatially resolved magnetization is required to unveil and disentangle the surface contribution. Half-polarized small angle-neutron scattering (SANSPOL) enables us to investigate the magnetization on the nanometer scale [6]. Our previous study has proven that the magnetic volume in ferrite NPs is not fixed at the coherent domain size but increases with the applied magnetic field [7]. This implies that the applied magnetic fields polarize the disordered surface spins, leading to an increase in the magnetic size of the NPs [7].

In this contribution, we will present the size dependence of the disorder energy and the surface anisotropy in spherical $CoFe_2O_4$ NPs with different coherent domain sizes range of 3.1(1), 6.3(2), and 8.6(1) nm synthesized using the oleate-based solvothermal method [8] with narrow size distribution confirmed by transmission electron microscopy (TEM) and small-angle X-ray scattering (SAXS). Rietveld's analysis shows that coherent domain size is smaller than mean particle size, suggesting a possible presence of a spin disorder or canting. The spatial magnetization distribution obtained from SANSPOL reveals significant magnetic field dependence of magnetized volume for each sample, but with different degrees of the total magnetized NP volume. Ultimately, we will discuss the particle and coherent size dependence of the surface anisotropy constant.

*We greatly acknowledge Dr. Jana Havličková for the TGA analysis, and Dušan Rohaľ for synthetizing 1 samples. We acknowledge the Institut Laue-Langevin, Grenoble, France for the provision of beamtime at the instrument D33 and Dr. Nina J. Steinke for the technical support at the instrument.*

1. E. Tronc et al., Journal of Magnetism and Magnetic Materials **221** (2000) 6379.
2. A. Omelyanchik et al., Nanomaterials. **10** (2020) 1288.
3. B. N. Pianciola et al., J. Magn. Magn.Mater. **377** (2015) 44.
4. V. Bonanni et al., Appl. Phys. Lett. **112** (2018) 022404.
5. D. S. Negi et al., Phys. Rev. B **95** (2017) 174444.
6. S. Mühlbauer et al., Rev Mod Phys. **91** (2019) 015004..7. D. Zákutná et al., Phys Rev X. **10** (2020) 031019.
8. M. Sanna Angotzi et al., J. Nanosci. Nanotechnol. **19** (2019) 4954.

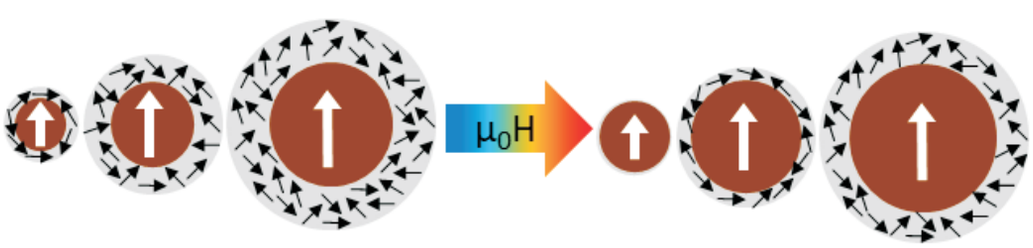


**Figure 1.** Schematic presentation of the size dependence of magnetized volume growth in applied magnetic field. Grey and brown particle part corresponds to the disorder and magnetized volume of nanoparticles.

SL4

# METAL CARBOXYLATES IN PAINTINGS – THE STUDY OF THEIR STRUCTURE AND BEHAVIOUR

**Ruslan Barannikov[1,2], Petr Bezdička[1], Eva Kočí[1], Silvia Garrappa[1], Libor Kobera[3], Jan Rohlíček[4], Jiří Plocek[1], Silvie Švarcová[1]**

*[1]Institute of Inorganic Chemistry of the Czech Academy of Sciences, ALMA Laboratory, Husinec-Řež 1001, 250 68 Husinec-Řež, Czech Republic*

*[2]Department of Inorganic Chemistry, Faculty of Science, Charles University in Prague, Hlavova 2030/8, 128 43 Prague 2, Czech Republic*

*[3]Institute of Macromolecular Chemistry of the Czech Academy of Sciences, Heyrovského nám. 2, 162 06 Praha 6, Czech Republic*

*[4]Institute of Physics of the Czech Academy of Sciences, Na Slovance 1999/2, 182 21 Praha 8, Czech Republic*

*barannikov@iic.cas.cz*

Saponification, resulting from pigment-binder interactions is one of the most dangerous degradation phenomena affecting the appearance and stability of paintings. The crystallization of metal carboxylates (soaps) is assumed as a critical point for the development of undesirable changes manifested as protrusions, efflorescence, darkening and etc. However, factors triggering this process are not fully understood, limiting the development of a suitable strategy for conservation and preservation of precious works of art.

Previous research of the portrait miniatures [1] has revealed presence of different types of crystalline metal carboxylates frequently in a conjoined occurrence of lead white ($2PbCO_3 \cdot Pb(OH)_2$) and cinnabar (HgS) pigments in paint layers, exceptionally even without presence of any lead-based pigment. These findings indicated that HgS assists to the formation of Pb and/or Hg carboxylates. Nevertheless, its role in the reaction mechanism has to be clarified.

The paucity of reliable reference structural data limited the experimental research of HgS effect on the pigment-binder interactions on molecular level. In our previous research [2], the long chain simple and mixed mercury (II) carboxylates in the series $Hg(C16)_x(C18)_{2-x}$ (x= 0.0; 0.2; 0.5; 0.8; 1.0; 1.2; 1.5; 1.8; 2.0) were synthesized in the form of pure polycrystalline powders and characterized by XRPD, ssNMR, FTIR and DSC. The crystal structure of the studied mercury carboxylates was described on the basis of complementary ssNMR and XRPD measurements, Rietveld refinement and DFT calculations. All the subjected compounds crystallize in a monoclinic lattice of the C2/c symmetry. Mercury atoms are arranged in a slightly distorted square antiprismatic geometry and are monodentatically bonded to carboxylate anions. The structural disorder at the aliphatic end of the stearic acid chains was detected in the mixed carboxylates.

The synthesized and characterized metal carboxylates were applied for the study of formation of metal soaps in model experiments simulating egg and/or oil-based paint systems consisted of lead and/or mercury-based pigments, and furthermore for the study of their crystallization in oil-based polymeric matrix.

1. S. Garrappa, D. Hradil, J. Hradilová, et al., Anal. Bioanal. Chem., 2021, 413, 263-278.
2. R. Barannikov, E. Kočí, P. Bezdička, et. al. Dalton Trans., 2022, 51, 4019–4032.

SL5

# TEMPORAL EVOLUTION OF OPTICAL ABSORPTION AND EMISSION SPECTRA OF THIOL CAPPED CdTe QUANTUM DOTS

**S. Gupta[1], S. Tomar[2, 3], A. Priyam[4], B. Bhushan[5], A. Singh[6], U. K. Dwivedi[7], R. K. Choubey[2]**

*[1]Department of Condensed Matter Physics, Faculty of Mathematics and Physics, Charles University, Ke Karlovu 5, Prague- 12116, Czech Republic*
*[2]Department of Physics, Amity Institute of Applied Sciences, Amity University, Noida Sector 125, Uttar Pradesh- 201313, India*
*[3]Applied Science and Humanities Department, ABES Engineering College, Campus- 1, 19th KM stone NH-24, Ghaziabad, Uttar Pradesh- 201009, India*
*[4]Department of Chemistry, School of Physical and Chemical Sciences, Central University of South Bihar, SH- 7, Gaya-Panchapur Road, Gaya, Bihar- 824236, India*
*[5]Department of Physics, School of Applied Sciences, Kalinga Institute of Industrial Technology, Bhubaneshwar, Odisha- 751024, India*
*[6]Department of Physics, Faculty of Natural Sciences, Jamia Millia Islamia, Central University, New Delhi-110025, India*
*[7]Department of Applied Physics, Amity School of Applied Sciences, Amity University Jaipur, Rajasthan-303002, India*
*suhaas96@gmail.com*

Quantum dots (QDs) are strongly confined semiconductor nanoparticles that exhibit novel and size-tunable properties as a result of quantum confinement effects in the particle size regime comparable to their Bohr excitonic radius. QDs have been rigorously studied to employ their desirable properties in optoelectronic devices; these very same size-tunable optoelectronic properties have also been investigated for potentially widespread use in sensing and imaging applications in biological systems [1-3]. CdTe is such a II-VI semiconductor compound, whose particle size can be tailored to exhibit luminescence across the visible spectrum [4]. However, to make CdTe a suitable material to be used in biological systems, it must be made water-soluble with the use of a biocompatible 'capping' material; capping the CdTe QD also affords it increased mechanical, chemical and luminescent stability [5]. The choice of functional group of the material used to cap the CdTe QD also lends to it easily tuneable surface properties that can be used in biomedical tracking and drug delivery applications [6].

In the present work, we have synthesised and studied a series of CdTe QDs capped with four different thiols: (i) Thioglycolic acid (TGA), (ii) Mercaptoethyl amine (MEA), (iii) L-Cysteine (L-Cys), and (iv) Glutathione (GSH). An aqueous route was employed to synthesise all the samples, with varying reflux times for the different thiols used for capping. Fig.1 illustrates the confirmation of the cubic CdTe phase of the seed material from the XRD analysis of the synthesised CdTe@TGA QDs refluxed for 15mins; highest intensity characteristic (111) peak was further analysed to calculate the lower limit of crystallite size (2.4nm), interplanar spacing (3.65 Å), lattice constant (6.32 Å), microstrain and dislocation density. HRTEM and SAED studies further supported the results obtained from the XRD analysis. Fig.2 shows the comparison of the FTIR spectra of the CdTe@MEA QDs with the FTIR spectra of MEA; evidence of cleavage of the H-SR bond in thiols and simultaneous formation of the Cd-SR bond was used to

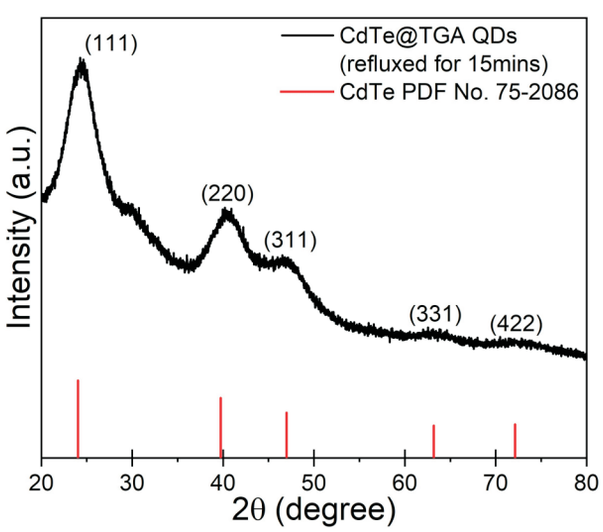


**Figure 1**. XRD analysis of the synthesised CdTe@TGA QDs refluxed for 15mins

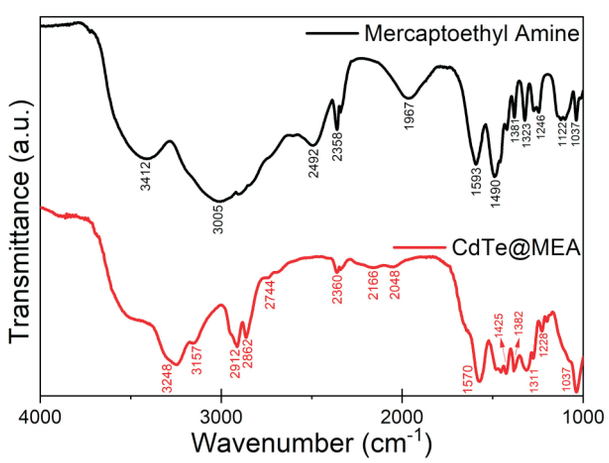


**Figure 2.** Comparison of the FTIR spectra of the synthesised CdTe@MEA QDs with the FTIR spectra of MEA

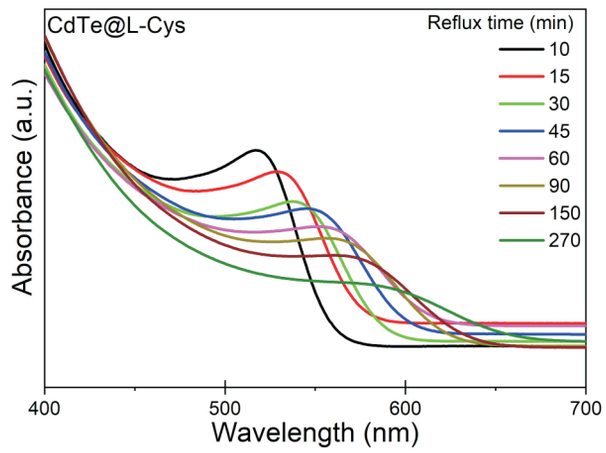


**Figure 3.** UV-visible absorption spectra of the synthesised CdTe@L-Cys QDs refluxed for different times.

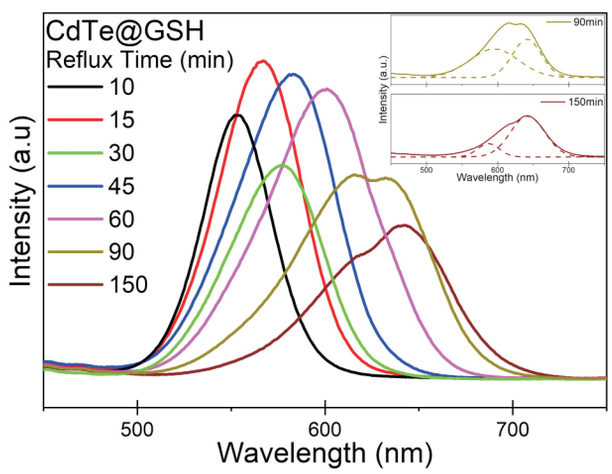


**Figure 4.** Photoluminescent emission spectra of the synthesised CdTe@GSH QDs refluxed for different times. Inset shows the deconvolution of the emission peaks at longer reflux times.

confirm the successful capping of all the thiols to the surface of the CdTe QDs.

Fig.3 shows the UV-visible absorption spectra of the synthesised CdTe@L-Cys QDs refluxed for different times. All synthesised samples exhibited blue-shift in absorption edge as compared to the bulk CdTe, confirming the strong size confinement of the nanoparticles; with increasing reflux time, the absorption edge shifted gradually to longer wavelengths for all samples. Band-gap energy was obtained from the Gaussian-fitted peak position of the 1st derivative of absorption v/s energy plot; tight binding approximation model was used to calculate the size of the QD from the band gap energy. Particle size growth with increasing reflux time was observed for all samples: CdTe@GSH reached a predetermined particle size (4nm) the fastest (90mins) when compared to the other thiol capped CdTe QDs, while the CdTe@MEA QDs were unable to attain the same particle size even after 390mins of reflux time. To understand the growth mechanics, variations of concentration and particle size distribution of the synthesised thiol-capped CdTe QDs with respect to increasing reflux time and particle size was studied. Evidence of separation between the nucleation and growth processes, and identification of three distinct growth regimes (focusing, defocusing and equilibrium) allowed us to confirm the dominance of Ostwald ripening processes during the particle growth.

Fig.4 shows the photoluminescent emission spectra of the synthesised CdTe@GSH QDs refluxed for different times. At shorter reflux times, all samples exhibit narrow-width single peak emission, which gradually shifts to longer wavelengths, from green to yellow to orange to red, with increasing reflux time and particle size. At longer reflux times, deconvolution of the emission peak into Gaussian components was done to qualitatively investigate the contribution of emission from different sized particles, as can be seen in the inset of Fig.4; comparison of the component peaks at different times suggests that as reflux time increases, emission intensity contribution from larger particle sizes increases. Zetapotential analysis was conducted to obtain the surface charge of the synthesised thiol-capped CdTe QDs to study the effect the different functional groups on the surface of the QD; DLS analysis was conducted to obtain the hydrodynamic diameter of the synthesised thiol-capped CdTe QDs.

1. I. L. Medintz, H. T. Uyeda, E. R. Goldman, H. Mattoussi, *Nature Materials*, **4(6)**, (2005), 435.

2. X. Gao, Y. Cui, R. M. Levenson, L. W. Chung, S. Nie, *Nature Biotechnology*, **22(8)**, (2004), 969.

3. C. Y. Zhang, H. C. Yeh, M. T. Kuroki, T. H. Wang, *Nature Materials*, **4(11)**, (2005), 826.

4. D. V. Talapin, S. Haubold, A. L. Rogach, A. Kornowski, M. Haase, H. Weller, *The Journal of Physical Chemistry B*, **105(12)**, (2001), 2260.

5. N. Gaponik, A. L. Rogach, *Physical Chemistry Chemical Physics*, **12(31)**, (2010), 8685.

6. L. Qi, X. Gao, *Expert Opinion on Drug Delivery*, **5(3)**, (2008), 263.

SL6

# IN-SITU LOADING ON DEFECT CONTAINING MATERIAL OBSERVED UNDER HIGH-RESOLUTION TOMOGRAPH

**Ahmed Ubaid**

*Institute of Physics, Czech Academy of Sciences, Na Slovance 1999/2, 180 00 Praha 8*

NiTi possess unique shape memory and pseudoelastic characteristics. In this research, a dog-bone shaped sample of NiTi is being analysed under X-ray Computed Tomography. Deformation characteristics of NiTi have been studied due to their increased demand in the miniaturized applications. The in-situ tensile testing was performed at -20C with different load i.e., 10N, 150N, 220N and 300N using Deben chamber of Xradia Versa 610, Zeiss. The sample had 4.2 mm gauge length, 1 mm width and 1 mm height. The reconstructed images and large number of pores/inclusions were being analysed using DragonFly software. Images obtained under different loading were compared, dimensional changes in the pores/inclusions were determined as well as changes in the distances amongst different pores were calculated. The sample showed 1 % deformation at 150N, 3.80 % at 220N and 5.4 % deformation at 300N.

1. Otani, J., & Obara, Y. (Eds.). (2004). Xray CT for Geomaterials: Soils, Concrete, Rocks International Workshop on Xray CT for Geomaterials, Kumamoto, Japan. CRC Press.
2. Carmignato, S., Dewulf, W., & Leach, R. (Eds.). (2018). Industrial X-ray computed tomography. Cham: Springer International Publishing.

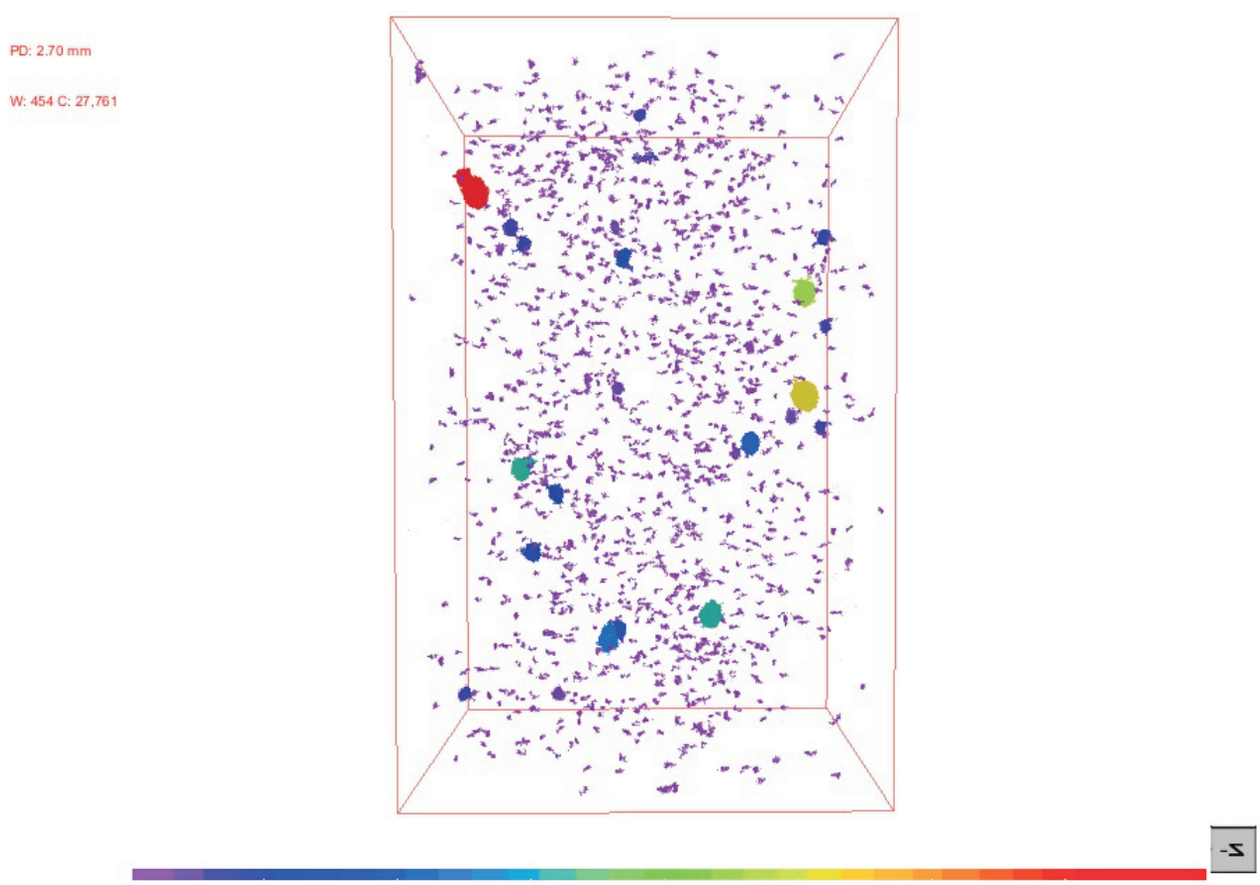


**Figure 1.** Different size pores shown with different colours at 220 N and -2 0°C.

Session II

SL7

# MICROSTRUCTURE OF HEXAGONAL $LuFeO_3$ THIN EPITAXIAL LAYERS

**P. Machovec, M. Dopita, L. Horák, V.Holý**

*Faculty of Mathematics and Physics, Charles University, Ke Karlovu 5, 121 16 Praha 2*
*machovec9@seznam.cz*

Hexagonal $LuFeO_3$ (h-$LuFeO_3$) is a multiferroic material that belongs to hexagonal ferrites. Magnetoelectric coupling at room temperature was theoretically predicted in this material. These properties make h-$LuFeO_3$ very interesting for potential use in spintronics [1, 2].

We investigated the real structure of the thin epitaxial layers of *h*-$LuFeO_3$ by means of X-ray diffraction (reciprocal space mapping) and X-ray reflectivity. Three samples of *h*-$LuFeO_3$ with (001) surface orientation were investigated. The first epitaxial layer was deposited on a sapphire substrate (001), the second layer was deposited on a platinum interlayer (111) on a sapphire substrate (001), and the third layer was deposited on an yttria-stabilized zirconia substrate (111). Despite the high mismatch between substrates and layer (up to 6.8 % for the *h*-$LuFeO_3$-platinum interface), epitaxial growth was achieved in all samples. The layer thickness determined from the X-ray reflectivity was (339±1) Å, (370±3) Å, and (370±1) Å, respectively.

Two symmetrical and two asymmetrical reciprocal space maps were measured for each layer (including the platinum interlayer). From the positions of the reciprocal lattice points, we determined that all layers were relaxed. All four reciprocal space maps belonging to one layer were simultaneously fitted using a model of X-ray scattering on mosaic layers [3]. This model assumes that the layer is composed of mosaic blocks in the shape of a rotational ellipsoid. These blocks are mutually slightly rotated, i.e., there is a small random tilt of the (001) planes. The layer is thus described by the following parameters: thickness, lateral and vertical average size of blocks, distribution width of block size, root mean square misorientation, vertical and lateral microstrain.

The reciprocal space maps of *h*-$LuFeO_3$ layer deposited directly on the sapphire substrate show two overlapping peaks. The more intense maxima correspond to almost spherical blocks with horizontal semi axis $R_L = (170\pm10)$ Å and vertical semi axis $R_V = (170\pm10)$ Å with misorientation $\Delta = (1.5\pm0.1)°$ and the less intense maxima correspond to blocks with $R_L = (100\pm20)$ Å and $R_V = (170\pm15)$ Å with misorientation $\Delta = (1.7\pm0.1)°$ and slightly smaller out of plane lattice parameter.

The platinum interlayer helps to improve the crystalline quality of the *h*-$LuFeO_3$ layer. The size of the mosaic blocks in the layer deposited on the platinum interlayer is $R_L = (125\pm7)$ Å and $R_V = (115.8\pm0.1)$ Å and misorientation of mosaic bocks is $\Delta = (0.10\pm0.02)°$. The platinum interlayer is composed of a wetting layer with low mosaicity and hills with mosaic blocks of size $R_L = (200\pm15)$ Å and $R_V = (200\pm15)$ Å and misorientation $\Delta = (0.25\pm0.03)°$ growing from this wetting layer.

In the last sample deposited on yttria-stabilized zirconia, we detected medium sized mosaic blocks $R_L = (183.6\pm6.6)$ Å and $R_V = (182.6\pm1.8)$ Å with medium misorientation $\Delta = (0.31\pm0.02)°$. The microstrain was highest in the sample deposited directly on a sapphire substrate and lowest in the sample deposited on an yttria-stabilized zirconia substrate.

1. Disseler, S.M.; Borchers, J.A.; Brooks, C.M.; Mundy, J.A.; Moyer, J.A.; Hillsberry, D.A.; Thies, E.L.; Tenne, D.A.; Heron, J.; Holtz, M.E.; et al. Magnetic Structure and Ordering of Multiferroic Hexagonal LuFeO3. *Physical Review Letters* 2015, ***114***.
2. Wang, W.; Zhao, J.; Wang, W.; Gai, Z.; Balke, N.; Chi, M.; Lee, H.N.; Tian, W.; Zhu, L.; Cheng, X.; et al. Room-Temperature Multiferroic Hexagonal LuFeO3 Films. *Physical Review Letters* 2013, ***110***.
3. Pietsch, U; Holý, V; Baumbach,T.; B. *High-Resolution X-Ray Scattering from Thin Films to Lateral Nanostructures - Second Edition*; 2004.

SL8

# STUDIUM PŘEDNOSTNÍ ORIENTACE LASEREM NAVAŘENÉ NÁSTROJOVÉ OCELE

**K. Trojan[1], J. Čapek[1], V. Ocelík[2], N. Ganev[1]**

*[1]Katedra inženýrství pevných látek, Fakulta jaderná a fyzikálně inženýrská, České vysoké učení technické, Trojanova 13, 120 00 Praha 2, Česká Republika*

*[2]Department of Applied Physics, Zernike Institute for Advanced Materials, Faculty of Science and Engineering, University of Groningen, Nijenborgh 4, 9747 AG, Groningen, The Netherlands*

*karel.trojan@fjfi.cvut.cz*

Cílem tohoto příspěvku je popsat přednostní orientaci laserem navařené nástrojové ocele AISI H13. Byl vytvořen návar z pěti vrstev, na jeho původním povrchu byla následně charakterizována přednostní orientace a ta byla porovnána s výsledky konvenčně zpracované ocele.

Nástrojová ocel AISI H13 pro práci za tepla je jedním z běžných materiálů používaných v průmyslu pro výrobu forem, zápustek nebo ozubených kol. Formy během své životnosti trpí silným poškozením v důsledku termodynamického namáhání [1]. Proto byly vyvinuty různé způsoby jejich oprav, které jsou levnější než výroba nových forem. Velkou výhodou laserového navařování je vysoká produktivita s minimálním ovlivněním základního materiálu díky nízkému vnesenému teplu. Vnesené teplo způsobuje deformace nebo zhoršení vlastností materiálu v důsledku popouštění. Laserové navařování proto umožňuje opravy forem bez dalšího tepelného zpracování [2]. Při navařování dochází k rychlému směrovému tuhnutí, které má za následek výraznou přednostní orientaci, což může významně ovlivnit mechanické vlastnosti nově vytvořeného materiálu. Proto je důležité sledovat a porozumět těmto změnám, následně lze tyto znalosti použít k návrhu postupu pro depozici větších objemů.

Laserové navařování bylo prováděno pomocí vláknového laseru *IPG 3kW Yt:YAG*. Laserovým svazkem o hustotě energie 90 J/mm$^2$ byl zhotoven návar s pěti vrstvami. Každá vrstva byla vytvořena ze šesti, nebo sedmi překrývajících se housenek na substrátu z nástrojové oceli AISI H11. Byl použit prášek s průměrnou velikostí částic 94 ± 24 μm.

Za účelem popsání přednostní orientace byly získány pólové obrazce linií {200}, {211} a {220} fáze α-Fe na přístroji *X'Pert PRO MPD* v klasické Braggově–Brentanově konfiguraci s kobaltovým zářením a křížovými clonami 0,5 × 1 mm$^2$. Program MATLAB$^{TM}$ *toolbox MTEX* [3] byl použit pro výpočet orientačně distribuční funkce a vykreslení inverzních pólových obrazců (IPO). Efektivní hloubka vnikání odpovídající tloušťce povrchové vrstvy, která poskytuje přibližně 63 % difraktované intenzity, je v případě použité vlnové délky ca 5 μm.

Na základě IPO, viz obrázek 1 a 2, je možné konstatovat, že obrazce jak navařené, tak konvenčně zpracované oceli se pro jednotlivé směry od sebe kvalitativně neliší. Ve směru L, tedy ve směru navařování, převládá krystalografický směr [100]. Ve směru T, kolmo na navařování, lze pozorovat dvě maxima a to ve směru [100] a [110]. Naopak

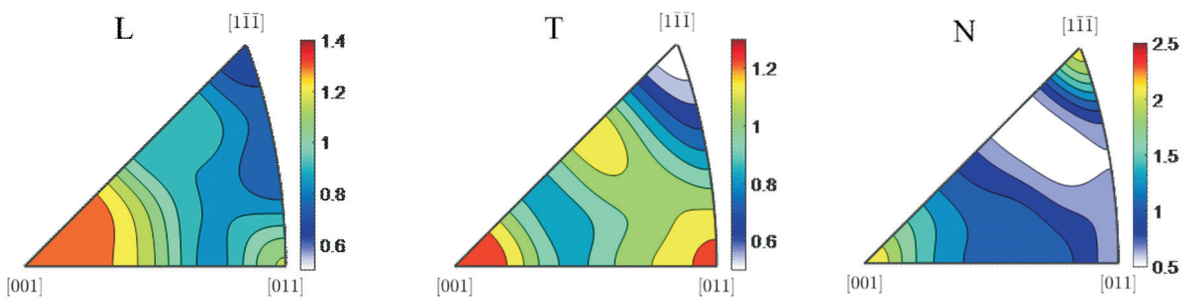


**Obrázek 1**. IPO laserem navařené ocele, kdy směr L je rovnoběžný se směrem navařování, směr T je kolmý a směr N je normálou povrchu.

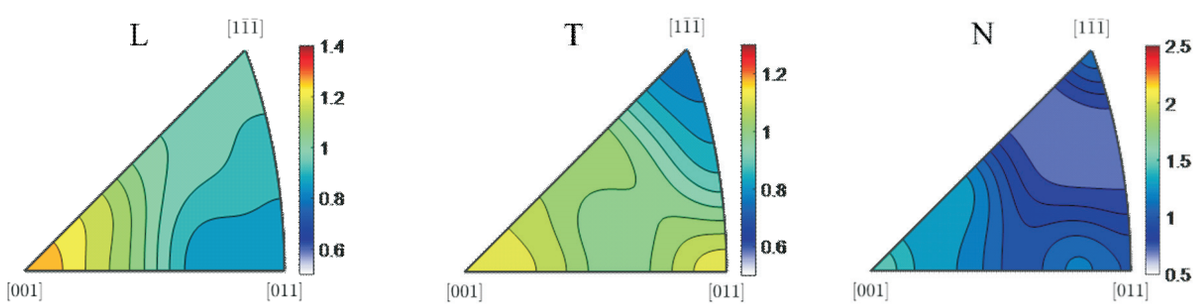


**Obrázek 2**. IPO konvenčně zpracované ocele, kdy směr L je rovnoběžný se směrem navařování, směr T je kolmý a směr N je normálou povrchu.

ve směru normály k povrchu jsou maxima ve směru [100] a [111]. Pro laserově navařenou ocel lze ve všech směrech pozorovat vyšší hodnoty násobku náhodné distribuce. Tato závislost je velice zajímavá, jelikož texturní data konvenčně zpracované ocele byla získána na ploše, kde následně proběhlo laserové navařování. Na základě těchto výsledků by tedy bylo možné vyslovit hypotézu, že přednostní orientace substrátu ovlivňuje přednostní orientaci navařené vrstvy tím, že dochází k nukleaci nových zrn na hranici natavené zóny substrátu a jejich dalšímu směrovému růstu. Tuto problematiku je potřeba detailněji prozkoumat a zhodnotit, zda se nejedná pouze o náhodu.

Laserové navařování nástrojové oceli H13 vykazuje velký aplikační potenciál. Ukázalo se, že přednostní orientace navařené oceli vykazuje podobný typ jako konvenčně zpracovaná ocel. Zkoumaná problematika, a především interpretace podobných získaných výsledků však dosud nebyly přesně popsány. K doplnění poznání v této oblasti bude nezbytný další výzkum.

1. R. G. Telasang, et al. Microstructure and Mechanical Properties of Laser Clad and Post-cladding Tempered AISI H13 Tool Steel. *Metall. Mater. Trans. A.* **46A**: 2309–2321, 2015.

2. M. Vedani, et al. Problems in laser repair-welding a surface-treated tool steel, *Surf. Coat. Tech.* **201**: 4518–4525, 2007.

3. F. Bachmann, et al. Texture Analysis with MTEX — Free and Open Source Software Toolbox, Solid State Phenomen. **60**: 63–88, 2010.

*Tato práce byla podpořena grantem Studentské grantové soutěže ČVUT č. SGS22/183/OHK4/3T/14 a projektem CZ.02.1.01/0.0/0.0/16_019/0000778 "Center for advanced applied science" v rámci Operačního programu Výzkum, vývoj a vzdělání, který je kontrolován Ministerstvem školství, mládeže a tělovýchovy České Republiky.*

**SL9**

## CHALLENGING MARTENSITES IN Ni-Mn-Ga-BASED ALLOYS: CAN MINOR CHANGES IN STRUCTURAL MODULATION AFFECT PHYSICAL PROPERTIES?

**P. Veřtát[1,2], L. Straka[2], M. Klicpera[3], O. Sozinov[4], O. Heczko[2]**

[1] *Faculty of Nuclear Sciences and Physical Engineering, Czech Technical University in Prague, 120 00 Praha 2, Czech Republic*

[2] *FZU - Institute of Physics of the Czech Academy of Sciences, 182 21 Praha 8, Czech Republic*

[3] *Faculty of Mathematics and Physics, Charles University, 121 16 Praha 2, Czech Republic*

[4] *Material Physics Laboratory, LUT University, 538 50 Lappeenranta, Finland*

*vertat@fzu.cz*

The structure of martensites of Ni-Mn-Ga-based magnetic shape memory (MSM) alloys represents a unique crystallography challenge. Not only do these alloys possess complex and practically inevitable *twined microstructure* (for some compositions even close to merohedral twins), but they also feature a structural *modulation* that evolves with temperature. Some of our new single-crystal studies even indicate that we might be dealing with twinned *composite crystals*, i.e., there is more than one ordering. To make things even more complicated, SEM and HRTEM indicate the presence of *nanotwinning* (at least close to the *a*/*c* twin boundaries) [1-3]. Despite the challenging nature of our martensites, all the said phenomena seem to be precursors for the extremely high mobility of the twin boundaries (very unusual property itself) which are essential for the magnetically induced reorientation of the martensite (MIR).

Aiming to solve one of the most difficult topics in the field – the *commensurate* or *incommensurate* question, we focused on the evolution of the 10M modulated martensite with temperature. We used a simple modulation approach to describe the detected changes in modulation satellites. We found a universal rule that seems to be valid for a wider range of Ni-Mn-Ga-based alloys. Our studies indicate a *commensurate* 10M modulated structure in the vicinity of the austenite phase. Upon cooling, the modulation evolves into *incommensurate* and continues to evolve until it at-

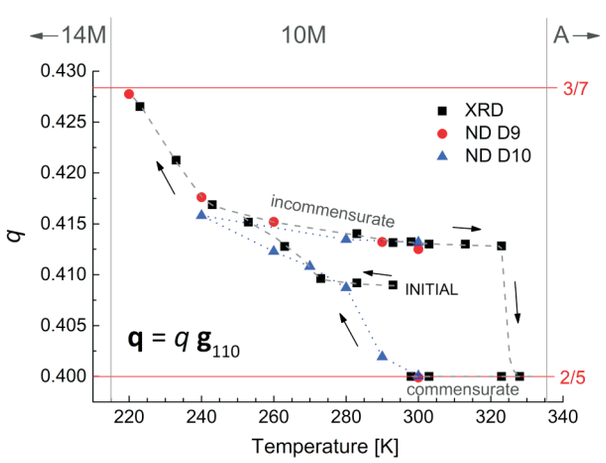


**Figure 1**. Evolution of the magnitude $q$ of the modulation vector **q** with temperature within 10M modulated martensite of the $Ni_{50}Mn_{27}Ga_{22}Fe_1$ alloy. Data from the conventional XRD and two ND experiments in ILL Grenoble (D9 and D10 instruments). Transformation temperatures are represented by vertical lines and phases are marked: A – austenite, 10M – five-layered modulated martensite, 14M – seven-layered modulated martensite. The commensurate metastable states are schematically marked by red vertical lines. Adapted from [4].

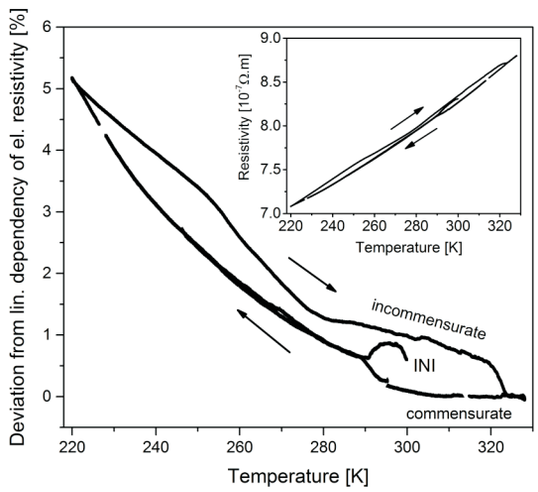


**Figure 2**. Deviation from linear dependency of electrical resistivity with temperature within 10M modulated martensite of the $Ni_{50}Mn_{27}Ga_{22}Fe_1$ alloy. Measured resistivity curve within the studied region of the 10M martensite phase is presented in the inset [4].

tains yet another *commensurate* metastable state followed by the intermartensitic transformation to 14M modulated martensite [4]. Observed changes in modulation exhibit a thermal hysteresis, Fig. 1. Interestingly, these minor changes in modulation can be corelated with the changes of physical properties, such as electrical resistivity, Fig. 2, and elastic moduli.

1. L. Straka, J. Drahokoupil, P. Veřtát, J. Kopeček, M. Zelený, H. Seiner, O. Heczko, *Acta Mater.*, **132**, (2017), 335-344.

2. P. Veřtát, L. Straka, J. Drahokoupil, O. Heczko, *Acta Physica Polonica A*, **134**, (2018), 859-862.

3. L. Straka, J. Drahokoupil, P. Veřtát, M. Zelený, J. Kopeček, A. Sozinov, O. Heczko, *Scientific Reports,* **8**, (2018), 11943.

4. P. Veřtát, H. Seiner, L. Straka, M. Klicpera, A. Sozinov, O. Fabelo, O. Heczko, *J. Phys.: Condens. Matter*, **33**, (2021), 265404.

*This work was supported by the Grant Agency of the Czech Technical University in Prague, grant No. SGS22/183/OHK4/3T/14, and by Czech OP VVV project MATFUN—CZ.02.1.01/0.0/0.0/15_003/0000487. We acknowledge the Institut Laue-Langevin and the project LTT20014 financed by the Ministry of Education, Youth and Sports, Czech Republic, for the provision of neutron radiation facilities and kindly thank O. Fabelo for assistance with the ND measurements.*

## Session III

### SL10

# PHOTOCHEMICAL DEGRADATION OF SELECTED PHARMACEUTICALS UNDER LIGHT CONDITIONS RELEVANT TO NATURAL WATERS AND STUDY OF TOXICITY OF PHOTOPRODUCTS

**M. Poncarová[1], Š. Klementová[1], M. Šorf[2]**

*[1]Faculty of Science, University of South Bohemia, Branišovská 1760, 370 05 České Budějovice*
*[2]Department of Agronomy, MENDEL University, ÚZRHV AF, Zemědělská 1, 613 00 Brno*
*poncam00@prf.jcu.cz*

Xenobiotics in the environment include a wide variety of compounds, e.g. pesticides, drugs, textile dyes, personal care products, stabilisers, and many others. Among xenobiotics, pharmaceuticals have recently acquired increasing attention [1, 2]. Pharmacological products enter natural waters mainly via wastewater either from manufacturing facilities or from municipal wastewater (excretion of unmetabolised drugs, disposal of unused drugs). The contamination of natural aquatic systems results in adverse negative effects on aquatic organisms.

In surface waters, physical, chemical, and biological processes contribute to the transformations of polluting substances. Photoinitiated processes may represent important degradation pathways in surface waters for compounds resistant to both biological degradation and chemical reactions such as hydrolysis [3]. Photochemical degradation may lead to a decrease in contaminant concentration, and, in some cases, generate photoproducts with even higher harmful effects than that of the parent compound [4].

Ecotoxicology represents a framework enabling to test a given compound and to reveal or at least estimate its potential harmful effect. This study is focused on aquatic organisms. In autotrophs, algae *Chlorella sp*. and *Desmodesmus sp*. are often used due to their simple laboratory maintenance [5, 6]. The flagship of heterotrophs toxicity testing in surface water is the planktonic microcrustacean *Daphnia magna* [7]. It has several characteristics that in toxicological tests, especially those targeted at acute toxicity estimation – it can be relatively easily maintained in the laboratory and, when under suitable conditions, *D. magna* reproduces parthenogenetically. A common model of vertebrates in ecotoxicology is the zebrafish *Danio rerio*. Although the extrapolation of the obtained results to higher vertebrates is not straightforward and should be done with care, the response of fish to xenobiotics is a significant indicator of how a particular compound (or products of its photodegradation) affect fish assemblages in surface waters.

In this study, toxicity of atorvastatin, a widely prescribed hypolipidemic drug, and the mixture of its photoproducts were investigated. The photoproduct mixture was produced by irradiation of the solution of atorvastatin ($c$ = 50 mg/l) by the radiation in the range between 300 – 350 nm (to imitate the short-wavelength solar radiation that reaches the Earth´s surface) for 15 minutes. Then, two toxicity assays based on OECD 202 [8] and 236 [9] guidelines were performed.

In the case of acute toxicity test on the model organism *Daphnia magna* (OECD 202), 2 juveniles not older than 24 h were introduced into 5 ml of pure media, other juveniles in pairs in the media with atorvastatin in the concentration range from 1 to 10 000 µg/l; photoproducts solutions were tested at concentration range of remaining atorvastatin in the irradiated solution up to 1000 µg/l. During this test (48 hrs) constant temperature was held at 18.7 ± 0.2 °C; photoperiod was 16 hrs light and 6 hrs dark and the juvenils were not fed. Atorvastatin did not cause any mortality, photoproducts caused 20 % mortality at the highest concentration used. The LC50 value could not be evaluated from this experiment. The data show that lethal concentration for 50 % of daphnids is higher than the highest used concentration. Photoproducts seem to be more toxic than atorvastatin itself since in addition to the observed mortality each daphind showed odd swimming at the highest concentration of photoproducts.

Toxicity assay based on OECD 236 guideline was done on embryos of *Danio rerio*. One fertilized egg was introduced into 2 ml of ISO water (control) or into 2 ml of atorvastatin or 2 ml of photoproducts (concentration ranges as in the tests with *D.magna)*. Tested embryos were kept in the incubator Climacell EVO line, for 96 hours at the temperature 25 – 26 °C and the photoperiod 14 hrs light/ 10 hrs darkness. The evolution of the embryos was monitored visually every 24 hours. Four key parameters indicating the lethality were sought for: coagulated embryos, lack of somite formation, non – detachment of the tail and lack of heartbeat. The value of LC50 for atorvastatin was determined by software Prism 6, its value is 1976 µg/l. Regarding photoproducts, 40 % mortality was observed at the photoproduct mixture with remaining 500 µg/l of atorvastatin. In the higher concentration there was also retardation in the development and the drug had adverse effect on blood formation – lack of cell flow, transparent cells without pigmentation.


1. M. Mezzelani, S. Gorbi, F. Regoli, *Marine Environmental Research*, **140**, (2018), 41.
2. M. de Oliviera, B. E. F. Frihling, J. Velasques et al., *Sci. Tot. Env.*, **705**, (2020), 135568.
3. A. Nikolaou, S. Meric, S. Fatta, *Anal. Bioanal. Chem.*, **387**, (2007), 1225.
4. Š. Klementová, M. Poncarová, D. Kahoun, M. Šorf, E. Dokoupilová, P. Fojtíková, *Environ. Sci. Pollut. Res.,* **27**, (2020), 35650.
5. OECD, Guidelines for testing chemicals 201, Freshwater Alga and Cyanobacteria, Growth Inhibition Test (2011).
6. E. Geiger, R. Hornek-Gausterer, M. T. Sacan, *Ecotox. Environ. Safe*, **129**, (2016), 189.
7. J. Seďa & A. Petrusek, *Journal of Limnology*, **70**, (2011), 337.
8. OECD, Guidelines for the testing of chemicals 202, *Daphnia sp.*, Acute Immobilisation Test (2004).
9. OECD, Guidelines for testing of chemicals 236, Fish Embryo Acute Toxicity (FET) Test (2013).


**SL11**

## DECORIN BINDING PROTEINS FROM EUROPEAN *BORRELIA* – DO STRUCTURAL DIFFERENCES INFLUENCE LIGAND BINDING?


**Libor Hejduk[1,2], Petr Rathner[3,#], Martin Strnad[1,2], Filip Dyčka[1], Libor Grubhoffer[1,2], Ján Štěrba[1], Ryan O. M. Rego[1,2], Norbert Müller[1], Adriana Rathner[4]**

*[1]Faculty of Science, University of South Bohemia, 37005 České Budějovice, Czech Republic*
*[2]Institute of Parasitology, Biology Centre, Czech Academy of Sciences, 37005 České Budějovice, Czech Republic*
*[3]Institute of Inorganic Chemistry, Johannes Kepler University, 4040 Linz, Austria*
*[4]Institute of Biochemistry, Johannes Kepler University, 4040 Linz, Austria*
*#Present address: Institute of Analytical Chemistry, University of Vienna, 1090 Vienna, Austria*


Adhesion of spirochetes from *Borrelia burgdorferi* sensu lato complex is the crucial step in early phase of Lyme disease infection. Decorin binding proteins (Dbp) are glycosaminoglycan (GAG) binding adhesins exposed on the surface of *borrelia* spirochetes. Dbps are expressed in two homologous forms A and B, both of them were characterized as main factors of *borrelia* virulence [1]. Based on the previous described differences in binding mechanisms of Dbp-GAG interaction [2], we focused on the relations between structural differences and GAG binding. We aim to describe the structural differences in detail among Dbps from european *Borelia* species and their particular interactions with different GAGs using solution nuclear magnetic resonance (NMR) spectroscopy at atomic resolution. Almost complete backbone and sidechain assignments of DbpA from *B. Afzelii* and *B. Bavariensis* have been achieved. Predictions of secondary structure propensity for both variants, calculated from assigned chemical shifts, were compared with available NMR structures of North American *borrelia* species. Backbone dynamics was described by T1 and T2 spin relaxations and $^{1}H$ $^{15}N$ heteronuclear NOE (Nuclear Overhauser effect) experiments. We performed initial protein-GAG interaction studies of both variants of DbpA with different GAGs by NMR

titrations including protein dynamics measurement by heteronuclear NOE experiments, hydrogen-deuterium exchange mass spectrometry (HDX-MS) and surface plasmon resonance (SPR) trial measurement. NMR-based prediction of secondary structure propensity and protein backbone dynamics combined with initial protein-ligand interaction experiments, which indicates interspecific differences in GAG binding, provided insight into structural characteristics of DbpA and will set the starting point for future extensive research of specific differences in structure and dynamics of Dbps and how it influence the interaction mechanism with GAG ligands.

1. Lin Y P, Benoit V, Yang X, Martínez-Herranz R, Pal U, & Leong J M (2014). Strain-specific variation of the decorin-binding adhesin DbpA influences the tissue tropism of the lyme disease spirochete. PLoS pathogens, 10(7).
2. Morgan A M, & Wang X (2015). Structural mechanisms underlying sequence-dependent variations in GAG affinities of decorin binding protein A, a Borrelia burgdorferi adhesin. The Biochemical journal, 467(3), 439–451.
3. Hejduk L, Rathner P, Strnad M, Grubhoffer L, Sterba J, Rego R.O.M., Müller N, Rathner A (2021). Resonance assignment and secondary structure of DbpA protein from the European species, Borrelia afzelii. Biomolecular NMR assignments, 15(2), 415–420.

**SL12**

# LIPOLYTIC SYSTEM IN THE HARD TICK *IXODES RICINUS*

**Tereza Kozelková[1,2], Filip Dyčka[2], Helena Frantová[1], Veronika Urbanová[1], and Petr Kopáček[1]***

[1]*Institute of Parasitology, Biology Centre of the Czech Academy of Sciences, Branišovská 31, 370 05, České Budějovice, Czech Republic*

[2]*Faculty of Science, University of South Bohemia, Branišovská 31, 370 05, České Budějovice, Czech Republic*

Ticks are obligatory blood-feeding ectoparasites capable of transmitting a wide variety of pathogens comprising bacteria, viruses, and protozoa to humans and animals. After mosquitoes, ticks are the second most dangerous vectors of arthropod-borne diseases. Hard tick *Ixodes ricinus* is a typical representative of the 3-host tick and its life cycle comprises three life stages. Each of the parasitic stages, except for adult males, feeds on a host. In contrast to mosquitoes, hard ticks *I. ricinus* feed much longer. Nymphal feeding takes typically from 3 to 4 days, adult females feed twice longer approximately 6 – 9 days. Adult ticks are capable to imbibe and digest huge amounts of host blood exceeding hundred times their unfed weight (Sonenshine, 1991).

Tick midgut lumen serves as the main organ for storage of the engorged blood. Most of the hematophagous ectoparasites (such as insect blood-feeders) digest host blood extracellularly in the midgut lumen. By contrast, digestion in ticks is a slow process occurring intracellularly in the midgut epithelium cells. Host blood is the sole source of energy and nutrients for overall tick development and reproduction. During feeding of each developmental stage, dynamic changes of tick midgut epithelium reflect the changes in the physiological processes occurring in this tissue (Sonenshine, 1991). Furthermore, the midgut serves as the primary interface between the tick and tick-borne pathogens that determines tick vector competence (O'Neal et al., 2020).

Limited information and functional studies about vector insect lipid metabolism are available. Lipids, in the form of sterols or free fatty acids, are the main and essential components of the insect dietary requirements (Canavoso et al., 2001; Toprak et al., 2020). However, insects are not able to synthesize sterols by themselves (Clark and Block, 1959; Jing and Behmer, 2020). During oxidation of the fatty acids (FAs), twice more energy (approximately 9 kcal/g) is released than during the complete oxidation of carbohydrates (approximately 4 kcal/g) (Toprak et al., 2020). The main source of lipids for these invertebrates is host blood. Lipid digestion occurs mainly in the midgut lumen, where lipases (EC 3.1.1.3; the major lipid digestive enzymes) catalyze the hydrolysis of the ester bond in triacylglycerols (TAGs) as well as in di- and monoacylglycerols (DAGs, MAGs) to the final products - glycerol and free fatty acids (FAs) (Derewenda, 1994; Toprak et al., 2020).

In *I. ricinus*, poor understanding of lipid metabolism exists. As mentioned above, digestion of proteins in tick midgut occurs intracellularly in the midgut epithelium cells. Nothing is known about digestion of lipids in ticks and no digestive lipases have been yet functionally characterized in any tick species. Some esterases and lipases involved in the incorporation of the nutrients to the oocytes were identified during embryogenesis in the eggs of the camel tick *Hyalomma dromedarii* (Fahmy et al., 2004). Earlier, Koh et al. (1991) described the utilization of the nutritional reserves stored in the form of lipid droplets in the midgut epithelium cells. These lipids droplets are used for the growth of tissues during feeding in the nymphal stage of hard tick *Haemaphysalis longicornis* (Koh et al., 1991). More recently, it was demonstrated in another tick species *Dermacentor variabilis*, that lipids are also exploited in the course of the long off-host starvation period, during which the large lipid droplets are released and used as the endogenous energy recourses (Rosendale et al., 2018). In the midgut transcriptome of *I. ricinu*s, lipases from several classes have been identified (Perner et al., 2016). Phospholipase A2, acid sphingomyelinase, and lipase (pancreatic-like type) were identified as the most up-regulated lipases in the midgut on the 3rd day of adult

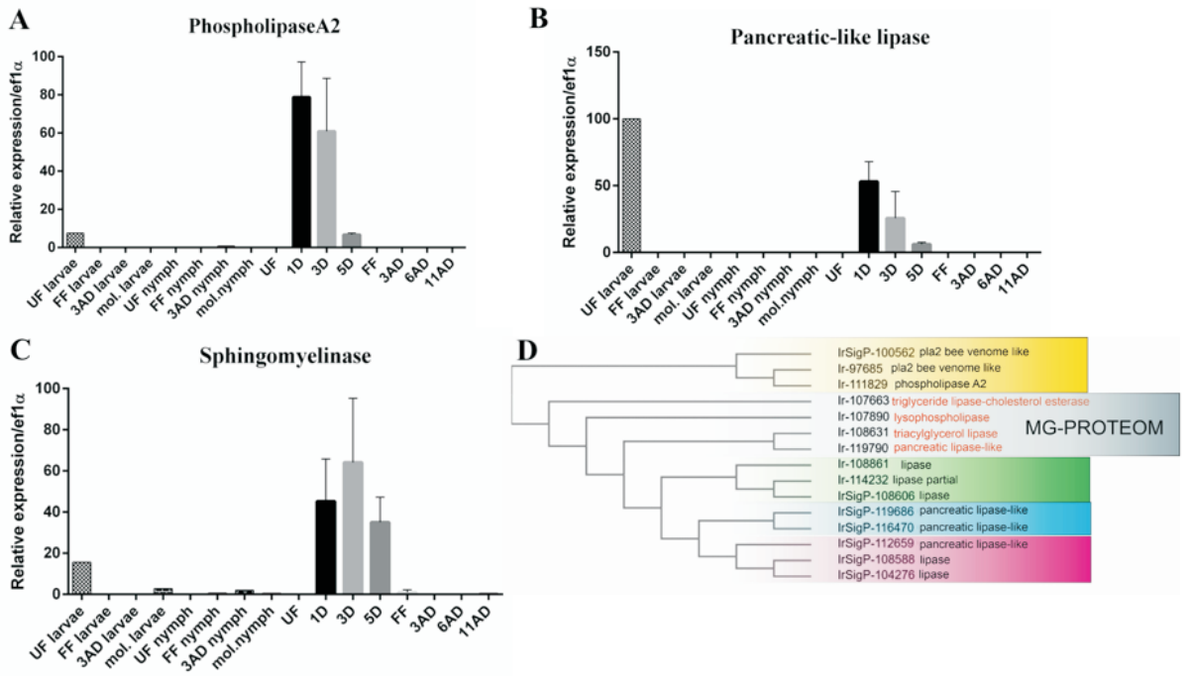


**Figure 1: (A-C) - mRNA expression of individual lipases in the midgut during developmental and feeding stages.** Quantitative real-time PCR (qRT-PCR) profiling of the phospholipase A2 (PlA2), pancreatic-like lipase, and sphingomyelinase. Bars indicate the standard deviation. UF: unfed; 1D,3D, 5D: one, three and five days of feeding; FF: fully fed females; 3AD, 6AD, 11AD: three, six and eleven days after detachment; mol.: molting. **(D) – Phylogenetic three of lipases identified in the midgut transcriptome (Perner et al., 2016a) and in the midgut proteome.** Lipases identified in the midgut proteome are highlighted grey. Phylogenetic tree was performed using ClustalOmega server (https://www.ebi.ac.uk/Tools/msa/clustalo/).

female feeding (Perner et al., 2016). Detailed analysis of these midgut-specific lipases using quantitative real time PCR (qRT-PCR) across tick development revealed that these lipases are mainly expressed during the early stage of adult female feeding (Fig. 1A-C). The RNAi mediated-knockdown (RNAi KD) of individual lipases in adult females did not show any phenotype differences between RNAi KD and control groups (data not shown). Furthermore, in the midgut proteome analysis, either form unfed females or from females fed for five days, only rare lipases were identified (Fig. 1D).

*Acknowledgement: Supported by GACR 21-08826S and ERDFunds (No.CZ.02.1.01/0.0/0.0/16_019/0000759)*

**Canavoso, L.E.**, Jouni, Z.E., Karnas, K.J., Pennington, J.E., Wells, M.A. (2001). Fat metabolism in insects. *Annu Rev Nutr 21, 23-46.*

**Clark, A.J**., Block, K. (1959). The absence of sterol synthesis in insects. J Biol Chem 234, 2578-2582.

**Derewenda, Z.S.** (1994). Structure and function of lipases. *Adv Protein Chem 45:1-52.*

**Fahmy, A.S.,** Abdel-Gany, S.S., Mohamed, T.M., Mohamed, S.A. (2004). Esterase and lipase in camel tick Hyalomma dromedarii (Acari: Ixodidae) during embryogenesis. Comp Biochem Physiol B Biochem Mol Biol 137, 159-168.

**Jing, X.,** Behmer, S.T. (2020). Insect Sterol Nutrition: Physiological Mechanisms, Ecology, and Applications. Annu Rev Entomol 65, 251-271.

**Koh, K.,** Mori, T., Shiraishi, S., Uchida, T.A. (1991). Ultrastructural changes of the midgut epithelial cells in feeding and moulting nymphs of the tick Haemaphysalis longicornis. Int J Parasitol 21(1):23-36.

**O'Neal, A.J.**, Butler, L.R., Rolandelli, A., Gilk, S.D., Pedra, J.H. (2020). Lipid hijacking: a unifying theme in vector-borne diseases. *Elife 9.*

**Perner, J.,** Provazník, J., Schrenková, J., Urbanová, V., Ribeiro, J.M., Kopáček, P. (2016). RNA-seq analyses of the midgut from blood- and serum-fed Ixodes ricinus ticks. Sci Rep 6:36695.

**Rosendale, A.J.,** Dunlevy, M.E., McCue, M.D., Benoit, J.B. (2018). Progressive behavioural, physiological and transcriptomic shifts over the course of prolonged starvation in ticks. Mol Ecol 28(1):49-65.

**Sonenshine, D.E.** (1991). Biology of ticks. *Oxford University Press*, New York. First ed., Vol. 1.

**Toprak, U.**, Hegedus, D., Dogan, C., Guney, G. (2020). A journey into the world of insect lipid metabolism. *Arch Insect Biochem Physiol 104, e21682.*

SL13

# STRUCTURAL STUDIES OF Si3 ENDOLYSIN MUTANTS

**D. Peramotava[1], P. Grinkevich[1], I. Kutá Smatanová[1], Daria. V. Vasina[2], T. Prudnikova[1]**

*[1]University of South Bohemia in České Budějovice, Branišovská 1760, 370 05 České Budějovice, Czech Republic*

*[2]Laboratory of Pathogen Population Variability Mechanisms, N. F. Gamaleya National Research Center for Epidemiology and Microbiology, 18 Gamaleya St., 123098 Moscow, Russia*

*daschaperemotova@gmail.com*

For more than half a century, antibiotics have been used as the most common tool in the fight against infectious diseases. However, due to the misuse and overuse of these substances, an increasing number of bacteria are emerging that are completely resistant to all currently known antibiotics (multidrug resistant). The emergence of these types of bacteria renders most, if not all, available antibiotics ineffective. This situation is a global health crisis that threatens effective prevention and control of ever-increasing infectious diseases. This crisis is also exacerbated by increasingly sophisticated development new antibiotics.

A way out of this crisis may be the use of novel substances in the fight against infectious diseases. One of the potential candidates are endolysins. These enzymes, originally derived from bacteriophages, are peptidoglycan hydrolases that destroy bacterial cell wall. They have high specificity, much higher capability and efficiency, and also have not been found to develop resistance [1, 2]. An extremely fast and efficient lysis of peptidoglycan leads to a

**Table 1.** Selected data collection statistics

| Parameters | lysECD7-SMAP | lysAAA | LysHE |
|---|---|---|---|
| Resolution (Å) | 1.70 | 1.43 | 2.00 |
| Average unit cell (*a, b, c* Å; $\alpha = \beta = \chi$ (°) | 48.66, 58.03, 196.63<br>90.00 | 66.307, 76.548, 65.633<br>90.00 | 48.183, 66.381, 119.26<br>90.00 |
| Space group | $P2_12_12_1$ | $C222_1$ | $P22_12_1$ |
| Number of molecules in asymmetric unit | 4 | 1 | 2 |
| R | 0.216 | 0.166 | 0.183 |
| $R_{free}$ | 0.260 | 0.204 | 0.221 |

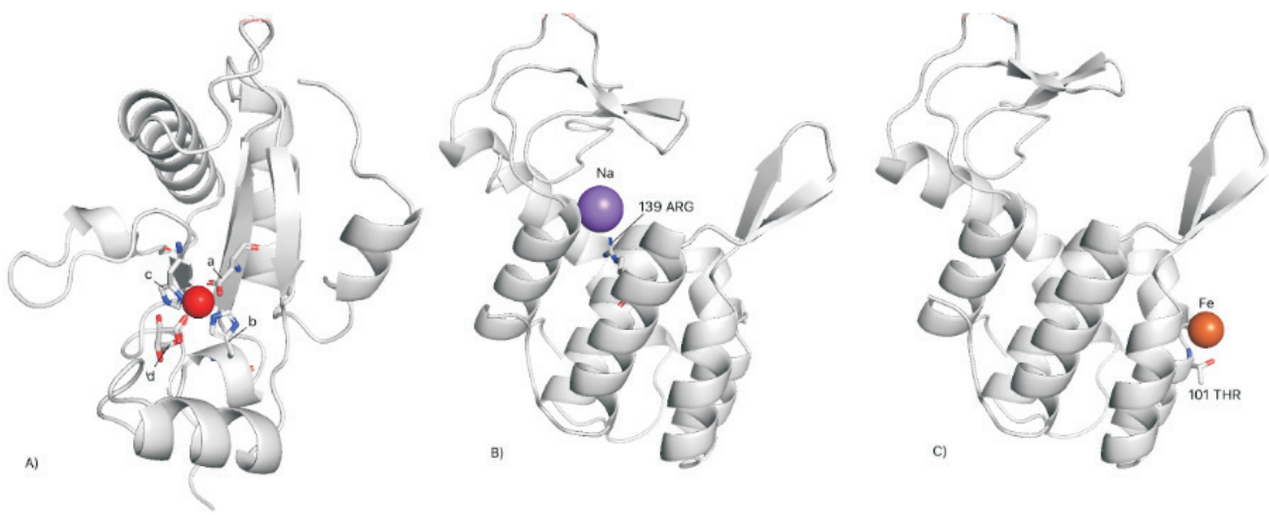


**Figure 1.** Secondary structures of Si3 mutants. A) the lysECD7-SMAP mutant molecule has a Zn atom (red ball) that is stabilized by amino acids 62 HIS (a), 69 ASP (b) and 117 HIS (c). Also shown is a glycerol molecule (d) located in the region of the Zn atom; B) lysAAA mutant with Na ion (purple ball); C) lysHE mutant, the structure contains the Fe ion (orange ball).

sudden drop in turgor pressure and osmotic lysis, causing bacterial cell death [3]. The most important aspect for us is how molecular engineering can be used to change lytic spectrum of endolysins [4].

The aim of our work was to obtain crystals of three Si3 endolysin mutants (lysAAA, lysHE and lysECD7-SMAP), followed by the study of their structure.

In the course of the work carried out, we obtained crystals of high diffraction quality for all three mutants presented above, which allowed us to study their structure in sufficient detail. X-ray diffraction data wore collected at BESSY II, Helmholtz Zentrum Berlin and processed used XDS-app and CCP4 software. The main statistical parameters are given in Table 1.

As can be seen from Figure 1, the structure of the lysECD7-SMAP mutant is fundamentally different from the structures of the lysAAA and lysHE mutants, which, in turn, are similar to each other. It is worth noting separately the presence of different metal atoms in the structure of each molecule; however, only in the lysECD7-SMAP mutant is the Zn atom stabilized by amino acid residues. ECD7-SMAP mutant has a 19-amino-acid C-terminal tail which changes overall conformation that may impact its enzymatic activity. It is, therefore, our main focus of further structural studies.

1. López, R.; García, E.; García, P., *Drug Discovery Today: Therapeutic Strategies*, **1**, 2004, pp 469–474;
2. Fischetti, V.A., *Trends Microbiology*, **13**, 2005, pp 491–496;
3. Vollmer, W.; Biochimica et Biophysica Acta (BBA) – Biomembranes, 1778, 2008, pp 1714–1734;
4. Kashani, H.H., Schmelcher, M., Sanzalipoor, H., Hosseini, E.S.Moniri, R., *Clin. Microbiol. Rev*., **31**, 2018, e00071-17.

**SL14**

## MOLECULAR, BIOCHEMICAL AND STRUCTURAL CHARACTERIZATION OF SECRETED FERRITIN II FROM *IXODES RICINUS*

**Anna Koutská[1], Petra Havlíčková[1], Ivana Kutá Smatanová[1], Zdeněk Franta[1] and Petr Kopáček[2*]**

*[1]Institute of Chemistry, Faculty of Science, University of South Bohemia, Branišovská 1760, České Budějovice, Czech Republic*
*[2]Institute of Parasitology, Biology Center of the Czech Academy of Sciences, České Budějovice, Czech Republic*
*kopajz@paru.cas.cz*

Ferritin is a ubiquitous protein with crucial role in tick biology. Ticks digest large amounts of host blood and are exposed to an enormous amount of free iron, which has to be treated properly to avoid its toxicity. Two types of ferritin were discovered in the tick *Ixodes ricinus* – tagged as ferritin I and ferritin II [1]. Ferritin I is a globular protein composing 24 subunits (25kDa each) and forming a hollow-sphere complex [2, 3]. Ferritin I functions as an intracellular scavenger of potentially toxic free iron and is capable to sequester up to 4 500 iron atoms [2]. The function of ferritin II is not entirely clear, but it probably plays a role in the transport of non-heme iron between the tick gut and the peripheral tissues. Silencing of ferritin II using RNA interference had a detrimental effect on tick development and reproduction [1]. The vaccination of mammalian hosts with recombinant ferritin II revealed its promising potential as an efficient anti-tick vaccine [4].

This study focus on the molecular, biochemical and structural characterization of ferritin II from *Ixodes ricinus.* We have cloned ferritin II into two *E. coli* expression vectors (pET-SUMO and pASK-37+), optimized its production in various expression cells and conditions (e.g., temperature, times and concentrations of inducer). Further, we will focus on improving the protein solubility and its purification in order to get sufficient amounts of pure recombinant ferritin II for following structural and biochemical studies.

1. Hajdusek, O., Sojka, D., Kopacek, P., Buresova, V., Franta, Z., Sauman, I., Winzerling, J., & Grubhoffer, L. (2009). Knockdown of proteins involved in iron metabolism limits tick reproduction and development. Proceedings of the National Academy of Sciences of the United States of America, 106(4).
2. Pham, D. Q., & Winzerling, J. J. (2010). Insect ferritins: Typical or atypical? Biochimica et biophysica acta, 1800(8), 824–833.3. H. J. Bunge, *Texture Analysis in Materials Science*. London: Butterworth. 1982.
3. Kopáček, P., Zdychová, J., Yoshiga, T., Weise, C., Rudenko, N., & Law, J. H. (2003). Molecular cloning, expression and isolation of ferritins from two tick species—Ornithodoros moubata and Ixodes ricinus. Insect biochemistry and molecular biology, 33(1), 103–113.
4. Hajdusek, O., Almazán, C., Loosova, G., Villar, M., Canales, M., Grubhoffer, L., Kopacek, P., & de la Fuente, J. (2010). Characterization of ferritin 2 for the control of tick infestations. Vaccine, 28(17), 2993–2998.

*This research is supported by the Czech Science Foundation (GACR 21-08826S) and ERDF CZ.02.1.01/0.0/0.0 /15_003/0000441.*

**Session IV**

**SL15**

# $Zn^{2+}$ TO $Ni^{2+}$ EXCHANGE IN Zn-DEPENDENT S1 NUCLEASE

**J. Hrubý[1,2], P. Kolenko[1,2], K. Adámková[2,3], B. Husťáková[2,3], M. Malý[1,2], L. H. Østergaard[4], T. Kovaľ[2], J. Dohnálek[2]**

[1]*Czech Technical University in Prague, Břehová 7, 115 19 Prague, Czech Republic*
[2]*Institute of Biotechnology of the Czech Academy of Sciences, Biocev, Průmyslová 595, Vestec,*
[3]*University of Chemical and Technology Prague, Technická 5, Prague, Czech Republic*
[4]*Dept. of Agile Protein Screening, Novozymes A/S, Krogshoejvej 36, Bagsvaerd, Denmark*
*hrubyj18@fjfi.cvut.cz*

The single-strand-specific S1 nuclease from *Aspergillus oryzae* is a metalloenzyme with a widespread use for biochemical analysis of nucleic acids [1,2]. It is a globular protein with a secondary structure composed mainly of α-helices (Fig. 1). Its activity depends on the presence of three $Zn^{2+}$ ions in the active site: Two $Zn^{2+}$ ions of the cluster are buried at the bottom of the active site, while the third $Zn^{2+}$ ion is closer to the surface of the nuclease. The core of the active site is composed of nine residues coordinating the zinc cluster.

We studied the possibility of replacing $Zn^{2+}$ with $Ni^{2+}$ using the X-ray anomalous dispersion and other biophysical assays. The mixture of deglycosylated S1 nuclease, chelating agent ethylenediaminetetraacetic acid and $NiCl_2$ in a molar ratio of 1: 5: 10, respectively, was crystallized using the vapor diffusion method. The obtained crystals were of sufficient quality for the diffraction experiment on the synchrotron radiation source Bessy II, Helmholtz Zentrum Berlin [3].

The diffraction data were collected at three different X-ray energies with the aim of detecting the presence of metals using anomalous scattering. Key data collection statistics are summarized in Tab. 1. The obtained anomalous difference maps (Fig. 2) confirmed the exchange of one $Zn^{2+}$ ion by $Ni^{2+}$ at the position M3 closest to the enzyme surface, while the other two $Zn^{2+}$ ions of the core (positions M1 and M2) remained unaffected. Despite the ion exchange, the residues of the active site and its surroundings are structurally conserved.

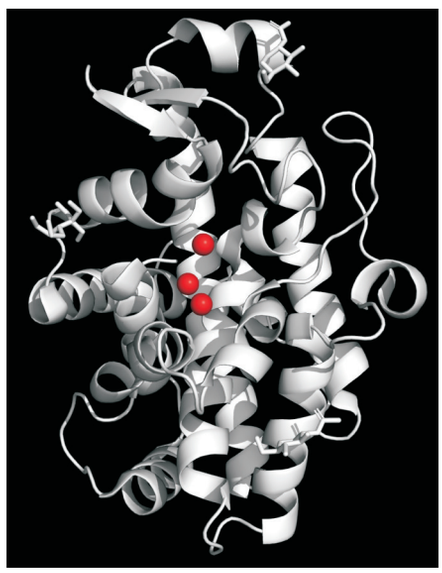

**Figure 1**. Secondary structure of S1 nuclease (PDB ID 5FB9). Zinc ions are represented using spheres. Graphics created using PyMOL [4].

1. T. Koval', L. H. Oestergaard, J. Lehmbeck, A. Nřrgaard, P. Lipovová, J. Dušková, T. Skálová, M. Trundová, P. Kolenko, K. Fejfarová, J. Stránský, L. Švecová, J. Hašek, J. Dohnálek, *PLoS ONE*, **11**, 2016, e0168832.
2. T. Koval', J. Dohnálek, *Biotechnology Advances*, **36**, 2018, pp. 603-612.

**Table 1**: Selected data collection statistics

| | |
|---|---|
| Space group | $P\ 2_12_12_1$ |
| X-ray energy (Ni-low ; Ni-peak ; Zn-peak) [keV] | 8.320 ; 8.346 ; 9.665 |
| Resolution [Å] | 1.6 |
| Rmerge (Ni-low ; Ni-peak ; Zn-peak) | 0.072 ; 0.075 ; 0.154 |
| Mean I/σ (Ni-low ; Ni-peak ; Zn-peak) | 28.8 ; 27.2 ; 15.8 |
| Avg. anomalous multiplicity | 13 |
| Completeness [%] | 98.9 |

3. U. Mueller, R. Foerster, M. Hellmig, F. U. Huschmann, A. Kastner, P. Malecki, S. Puehringer, M. Roewer, K. Sparta, M. Steffien, M. Uehlein, P. Wilk, M. S. Weiss. *The European Physics Journal Plus*, **130**, 2015, pp. 141/1-10.

4. L. Schrödinger, W. DeLano, PyMOL, 2020, available from: http://pymol.org/pymol.

5. P. Emsley, B. Lohkamp, W. G. Scott, K. Cowtan, *Acta Crystallographica Section D*, **66**, 2010, pp. 486 – 501.

*This work was supported by the MEYS CR (projects CAAS – CZ.02.1.01/0.0/0.0/16_019/0000778 and ELIBIO – CZ.02.1.01/0.0/0.0/15_003/0000447) from the ERDF fund, by the Czech Academy of Sciences (grant No. 86652036), and by the GA CTU in Prague (SGS22/114/OHK4/2T/14). We acknowledge CMS- BIOCEV Crystallization and Diffraction, part of Instruct-ERIC, supported by the MEYS CR (LM2018127).*

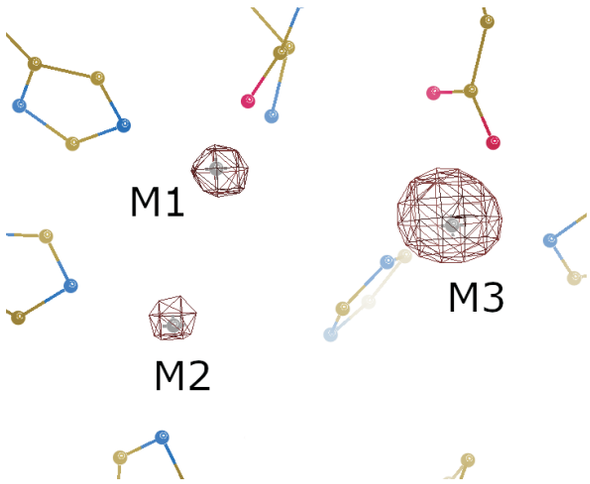


**Figure 2.** Anomalous difference map (data set Ni-peak) at a level of 10 σ. Significant peak at the position M3 proves the presence of Ni. Graphics created using Coot [5].

**SL16**

## STRUCTURAL INSIGHT INTO ANTIBIOTIC-INACTIVATING ENZYME FROM *STENOTROPHOMONAS MALTOPHILIA*

**M. Malý[1,2], P. Kolenko[1,2], J. Dušková[1], T. Kovaľ[1], T. Skálová[1], M. Trundová[1], J. Stránský[1], L. Švecová[1], K. Adámková[1,3], B. Husťáková[1,3], J. Dohnálek[1]**

[1]*Institute of Biotechnology of the Czech Academy of Sciences, Biocev, Průmyslová 595, Vestec*
[2]*Czech Technical Univ. in Prague, Fac. of Nuclear Sciences and Physical Engineering, Břehová 7, Prague*
[3]*Univ. of Chemical and Technology Prague, Dep. of Biochemistry and Microbiology, Technická 5, Prague*
*martin.maly@ibt.cas.cz*

*Stenotrophomonas maltophilia* is an opportunistic bacterial pathogen responsible for a serious number of infections globally. It exhibits broad antibiotic resistance that has been further extended via the acquisition of antibiotic-resistance genes and mutations [1]. We carried out a bioinformatic analysis of its sequenced genomes to investigate not yet characterised antibiotic-inactivating enzymes.

Several chosen proteins were expressed in *Escherichia coli* strain Lemo21 (DE3) and purified using Ni-NTA and size-exclusion chromatography. Their proposed function – enzymatic modification of antibiotics – was inspected with an activity assay. The enzyme with the confirmed activity was successfully crystallized and diffraction patterns were collected. The data exhibited serious anisotropy: a resolution cutoff determined in *Aimless* [2], according to the criterion of $CC_{1/2} > 0.30$, varied from 2.43 Å to 1.92 Å in different reciprocal space directions. Thus, the data were corrected with *STARANISO* [3]. After the solution of the phase problem in *MoRDa* [4], the model was refined in *REFMAC*5 [5]. The choice of the anisotropic high-resolution diffraction limit (1.88 Å) was confirmed with paired refinement in *PAIREF* [6].

The solved X-ray crystal structure reveals an atomic arrangement of the putative substrate-binding pocket that allows further structural analysis (*in silico* or *in vitro*) of complexes with potential inhibitors or antibiotic substrates. The overall fold is very close to the tetracycline destructases [7] or the reductase involved in the abyssomicin biosynthesis pathway [8]. However, the putative active site differs significantly. Our study leads to a better understanding of the involvement of this enzyme in the antibiotic resistance and could contribute to the development of new strategies of antibiotic therapies. Remarkably, the solved structure is composed of a homodimer linked with two disulfides. Nevertheless, further investigation using small-angle X-ray scattering, mass spectrometry

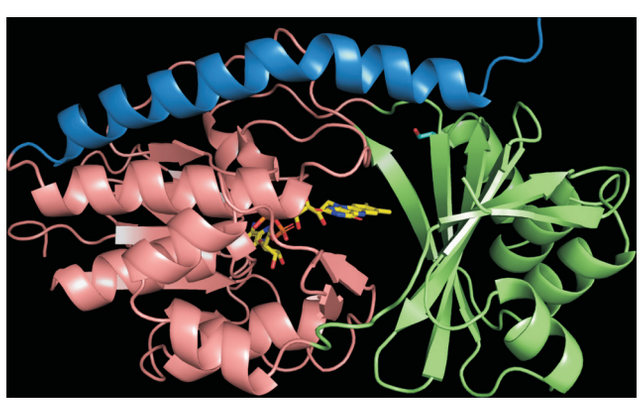

**Figure 1**. Overall structure of the antibiotic-inactivating enzyme from *Stenotrophomonas maltophilia* in secondary structure representation. Flavin adenine dinucleotide (FAD) is shown in stick representation in yellow. The substrate-binding domain is coloured in green, the FAD-binding domain in pink and the C-terminal helix in blue.

and dynamic light scattering showed that the protein is monomer in solution.

1. T. Gil-Gil, J. L. Martínez, P. Blanco, *Expert Review of Anti-infective Therapy*, **18**, (2020), pp. 335-347.
2. P .R. Evans, G. N. Murshudov, *Acta Cryst., D***69**, (2013), pp. 1204-1214.
3. I. J. Tickle, C. Flensburg, P. Keller, W. Paciorek, A. Sharff, C. Vonrhein, G. Bricogne. (2018). STARANISO (http://staraniso.globalphasing.org/cgi-bin/staraniso.cgi). Cambridge, United Kingdom: Global Phasing Ltd.
4. A. Vagin, A. Lebedev, *Acta Cryst., A***71**, (2015), s19.
5. G. N. Murshudov, P. Skubak, A. A. Lebedev, N. S. Pannu, R. A. Steiner, R. A. Nicholls, M. D. Winn, F. Long, A. A. Vagin, *Acta Cryst., D***67**, (2011), pp. 355-367.
6. M. Malý, K. Diederichs, J. Dohnálek, P. Kolenko, *IUCrJ*, **7**, (2020), 681-692.
7. J. L. Markley, T. A. Wencewicz, *Frontiers in microbiology*, **9**, (2018), 1058.
8. J. A. Clinger, X. Wang, W. Cai, Y. Zhu, M. D. Miller, C. G. Zhan, S. G. Van Lanen, J. S. Thorson, G. N. Phillips Jr., *Proteins*. **89**, (2021), pp. 132-137.

*This work was supported by the MEYS CR (projects CAAS – CZ.02.1.01/0.0/0.0/16_019/0000778, BIOCEV – CZ.1.05/1.1.00/02.0109, and ELIBIO – CZ.02.1.01/0.0/0.0 /15_003/0000447) from the ERDF fund; by the Czech Academy of Sciences (86652036); by the GA CTU in Prague (SGS22/114/OHK4/2T/14); by the Czech Science Foundation (20-12109S); and from the grant of Specific university research (A1_FPBT_2021_003). We acknowledge CMS-Biocev (Biophysical techniques, Crystallization, Diffraction, Structural mass spectrometry) supported by MEYS CR (LM2015043 and LM2018127).*

**SL17**

# STRUCTURAL STUDIES OF HUMAN PURINE NUCLEOSIDE PHOSPHORYLASE AND CYCLIN-DEPENDENT KINASE 2 INHIBITORS

**S. Djukic[1], J. Skácel[1], J. Brynda[1,2], P. Pachl[1], T. Vučková, M. Fábry [2], M. Rumlová[3], T. Bílek[1,3], J. Voldřich[1,3], H. Mertlíková-Kaiserová[1], Z. Janeba[1], J. Škerlová[1], M.Peřina[4], R.Jorda[4], V. Kryštof[4], P. Řezáčová[1,2]**

*[1]Institute of Organic Chemistry and Biochemistry, AS CR, Prague 6, Czech Republic*
*[2]Institute of Molecular Genetics, AS CR, Prague 4, Czech Republic*
*[3]University of Chemical Technology, Prague 6, Czech Republic*
*[4]Department of Experimental Biology, Faculty of Science, Palacky University Olomouc, Czech Republic*
*Stefan.dukic@uochb.cas.cz*

Purine nucleoside phosphorylase (PNP) represents one of the key enzymes of the purine salvage pathway, which is considerably more energy-efficient than *de novo* pathway. It hydrolyses ribose from inosine and guanosine in the presence of an inorganic phosphate, producing hypoxanthine and guanin which can then be recycled trough the salvage pathway or be further degraded to uric acid. PNP's activity is increased during processes which require rapid cell division and proliferation, which makes it a target in treatment of different types of cancer, autoimmune and other conditions in human, as well as treatment for different parasitic diseases such as tuberculosis (caused by *Mycobacterium tuberculosis)* where PNP is essential during transition from latent to active infection. Both human and Mtb PNP are trimers with three active sites. Even though there is a small sequence similarity, overall fold and active site are conserved which presents a challenge in design of selective inhibitors [1,2].

Cyclin-dependent kinase 2 (CDK2) is a Ser/Thr protein kinase that is active during G1 and S phase of the cell cycle and works as check point control. During the G1 phase of the cell cycle, it is activated by binding to cyclin E and in S phase by binding to cyclin A [3]. It is dispensable in healthy cells, as other CDKs can take over its role, but it is essential for proliferation of cancer cells. This makes CDK2 an interesting target in discovery of anticancer compounds [4].

We utilize X-ray crystallography in the structure-based drug discovery approach.

Enzymes were prepared by heterologous expression in *E. coli* and purified in high yields and purity necessary for crystallographic studies. Crystallization conditions for all three enzymes were identified through wide screening and optimization. Diffraction data have been collected on BL14.1 at the BESSY II electron storage ring operated by the Helmholtz-Zentrum Berlin and crystal structures were determined at high resolution (Figure1).

The knowledge of binding properties of these inhibitors will provide us crucial information which will be used to further optimize affinity and selectivity of both PNP and CDK2 inhibitors.

1. Nyhan, W. L. Encyclopedia of life sciences 2005, John Wiley & Sons, Ltd.
2. Bzovska, A, Kulikovska, E., Shugar, D. Pharmacology and Therapeutics., 88 (3) 2000, 349-425.
3. Echalier A, Endicott JA, Noble ME: Biochimica et Biophysica Acta (BBA) - Proteins and Proteomics 2015, 1804 (3): 511–9
4. Wood DJ et al. Cell Chemical Biology. 2018; 26 (1): 121–130.e5.
5. Dayal N et al. J Med Chem 2021; https://doi.org/10.1021/acs.jmedchem.1c00330.

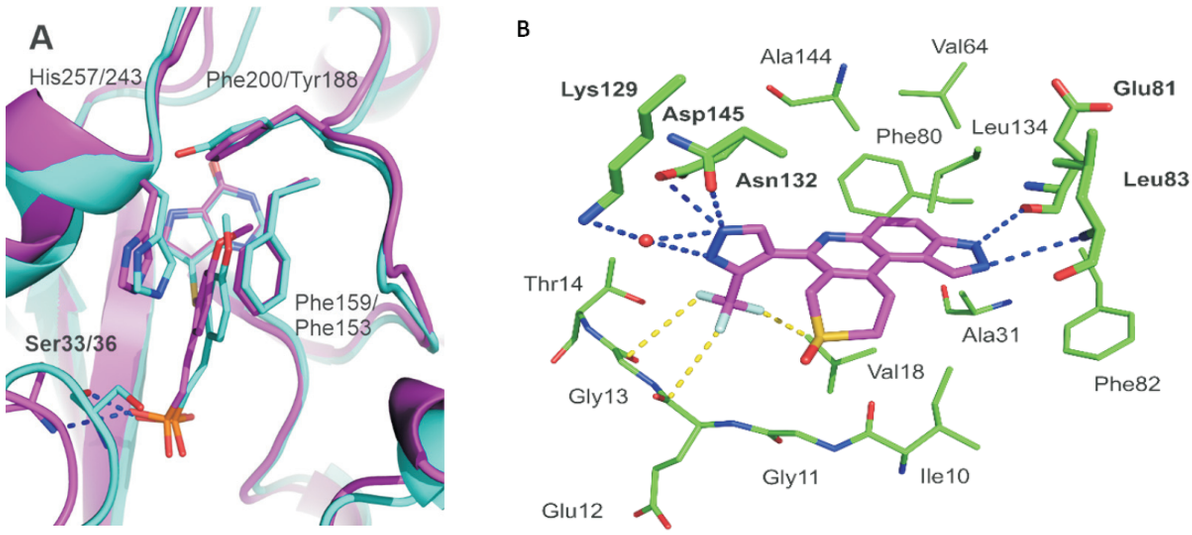


**Figure1. A)** Overlay of structures of human PNP (magenta) and Mtb PNP (cyan) in complex with one of the inhibitors. **B)** Active site of CDK2 in complex with an inhibitor [5].

**SL18**

## STRUCTURAL TRANSITION OF THE SALIVARY SERPIN FROM *IXODES RICINUS* TICK

**Barbora Kascakova[1], Jan Kotal[2, 3], Petra Havlickova[1], Tatyana Prudnikova[1], Pavel Grinkevich[1], Michal Kuty[1], Jindrich Chmelar[2*] and Ivana Kuta Smatanova[1*]**

*[1] Dep. of Chemistry, Faculty of Science, Univ. of South Bohemia in Ceske Budejovice, 37005, Czech Rep.*
*[2] Department of Medical Biology, Faculty of Science, University of South Bohemia in Ceske Budejovice, 37005, Czech Republic*
*[3] Institute of Parasitology, Biology Centre of the Czech Academy of Sciences, Ceske Budejovice, 37005, Czech Republic*
**ivanaks@seznam.cz*

Serpins are a large superfamily of structurally conserved protease inhibitors that are widely distributed in nature [1]. A structural study of serpins found in tick saliva revealed members' uniformity of structure but not their functions. This group of proteins has primarily immunological and haemostatic functions, but their functions can vary according to their specificity. The tick serpins act as modulators of immune responses by using their anti-coagulation, and anti-complementary functions and play role in immunosuppression [2].

The structural transition to the different conformation is required for inhibitory activity. The secondary structure typically consists of 3 β-barrels, 7-9 α-helices and an exposed, flexible reactive center loop that acts as proteinase "bait". There are different types of conformation and each of these structural rearrangements is important in the inhibitory pathway. The serpins are irreversible inhibitors that adapt the suicide substrate mechanism [3].

Iripin-4 with hitherto unexplained function, crystallized in two different structural conformations. The native structure was solved at 2.3A resolution and the structure of cleaved conformation at 2.0A resolution. Furthermore, structural changes during the reactive-centre loop transition from native to cleaved conformation were observed. In addition to this finding, we confirm that the main substrate-recognition site for the inhibitory mechanism is represented by Glu341. Further research on Iripin-4 should focus on the functional analysis of this interesting serpin.

1. J. Potempa, E. Korzus & J. Travis (1994) *J. Biol. Chem.* **269**, 15957-15960.
2. Ooi, C. P., Haines, L. R., Southern, D. M., Lehane, M. J., & Acosta-Serrano, A. (2015). PLoS Negl. Trop. Dis. 9:e3448. doi: 10.1371/journal.pntd.0003448.
3. P. G. W. Gettins, P. A. Patston & S. T. Olson(eds) (1996) Serpins: Structure, Function and Biology, *Molecular biology Intelligence Unit*, R. G. Landes Co., and Chapman & Hall, Austin, TX

*This research was supported by European Regional Development Fund-Project, MEYS (No. CZ.02.1.01/0.0/0.0/15_003/0000441); by the Grant Agency of the Czech Republic (Grant No. 19-14704Y) and by the Grant Agency of the University of South Bohemia (grant No. 105/2019/P and 04-039/2019/P).*

SL19

# STRUCTURAL AND FUNCTIONAL STUDIES OF TBEV NON-STRUCTURAL PROTEIN 5

**Petra Havlíčková[1], Joel A. Crossley[1], Zdeno Gardian[1, 2], Filip Dyčka[1], Ivana Kutá Smatanová[1] and Zdeněk Franta[1]**

[1] *Institute of Chemistry, Faculty of Science, University of South Bohemia, Branišovská 1760, České Budějovice, Czech Republic*

[2] *Institute of Parasitology, Biology Center of the Czech Academy of Sciences, České Budějovice, Czech Republic*

*zfranta@prf.jcu.cz*

Tick-borne encephalitis virus (TBEV) is a major human pathogen, transmitted by ticks from family Ixodidae. TBEV is an enveloped virus with a ~ 11 kb positive-sense single-strand RNA genome, encoding a single 375 kDa polyprotein. During the infection, the polyprotein is cleaved into three structural and seven non-structural (NS) proteins. While structural proteins are involved in the assembly of new virions, non-structural proteins are responsible for the virus replication [1].

NS5 is a large conserved protein comprising of two domains connected by a highly flexible linker, which is important for the activity as well as for the overall shape of the protein. N-terminal methyltransferase (MTase) domain is involved in the capping process. C-terminal RNA-dependent RNA polymerase (RdRp) is crucial for virus replication [2].

This project focuses on structural and functional studies of TBEV NS5 protein. Various constructs were designed – NS5 full length, RdRp domain and MTase domain. Expression and purification of individual constructs have been optimized and pure samples were used for initial crystallization screening, cryo-EM analysis and functional assays.

So far, we have obtained cryo-EM data for RdRp domain, using Titan Krios equipped with Falcon 4 camera and Relion processing pipeline yielded a reconstruction of 6Å resolution. Tiny protein crystals of RdRp grew in several crystallization conditions. Furthermore, we have carried out fluorescence-based binding and activity assays with TBEV RdRp as well as DENV RdRp, that revealed revealed substrate affinity and specificity.

1. Mackenzie, J. (2005). Traffic. 6, 967-977.

2. Bollati, M. et al. (2009). Antiviral Res. 87, 125-148.

*This research is supported by ERDF No. CZ.02.1.01/0.0/0.0/15_003/000041.*

SL20

# INVESTIGATION OF THE $R_{WP}$ FACTOR AND ENERGY OF PARACETAMOL CRYSTAL STRUCTURE

**Milan Kočí[1] and Jan Drahokoupil[1, 2]**

[1]*Department of Solid State Engineering, Faculty of Nuclear Science and Physical Engineerging, Czech Technical University in Prague, Trojanova 13, Prague*
[2]*Department of Material Analysis, Institute of Physics, Czech Academy of Science, Na Slovance 1999/2, Prague*

The combination of energy evaluation of crystal structure and powder diffraction data may successfully be used in structure determination. Using only powder diffraction factors (e.g. $R_{wp}$ factor) cannot guarantee finding reasonable crystal structure. Some structures with acceptable $R_{wp}$ factor are physically unrealistic because their atoms are too close to each other. This problem can be solved by setting restrains to atomic distances or by calculating the energy of the system. We use the energy evaluation because it can tell us not only which structure is unrealistic but also which structure is more preferred in nature. The energy of the crystal structure can be calculated in two ways - by Molecular Mechanics (MM) or by Density Functional Theory (DFT). MM is based on substitution to the preset mathematical relation so it is fast to compute (compared with DFT). The advantage of DFT is its accuracy. MM was used in our work. We expect that MM could be used to speed up the convergence of structure determination and DFT could be used for the final validation of the structures. The crystal structure can be predicted only with energy evaluation.

Another possibility of speeding the structure determination up is to use optimizing algorithms. For example global optimizing algorithm simulated annealing is used in program Dash [1] and parallel tempering and also simulated annealing are used in program FOX [2]. The diffraction pattern data can be combined with the energy value of the structure to new cost function which we minimize. The usage of the combination of powder diffraction data and energy evaluation can accelerate the structure determination, help to avoid wrong solutions of the crystal structure, or tell us more information about the determined structure (e.g. if it could be a metastable structure of the material).

We made the examination of energy and $R_{wp}$ functions on the structure parameter was made. For simplicity, we used only three structure parameters and made cuts through the hypersurface of the functions. We made the examination of energy and $R_{wp}$ factor of the crystal structure of paracetamol with two or three deviated parameters. To gain pictures of the hypersurface of the $R_{wp}$ and the energy function of paracetamol it must be done cuts through the hypersurface. Our hypersurface has six parameters: $\Delta x$, $\Delta y$, $\Delta z$, $\Delta\alpha$, $\Delta\beta$ and $\Delta\gamma$. These parameters correspond to motion parameters of the molecule of paracetamol - $\Delta x$ means deviation of the molecule in the direction of lattice vector $\vec{a}$, similarly $\Delta y$ is the deviation of the molecule in direction of $\vec{b}$ and $\Delta z$ is the deviation of the molecule in direction of $\vec{c}$; $\Delta\alpha$ means rotational deviation of the molecule about the molecule's own Axis 1, similarly $\Delta\beta$ is the rotational deviation of the molecule about the molecule's Axis 2 and $\Delta\gamma$ is the rotational deviation of the molecule about the molecule's own Axis3 (in the Figure 1 there are the translational degrees of freedom; in Figure 2 there are the rotational degrees of freedom). We chose three degrees of freedom i.e. $\Delta x$; $\Delta\gamma$; $\Delta y$ as parameters which we deviated from the crystal structure.

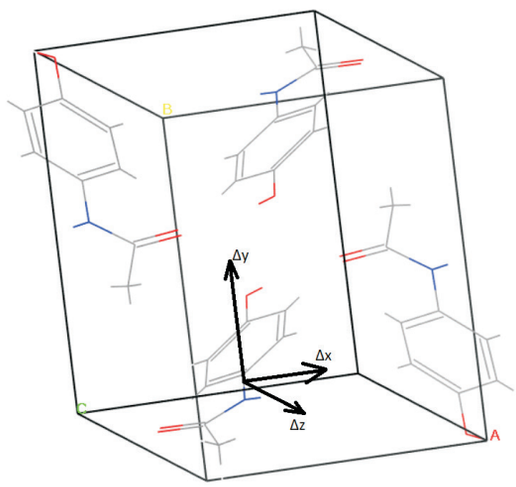


**Figure 1.** Crystal structure of paracetamol with illustrated translational degrees.

We made three cuts though the $R_{wp}$ function hypersurface. The parameters $\Delta x$ and $\Delta\gamma$ went through all their possible combinations and parameter $\Delta y$ was set consecutively to 0.0 Å, 0.5 Åand 2.0 Å.

The diffraction pattern was obtained by simulating the diffraction pattern of paracetamol crystal structure [3] in

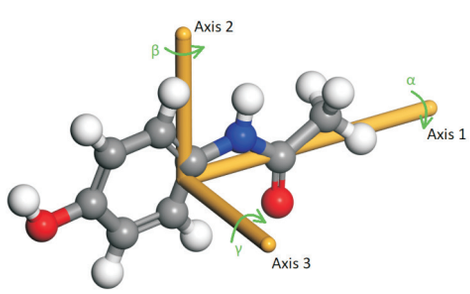


**Figure 2.** The molecule of paracetamol with illustrated rotational degrees of freedom.

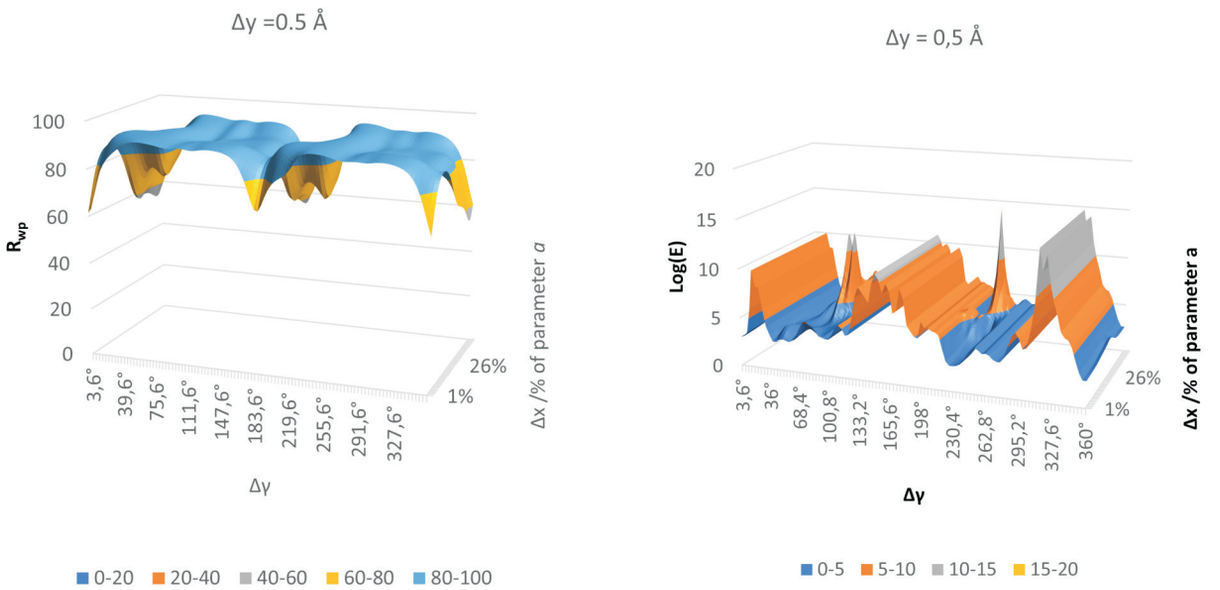


a) b)

**Figure 3**. Cut through paracetamol $R_{wp}$ function hypersurface (3a). The hypersurfaces were cut in Δx and Δγ degrees of freedom and Δy = 0.5 Å. The local minimum can be observed at 180 °Δγ in Figure 3a. In energy cut the local minimum at 180 °Δγ is not.

the program Materials Studio in the module Reflex. The parameters of diffraction were set: the refinement method Rietveld, convergence quality Medium, the range of diffraction pattern from 5 to 45 °2θ with step 0.015° 2θ, Bragg-Brentano instrumental geometry, zero-point shift 0.013, Pseudo-Voigt profile function, profile parameters U = 0.02192; V = -0.01152; W = 0.00788; $N_A$ = 0.1615; $N_B$ = -0.00075. The other diffraction patterns were simulate with the same settings of the module. The energy was calculated with the program Materials Studio, too Module Forcite was chosen because it can quickly compute the energy of the structure (it uses Molecular Dynamics). The parameters were set to compute only the energy of the structure, use forcefield COMPASS [4, 5, 6], quality was set to Ultra-fine, charges were assigned by the forcefield and summation methods were made atom-based.

We have found some interesting results which the $R_{wp}$ function follow with changes of structure parameters. The first one is that when the molecule rotates there are not many local minima in the $R_{wp}$ function and the second one is that when the molecule is translated there is only one - global minimum in the $R_{wp}$ function. In energy hypersurface, there are significantly more local minima and local maxima. From this view we can easily recognize the structures with too high energy and discard them instead of optimizing them. The cut through hypersurface of $R_{wp}$ function is plotted in Figure 3a. The cut through hypersurface of the energy function is plotted in Figures 3b. When comparing these two cut there is a local minimum in $R_{wp}$ function at 180°Δγ but in the energy function at 180°Δγ the local minimum is not. So the energy evaluation can help us to avoid searching the structure with this parameter set.

*Computational results were obtained by using Dassault Systèmes BIOVIA software programs. BIOVIA Materials Studio was used to perform the calculations and to generate the graphical results. This work was supported by the Grant Agency of the Czech Technical University in Prague, grant No. SGS22/183/OHK4/3T/14.*

1. David W. I. F., Shankland K., Van de Streek J., Pidcock E., Motherwell W.D. S., Cole J. C. DASH: A program for crystal structure determination frompowder diffraction data *J. Appl. Cryst*., **39**, 910-915 (2006).
2. Favre-Nicolin V., Cerny V. FOX, free objects for crystallography: a modular approach to ab initio structure determination from powder diffraction *J. Appl. Cryst.* **35**, 734-743 (2002).
3. Nichols C., Frampton C. S. CCDC 135451: Experimental Crystal Structure Determination (2000).
4. Sun, H. COMPASS: An ab Initio Forcefield Optimized for Condensed-Phase Applications - Overview with Details on Alkane and Benzene Compounds, *J. Phys. Chem. B*, **102**, 7338 (1998).
5. Sun, H.; Ren, P.; Fried, J. R. The COMPASS Forcefield: Parameterization and Validation for Polyphosphazenes *Comput. Theor. Polym. Sci.*, **8**, 229 (1998).
6. Rigby, D.; Sun, H.; Eichinger, B. E. Computer simulations of poly(ethylene oxides): Forcefield, PVT diagram and cyclization behavior, *Polym. Int.,* **44**, 311-330 (1998).

**Posters**

**P1**

# HYDROTHERMAL CONVERSION OF CERIUM OXALATE INTO $CeO_2.nH_2O$ OXIDE

**N. Assi, V.Tyrpekl**

*Department of Inorganic Chemistry, Faculty of Science, Charles University, Hlavova, 2030 Prague, Czech Republic*

## 1. Introduction

In the last few decades, various methods were applied for the synthesis of micro and nano structures of metal oxide which consist of precipitation, combustion, ionic liquid route, and sol-gel. The inconveniences presented in these methods such as pH control, the high temperature used, long reaction time and low purity, encouraged the researcher to find the suitable substitution methods. Thermal decomposition methods could be employed as an alternative approach. The utility of thermal decomposition for inorganic salts such as hydroxide, carboxylate, acetate, and oxalate has been extensively used to obtain metal oxides [1].

Oxalate hydrate could be a good precursor for the preparation of metal oxide due to its large quantity mass loss in the hydrothermal process (more than 50 wt %), low cost, easy synthesis, and low decomposition temperature in the air. Indeed, the hydrothermal decomposition of metal oxalates is a clean, flexible and powerful approach toward metal oxide with possible scale-up potential [2].

Metal oxalate hydrates can be dehydrated and decomposed by pressure and heating and finally converted to metal oxide. Ergo, metal oxalate hydrates have been exploited as a precursor to convert metal oxides with solid-state reaction methods [3].

In this study, we prepared a ceria solid solution with simple oxalate precipitation [4]. The obtain powder which consist $Ce_2(C_2O_4)_3.10H_2O$ was used for conversion to $CeO_2$ with hydrothermal treatment. The impact parameters such as pH, and hydrothermal temperature were evaluated on the physicochemical characterization of the final powder.

## 2. Experimental and Instrumental section

All the reagents used in this work were analytical grade and all solutions were prepared with Millipore water. Briefly, appropriate amount of oxalic acid (0.1 M) add to the cerium(III) nitrate hexahydrate (0.1 M) mixed together. The white precipitation was washed 3 times with Millipore water, centrifuged and dried at 50 °C in an oven. 0.25 g of the obtained powder with 21 mL of diluted nitric acid was transferred to the Teflon-lined autoclave for hydrothermally treatment. The final product washed 3 times with Millipore water, centrifuged and dried at 50 °C in an oven. The final powder was characterized with XRD and SEM.

## 3. Result and Discussion

Several parameters are affected to synthesis metal oxide from metal oxalate as precursor. The pH value is the significant key factor for the nature and crystallinity [5]. Therefore, the influence of the initial pH during the $Ce_2(C_2O_4)_3.10H_2O$ hydrothermal treatment was investigated in the 1, 2 and 3. The target pH was reached by adding different concentration of nitric acid. The XRD patterns of the final powder prepared in 220 °C at different adjusted pH for 24 h are shown in the Fig. 1.

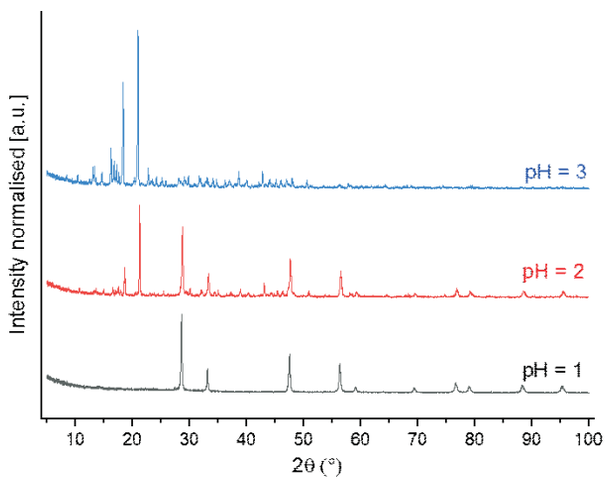


**Figure 1.** Powder X-ray diffraction diagrams obtained after hydrothermal treatment of $Ce_2(C_2O_4)_3.10H_2O$ in variation initial pH

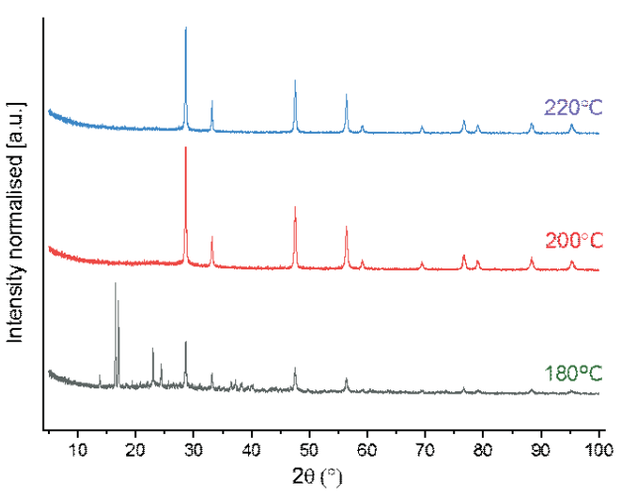


**Figure 2.** Powder X-ray diffraction diagrams obtained after hydrothermal treatment of $Ce_2(C_2O_4)_3.10H_2O$ with various temperatures in pH 1 during 24 h.

Other main effective parameter on the materials physicochemical properties is temperature [8]. Therefore, the effect of hydrothermal treatment for converting $Ce_2(C_2O_4)_3.10H_2O$ to $CeO_2$ was evaluated at 180, 200 and 220 °C with adjusted pH 1 for 24 h. As the XRDs are illustrated in the Fig. 2 with increasing hydrothermal temperature the initially precipitated of $Ce_2(C_2O_4)_3.10H_2O$ converted to $CeO_2$.The optimum temperature for the conversion is 200 °C and in higher temperature it just lead to sharp peaks and consequently growing crystallise structure.

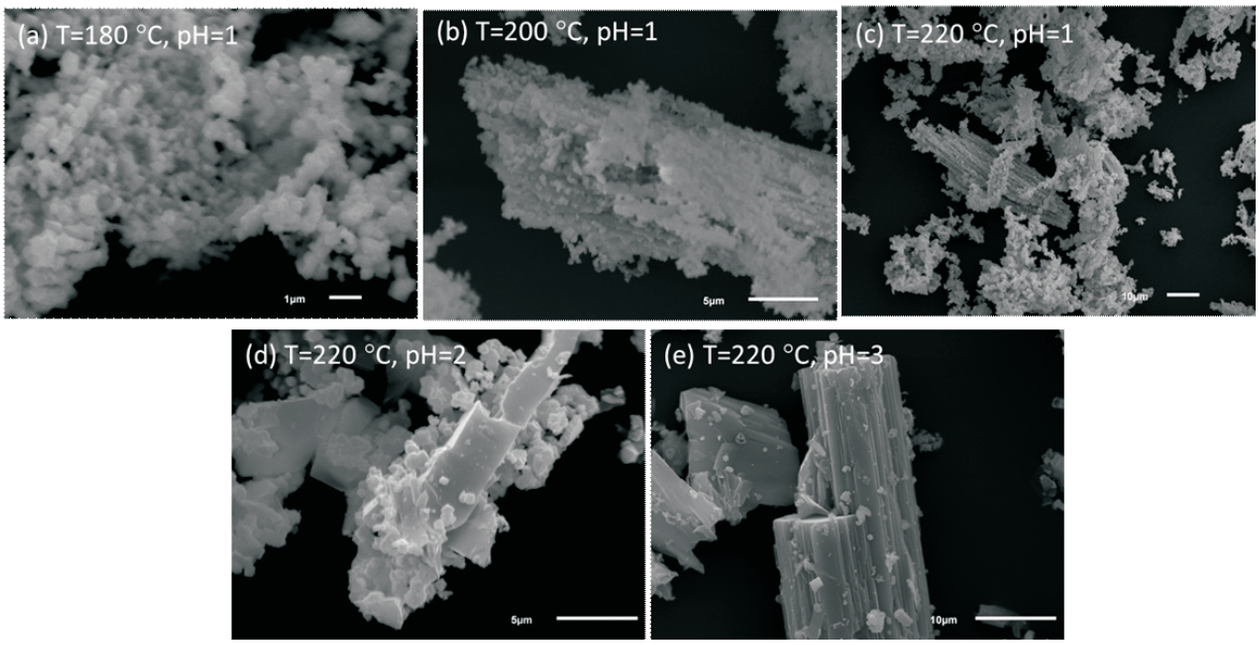


**Figure 3.** SEM images of $Ce_2(C_2O_4)_3.10H_2O$ conversion to $CeO_2$ in different hydrothermal treatment (a-c) and pH (c-e) during 24 h.

Final structure such as size, crystal thickness, aggregation and purity are related to the synthesis condition, as confirmed by our achievement. However, Fig. 3 shows the size and morphology of the achieved powder from hydrothermal treatment of $Ce_2(C_2O_4)_3.10H_2O$ to the $CeO_2$. Such modification of this conversion was correlated to increase crystallite phase with temperature and pH as already evidenced by XRD measurements. As it illustrated in Fig. 3 (a-c) with increasing the temperature from 180 to 220 °C aggregation of the nano powder sticking together to formation bigger structure was occurred. Also with increasing pH from 1 to 3, gradually conversion of $Ce_2(C_2O_4)_3.10H_2O$ to the $CeO_2$ was decreased and porous powders in the low pH change to the rods and it shown in Fig. 3 (c-e).

## 4. Conclusion

Cerium (III) precipitated with oxalic acid in the aqueous solution and the white powder of $Ce_2(C_2O_4)_3.10H_2O$ was achieved. Entirely conversion of $Ce_2(C_2O_4)_3.10H_2O$ to the $CeO_2$ was done with hydrothermal treatment. This conversion was profoundly related to several parameters such as pH solution and temperature in the process of hydrothermal treatment which optimized in this procedure.

## References

1. L. Guo, H, Arafune, N. Teramae, *Langmuir*, **29**, (2013), 4404.
2. O. Walter, K. Popa, O.D. Blanco, Open Chemistry, **14**, (2016), 170.
3. C. Hu, J. Mi, S. Shang, J. Shangguan. *J. Therm. Anal. Calorim.*, **115** (2014), 1119.
4. V. Tyrpekl, P. Markova, M. Dopita, P. Brázda, M. A. Vacca, Inorg. Chem., **58**, (2019),10111.
5. A. I. Y. TokF, Y.C. Boey, Z. Dong, X.L. Sun, J. Mater. Process. Tech.,**190**, (2007), 217.
6. J. Manaud, J. Maynadié, A. Mesbah, M. O. J. Y. Hunault, P. M. Martin, M. Zunino, N. Dacheux, N. Clavie, Inorg. Chem., **59**, (2020), 14954.

P2

# THE INFLUENCE OF ENERGY-FILTERING ON KINEMATICAL AND DYNAMICAL STRUCTURE REFINEMENT FROM 3D ED DATA

**M. Cabaj[1], L. Palatinus[1], I. Andrusenko[2], M. Gemmi[2]**

*[1]Department of Structure Analysis, Institute of Physics, Czech Academy of Sciences, Prague, Czech Rep.*
*[2]Istituto Italiano di Tecnologia, Center for Materials Interfaces, Electron Crystallography, Pontedera, Italy - Pontedera (Italy)*
*mkcabaj@fzu.cz*

X-ray diffraction data is a well-established and reliable approach of solid-state structure solution and refinement. Compared to it, electron diffraction is still not as commonly used due to various reasons, one of them being higher figures of merit indicating poorer accuracy of structure refinement. There are many ways to address this problem, ranging from using more complex theoretical approach for structure refinement, to installing additional parts of equipment, which enable collection of higher quality data.

In this work we investigate the influence of energy-filtering on data refined with kinematical and dynamical approach.

Four sets of data – two filtered and two unfiltered – were collected from two crystals of metal-organic polymer containing Zn(II), water and 4,4'-biphenyldicarboxylic acid. For first crystal, the unfiltered data were collected first and the filtered – second. For the other crystal the order of data collection was reversed. This protocol ensures that the observed differences are not due to the radiation damage.

All datasets were processed with PETS2 [1], and then solved and refined with JANA2020 [2]. We processed all four data set in an identical manner to ensure a reliable and unbiased comparison.

In each case we observed some differences in R-factors. For kinematical refinement the R factors were slightly lower for the unfiltered data (less than 1% of difference), with the except of R(all), which was higher for the filtered data. The situation was different for the dynamical approach – all R factors were higher for the unfiltered data, and again – the difference was usually less than 1%.

The obtained results confirm the preliminary hypothesis that the energy-filtering affects the kinematical and dynamical data refinement process in a different way. The change in all R factors is not considerable, but still measurable. Adding an energy-filter negatively affects kinematical refinement, but improves the dynamical one.

1. L. Palatinus, P. Brázda, M. Jelínek, J. Hrdá, G. Steciuk and M. Klementová, "Specifics of the data processing of precession electron diffraction tomography data and their implementation in the program PETS2.0," Acta Cryst. B, vol. B75, pp. 512-522, 2019.
2. V. Petricek, M. Dusek and L. Palatinus, "Crystallographic Computing System JANA2006: General features," Z. Kristallogr., vol. 229, no. 5, pp. 345-352, 2014.

*This work was supported by the Czech Science Foundation, project number 21-05926X.*

**Table 1**. The differences in R-factors for each dataset.

| | Crystal 1 | | | Crystal 2 | | |
|---|---|---|---|---|---|---|
| | Filter off | Filter on | Difference (off-on) | Filter on | Filter off | Difference (off-on) |
| Kinematical refinement | | | | | | |
| R(obs) | 24.94 | 25.13 | -0.19 | 26.11 | 25.95 | -0.16 |
| wR(obs) | 29.00 | 29.51 | -0.51 | 30.02 | 28.91 | -1.11 |
| R(all) | 32.47 | 30.78 | 1.69 | 29.35 | 31.46 | 2.11 |
| wR(all) | 29.91 | 30.35 | -0.44 | 30.37 | 29.36 | -1.01 |
| Dynamical refinement | | | | | | |
| R(obs) | 10.27 | 9.78 | 0.49 | 12.46 | 12.94 | 0.48 |
| wR(obs) | 11.73 | 11.12 | 0.61 | 14.16 | 15.33 | 1.17 |
| R(all) | 16.71 | 16.24 | 0.47 | 15.35 | 16.26 | 0.91 |
| wR(all) | 13.34 | 12.78 | 0.56 | 14.82 | 15.94 | 1.12 |

P3

## SOLUTION OF CRYSTAL AND MAGNETIC STRUCTURES IN JANA2020

**M. Henriques, C. A. Correa, V. Petříček and M. Dušek**

*Department of Structure Analysis, Institute of Physics, Academy of Sciences of the Czech Republic, 18221 Praha, Na Slovance 2, Czech Republic*
*henriques@fzu.cz*

The new Jana2020 is a natural successor to the previous version of the Jana2006 program [1], which was used to solve regular, modulated, and magnetic structures. The most important changes include a major improvement in the graphical interface, which allows the user full control of the individual steps of the solution and specification of crystal structures. Current changes in the structure can be monitored either in the mode of displaying the crystal structure, or by comparison of the measured and calculated profile from the powder data.

Since the formation of modulated and magnetic phases is very often associated with phase transitions, the procedure for detecting the coexistence of more independently diffracting domains has been significantly improved in the new version. In some cases, during the test of the space and superspace group, we receive incorrect information about the symmetry of the crystal, but also about its actual translational symmetry [2]. Therefore, the procedure was supplemented by an analysis of possible domain overlap.

Another significant improvement of the program is the ability to perform a series of structure refinements the system of data measured under different conditions (temperature, pressure, time). After solving and specifying the initial structure, automatic refinement takes place on all blocks of measured data. The procedure is supplemented by a graphical display of changes in advanced parameters.

*The authors are grateful to the Czech Science Foundation, project No. 18-10504S.*

1 V. Petříček, M.Dušek, L.Palatinus, Z.Kristallogr.-Crystalline Materials 229, (2014), 345-352.

2. V. Petříček, M.Dušek, L.Plášil, Z.Kristallogr.-Crystalline Materials, 231, (2016), 583-599.

P4

## CRYSTAL AND MAGNETIC STRUCTURES IN THE $Nd_{1-x}Sr_xFeO_3$ ($0.1 \leq x \leq 0.9$) SOLID SOLUTIONS

**H. Nakatsugawa[1], Y. Kamatani[1], C. H. Hervoches[2]**

*[1]Yokohama National University, Japan*
*[2]Nuclear Physics Institute, Rež, Czech Republic*

Rare-earth orthoferrites $RFeO_3$ (R = La,Nd,Dy,…) are of particular interest due to their potential multiferroicity, magnetoelectric effects, and other functional properties.

In this study, the $Nd_{1-x}Sr_xFeO_3$ series ($0.1 \leq x \leq 0.9$) have been prepared. Magnetization measurements from 5K to 700K show weak antiferromagnetic behaviour and paramagnetism following the typical Curie-Weiss law above 600K.

To clarify the correlation between the crystal structure and magnetic structure of $Nd_{1-x}Sr_xFeO_3$ ($0.1 \leq x \leq 0.9$) , powder neutron diffraction (PND) data of the $Nd_{1-x}Sr_xFeO_3$ ($0.1 \leq x \leq 0.9$) samples were collected at 15 K, 298 K, and 500 K with the medium resolution neutron powder diffractometer (MEREDIT), part of the CANAM infrastructure, at the Nuclear Physics Institute, Czech Republic. All Rietveld refinements were carried out using the GSAS-II suite of programs [1].

It is confirmed that the $FeO_6$ octahedron distortion is relaxed as *x* increases and approaches the crystal structure of the pseudo-cubic. Fig 1 shows the evolution of Fe-O-Fe angles with *x* in $Nd_{1-x}Sr_xFeO_3$ ($0.1 \leq x \leq 0.9$) .

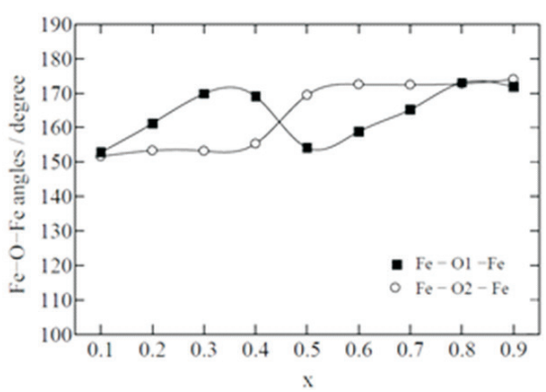


**Figure 1**. Evolution of Fe-O-Fe angles vs *x*.

At room temperature, the materials present antiferromagnetic order, with magnetic moment of Fe decreasing from ~ 3.2 μB for x = 0.1 to ~1.0 μB for x = 0.6 and magnetic spins oriented in the *a*- or *c*-axis (BNS Magnetic Space Group: P21'/*m*', P*n*'*ma*', or P*nma*).

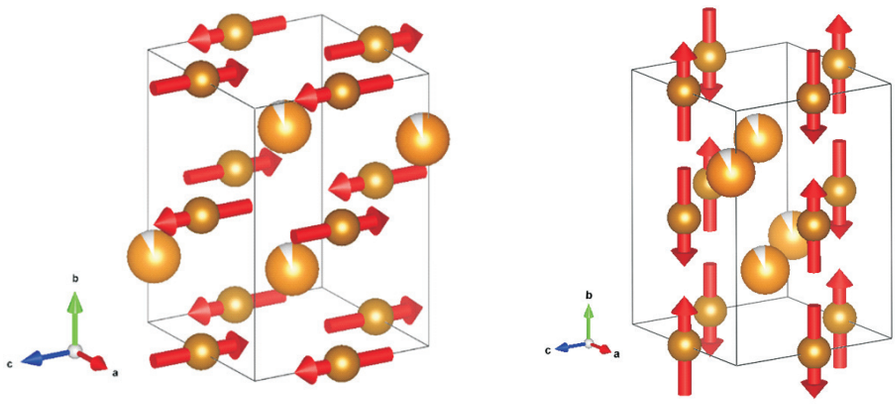

**Figure 2**. Magnetic structure of $Nd_{0.9}Sr_{0.1}FeO_3$ ($x$ = 0.1) at room temperature and 15K.

At 15 K, in the range x = 0.1 – 0.4, the magnetic spins order in the *b*-axis direction (BNS Magnetic Space Group: P21'/*m*' or P*n*'*ma*'); A more complex magnetic structure is observed for x≥ 0.5.

The magnetic structures for $Nd_{0.9}Sr_{0.1}FeO_3$ at RT and 10K are shown in fig 2. Crystal and magnetic structures were drawn using VESTA [2].

1. B.H. Toby and R.B.Von Dreele, J. Appl. Cryst. 46, 544-549 (2013).

2. K.Momma and F.Izumi, J.Appl.Crystallogr. 41, 653-658 (2008).

*The authors acknowledge CANAM (MŠMT project No. LM2011019), and the infrastructure Reactors LVR-15 and LR-0 (MŠMT project No. LM2018120) supported by the Ministry of Education, Youth and Sports of the Czech Republic.*

P5

## CRYSTAL STRUCTURE STUDY OF XENON COMPOUNDS USING 3D ELECTRON DIFFRACTION

**Kshitij Gurung**

*Institute of Physics, Czech Academy of Sciences, Prague*

The low stability of the xenon compounds in the atmosphere and under the electron beam makes it quite a challenge for their crystal-structure studies using electron diffraction. At the same time, some of these compounds are difficult to crystallize in large crystals, and electron diffraction is the only way to elucidate their structure. Recent progress in 3D electron diffraction (3D ED) makes it a promising technique for studying the crystal structures of these largely unexplored compounds. To verify the feasibility of the application of 3D ED to these compounds, we investigated $XeF_2$ and $[XeF][TaF_6]$. Sample loading was achieved by the use of a glovebox and a homemade construct that utilized liquid nitrogen, preventing the exposure of the sample to moisture. Energy-dispersive X-ray spectroscopy (EDS) confirmed the presence of xenon and fluorine in the loaded sample. The electron diffraction on $XeF_2$ confirmed the presence of this phase. However, the crystal quality was not sufficient to obtain a full single crystal 3D ED data set. However, the compound turned out to be sufficiently stable under the electron beam to potentially permit a 3D ED data collection. These results, albeit preliminary, demonstrate that it is possible to investigate nanocrystalline xenon-containing compounds as well as other air-sensitive and reactive materials by 3D ED.

P6

# X-RAY DIFFRACTION AND NEUTRON DIFFRACTION OF THE SKIN BARRIER MODEL

**P. Pullmannová[1], N. Kučerka[2,3], R. Georgii[4], B. Demé[5], J. Maixner[6], B. Čuříková-Kindlová[6], K. Dvořáková[6], V. Ondrejčeková[1], J. Zbytovská[1,6], K. Vávrová[1]**

*[1]Skin Barrier Research Group, Charles University, Faculty of Pharmacy, Hradec Králové, Czechia*
*[2]Faculty of Pharmacy, Comenius University, Bratislava, Slovakia*
*[3]Frank Laboratory of Neutron Physics, Joint Institute for Nuclear Research, Dubna, Russia*
*[4]Heinz Maier-Leibnitz Zentrum (MLZ), Technische Universität München, Garching, Germany*
*[5]Institut Laue-Langevin - 71 avenue des Martyrs, CS 20156, 38042 Grenoble Cedex 9 – France*
*[6]University of Chemistry and Technology Prague, Faculty of Chemical Technology, Prague, Czechia*
*pullmanp@faf.cuni.cz*

The physical barrier of the skin is located in its outermost layer – the stratum corneum (SC). SC consists of cornified cells embedded in the highly organized extracellular lipid matrix containing mainly ceramides (Cer), free fatty acids (FFA), and cholesterol (Chol). The skin lipids behaviour is studied in models of various complexity. We have studied the simple model based on Cer with C24 acyl chain (type NS or NH), FFA (C16 – C24 chains), and Chol at the equimolar ratio and a complex model prepared from isolated and purified human skin lipids (but still missing cornified cells). The models were prepared in the form of thin layers applied onto supporting wafers. They were annealed at the temperature above the melting point at low or high humidity. The regular structure was evaluated by the following methods:

1. X-ray diffraction measured with an X'pert PRO θ–θ powder diffractometer with the Bragg-Brentano geometry (PANalytical B.V., Netherlands)
2. Neutron diffraction using a cold-neutron three-axis spectrometer MIRA located at the neutron source in Heinz Maier-Leibnitz Zentrum (Garching, Germany) (a simple model)
3. Neutron diffraction using a D16 small-*q* diffractometer (Institut Laue-Langevin, Grenoble, France) (the human skin lipids)

The simple model based on Cer C24/FFA/Chol showed immense structural variability dependent on the annealing conditions. Bragg peaks at small angles provided a repeat distance (*d*) of 5.3 nm (Fig. 1A a), which is known from the literature [1], but also the repeat distances of 10.6 nm (Fig.1A b), 15.9 nm (Fig.1A c), and 21.2 nm (Fig. 1A d) were found [2]. All the peaks belong to the one-dimensional lamellar structures with an orthorhombic lipid chain sublattice (peaks at wide angles). The separated Chol (*) was also found. The repeat distance of 10.6 nm is double the theoretical maximal length of a two-chain Cer molecule in the splayed-chain conformation. The composition of the simple model with $d$ = 10.6 nm was adjusted for the neutron diffraction experiment at different contrast conditions ($D_2O/H_2O$ ratio). The relative neutron scattering length density ρ(z) was calculated according to the equation (1):

$$\rho(z) = \sum_{h=1}^{h\max} F_h \cos\left(\frac{2\pi\, hz}{d}\right) \qquad (1)$$

$F_h$ is the scattering form factor for the order $h$ and $z$ is the distance from the lamellar centre. The phase angles for a centrosymmetric structure attain the values of +1 or -1. We calculated 57 ρ(z) profiles at 100% $D_2O$ based on different combinations of the phase angles in two subsequent steps. The most plausible ρ (z) profiles (Fig. 1B) were selected to be consistent with the molecular composition of the sample and to provide feasible water distribution profile. The plausible r(z) profiles rely on a splayed-chain conformation of Cer [3] leading to the asymmetric distribution of hydrocarbon chains in leaflets. The isolated human skin lipids formed a lamellar phase with a longer $d$ of 13.4 nm due to the presence of ultra-long skin Cer. This long periodicity phase (LPP) [1] has a feature common with the structure with $d$ = 10.6 nm – low intensity of the 1st order peak. The human skin lipids were measured by neutron diffraction at different contrast conditions ($D_2O/H_2O$ ratio). The ρ(z) profile of LPP based on one combination of the phase angles for 6 $F_h$ is shown in Fig. 1C. We suppose that the molecular arrangement of the LPP is also based on the splayed-chain conformation of Cer. The ρ(z) profiles of LPP need to be corroborated with electron density profiles and other experiment to verify the plausibility of our model.

1. J. A. Bouwstra, G. S. Gooris, M. A. S. Vries, J. A. van der Spek and W. Bras, *Int. J. Pharm.*, **84**, (1992), 205.
2. P. Pullmannová, E. Ermakova, A. Kováčik, L. Opálka, J. Maixner, J. Zbytovská, N. Kučerka and K. Vávrová, *J. Lipid Res.*, **60**, (2019), 963.
3. R. Corkery, *Colloids Surf., B*, **26,** (2002), 3.

*The study was supported by the Czech Science Foundation (19-09135J and 19-09600S), Charles University (SVV 260 547), EFSA-CDN (No. CZ.02.1.01/0.0/0.0/16_019/ 0000841) co-funded by ERDF, Heinz Maier-Leibnitz Zentrum, and Institut Laue-Langevin.*

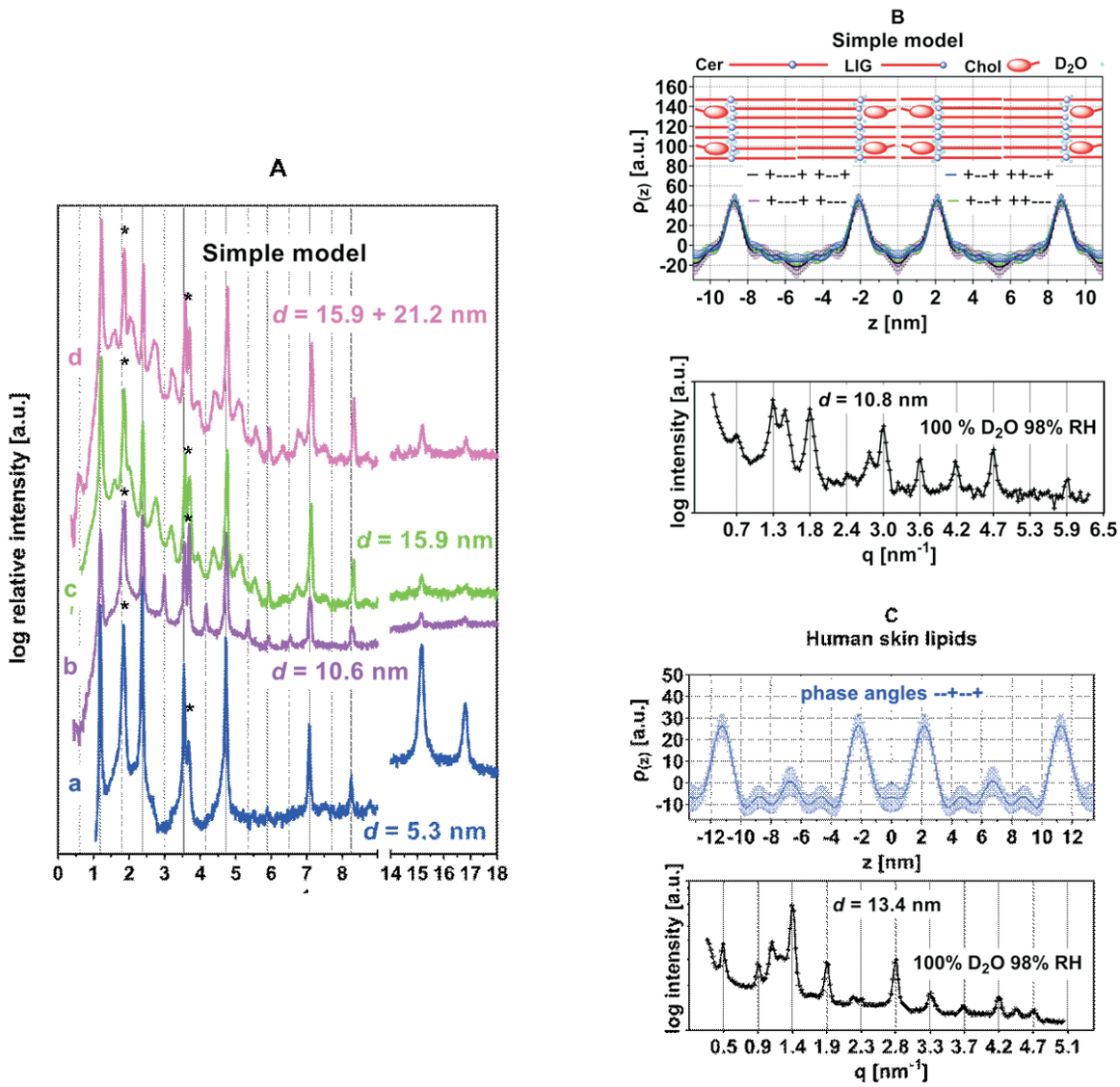


**Figure 1.** X-ray diffraction patterns of the simple models based on the Cer NS24/FFA/Chol mixture prepared at various annealing conditions. Asterisks indicate the peaks of separated crystalline Chol. Full grid lines predict the peaks at $d = 5.3$ nm, dashed grid lines predict the odd orders of peaks at $d = 10.6$ nm. The peaks of the orthorhombic chain sublattice are apparent in the wide-angle region (panel **A**). Neutron diffraction patterns and ρ(z) profiles of the simple model based on the Cer NH24/Cer NS24/FFA/Chol (panel **B**) and human skin lipids (panel **C**).

# Profesor RNDr. Václav Janovec, CSc.

Václav Janovec na 298. Rozhovorech o aktuálních otázkách rt a neutronové strukturní analýzy, 6.11.2015, Ústav makromolekulární chemie AV ČR, Praha

Dne 16. února 2022 zesnul profesor RNDr. Václav Janovec, CSc., významný český fyzik a krystalograf.

Václav Janovec se narodil v rolnické rodině 20. února 1930 v Pěčíně v podhůří Orlických hor. Otci, který se věnoval radiofonii a fotografování, se podařilo nadanému synkovi vštípit vztah k technice. Mladý hoch ve čtrnácti letech postoupil na reálné gymnázium a v roce 1949 byl přijat na přírodovědeckou fakultu. Téma diplomové práce věnované elektrickým vlastnostem feroelektrického $BaTiO_3$ a vlivu elektrického pole na difrakční intenzity dostal od prof. Václava Petržílky. Zadání tématu bylo zřejmě určujícím impulsem pro jeho další vědeckou kariéru. Jako čerstvý absolvent nastoupil spolu se svými spolužáky Janem Fouskem, Zdeňkem Fraitem a Zdeňkem Málkem do Laboratoře experimentální a teoretické fyziky, ze které později sloučením s Laboratoří nukleární fyziky vznikl Fyzikální ústav ČSAV. Ve své aspiranské práci v roce 1958 vysvětlil a z mikroskopických představ odvodil vztah nepřímé úměry mezi dvěma důležitými veličinami: minimálním elektrickým napětím nutným k překlopení polarizace feroelektrické destičky a třetí odmocninou kvadrátu její tloušťky. Znovu jej v roce 1962 v Bristolu odvodili a ověřili H. F. Kay a J. W. Dunn - a proto je tento vztah dnes uváděn jako Janovcův-Kayův-Dunnův zákon.

Janovec s Fouskem začali pracovat ve skupině dielektrik. Vedení dielektrické skupiny Janovec převzal přímo od prof. Josefa Beneše v březnu 1960 a stal se tak prvním interním vedoucím této skupiny, později a dodnes nazývané oddělením dielektrik. V létě 1966 se dielektrickému oddělení podařilo v Praze zorganizovat první mezinárodní konferenci o feroelektřině. Konala se za účasti předních vědců za západu i východu od železné opony a měla zásadní význam pro další budoucnost skupiny. Začátkem srpna 1968 Fousek a Janovec odeslali do tisku dnes již klasickou práci, která elegantně řeší problém prostorové orientace doménových rozhraní ve feroelektrických krystalech. Fousek i Janovec také spolu významně přispěli i k založení mezinárodního oborového časopisu FERROELECTRICS, což se stalo v roce 1970.

Za průlomový objev lze považovat Janovcovu teorii o symetrii doménových stěn z pohledu tzv. černobílé symetrie. Ačkoliv Janovec o této své teorii psal a přednášel už od 70. let a sám ji považoval za svůj nejdůležitější výsledek, ve světě zůstávala bez větší odezvy. Důvody proto patrně spočívají jak v neobvyklém teoretickém aparátu, tak v nepatrné, nanometrové šířce doménových stěn, kvůli kterým se teprve dnes začíná dařit tak malé objekty detailněji pozorovat.

Největším počinem byla systematická práce z roku 1975, na které pracoval spolu s Dr. Vladimírem Dvořákem a Dr. Janem Petzeltem. Práce vycházela z myšlenek tzv. Landauovy teorie fázových přechodů. Všem třem jmenovaným vědcům se podařilo Landaovu úlohu vyřešit vypsáním všech možných způsobů narušení všech 32 možných tříd makroskopické symetrie krystalů, a to včetně rozboru všech možných důsledků pro vlastností takových krystalů. Janovec použitý přístup dále rozpracoval a zdokonalil zejména při své mnohaleté práci na koncepci a reedicích svazku *D* Mezinárodních krystalografických tabulek, na nichž se z pověření Mezinárodní krystalografické unie podílel jak autorsky, tak organizačně v rámci mezinárodního týmu, jehož členy byli profesoři Th. Hahn, H. Wondratschek, J. Přívratská, H. Klapper a další.

Podle pamětníků se Janovec neprojevoval nápadnými protirežimními gesty, ale jeho mravní a politický kód byl po pár větách rozhovoru s ním zřejmý, přičemž kde mohl, tam se snažil pomoci. Mimo jiné byl jedním z nejštědřejších pravidelných přispěvovatelů na finanční pomoc pro rodinu svého kolegy Dr. Tomáše Růžičky, který byl vyhozen z Fyzikálního ústavu ČSAV a pronásledovaný kvůli Chartě 77. Podotkněme, že honorář, který za dlouholetou práci na krystalografických tabulkách obdržel od

prof. Hahna, věnoval Krystalografické společnosti na financování cen mladým vědcům. Příznačně si přál, aby se o tomto jeho příspěvku nemluvilo a zůstal jako anonymní dárce.

V 90. letech se Janovcovi otevřely příležitosti k mnoha pobytům a k ještě širší mezinárodní spolupráci. Kolem roku 1995 ovšem Akademie věd začala čelit významným finančním škrtům. Tehdejší ředitel ústavu Dr. Dvořák vyzval vědce v důchodovém věku k odchodu, nebo k výraznému snížení úvazků. Přitom si pochopitelně přál, aby jeho bývalé oddělení šlo příkladem. Janovec měl ve svých 65 letech už na kontě téměř stovku publikací, 4 patenty, několik medailí, rozsáhlou síť spolupracovníků z celého světa a byl považován za zakladatele pražské doménové školy. Spolu s prof. L. A. Shuvalovem inicioval novou sérii konferencí, které byly zaměřeny na jeho oblíbenou problematiku doménových stěn. Měl za sebou velké zkušenosti z přednášek na Univerzitě Karlově i na zahraničních univerzitách v Curychu, Dijonu, Karlsruhe, Montpellier a Rennes. Janovec a Fousek proto místo odpočinku přijali pozvání od prof. Jana Tichého, který se vrátil z exilu na Technickou univerzitu v Liberci, aby tam obnovil výzkum a výuku v oblasti piezoelektrických materiálů. Janovec se na Technické univerzitě v Liberci habilitoval a v roce 1995 ho prezident Václav Havel jmenoval profesorem. Na pedagogické fakultě byl pak zaměstnán v letech 1995-2008 a kromě svého výzkumu přednášel studentům termodynamiku, statistickou fyziku, tenzorový počet a další předměty. Je příznačné, že v rámci svých zkoušek vybízel studenty, aby sami zformulovali dotaz.

V r. 2009 – ve svých 79 letech - Janovec opětovně nastoupil do oddělení dielektrik Fyzikálního ústavu na formálně malý úvazek, který ale byl významný pro celé oddělení, protože Janovec byl zkrátka inspirativní osobnost, která předávala své nápady a zkušenosti ostatním mladším kolegům. Živě se zajímal se o novinky v oboru i v oddělení a vytrvale pracoval na použití teorie grup v krystalografii zdvojčatělých krystalů. Pravidelná setkávání autorů tohoto textu s naším milým kolegou Janovcem se často táhla do pozdních večerních hodin.

Prof. Janovec stihl během svého života být oporou nejen pro mnohé přátele z řad hudebníků, členů Sokola či vědců, ale především pro svoji rodinu, hlavně pro svého mladšího bratra Zdeňka, pro manželku Evu, která zemřela na následky těžké nemoci v roce 1999, pro svoji dceru Irenu s manželem Stevenem a vnoučaty Samuelem a Abrahamem a pro svoji blízkou přítelkyni Miluši a její rodinu. Poslední dva roky Janovcova života po nástupu epidemie byly poznamenány zhoršujícím se zdravím. Ale ti, kdo měli s ním možnost hovořit před jeho skonem, zaznamenávali neutuchající dobrotu, zájem o dění ve světě, stejně jako jeho klidnou vyrovnanost.

Život prof. Václava Janovce, CSc. byl dlouhý a naplněný, a přece krátký pro tak tvořivého, inspirativního a laskavého člověka. Bude nám chybět!

Jiří Hlinka
Jan Fábry

FZÚ AVČR

## Juraj Sedláček

### 4.8.1943–1.9.2021

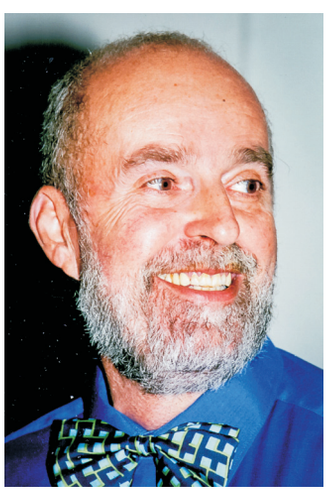

Juraj Sedlacek has passed away on September 1, 2021 after his battle with cancer.

He was born in Slovakia on August 4, 1943 and he never missed an opportunity to emphasize that gun salvos fired on that day in Moscow were not only a tribute to the victory at Kursk but also to his birth.

He started his education at the Czech Technical University, Prague, where he obtained M.Sc degree in nuclear physics. After that a rich scientific career followed, he was among the pioneers of recombinant DNA technology and molecular biology in Czechoslovakia/Czech Republic and he has educated a number of PhD students.

He was instrumental in establishing the first protein crystallographic facility in the Czech Republic in year 1998.

He was also an important member of the Heart of Europe crystallographic community since the very first meeting in 1998 and he personally participated in almost all HEC meetings.

But above all, he was a kind, generous and witty personality for which he will be remembered and sorely missed by his friends and colleagues.

Milan Fábry
IMG Prague

# 25th ASSEMBLY AND CONGRESS OF THE INTERNATIONAL UNION OF CRYSTALLOGRAPHY (IUCr). HYBRID CONGRESS IN THE TIME OF PANDEMIC, AUGUST 2021

**R. Kužel**

*Faculty of Mathematics and Physics, Charles University, Ke Karlovu 5, 121 16 Praha 2*

The IUCr organizes its congresses in conjunction with assemblies once every three years. In the meantime, there are conferences of its regional associates, ACA, AsCA, LACA, and ECA. In the Czech Republic the adhering body is the Regional Committee of Czech and Slovak Crystallographers included now in the Crystallographic association (Krystalografická společnost registered in the Czech Republic - international name Czech and Slovak Crystallographic Association (CSCA). Since modern crystallography is very interdisciplinary and no single institution (university, institute) can cover its whole scope, it was just CSCA that took the effort to organize the congress in Prague, and after several attempts we won the bid in 2014 during the congress in Montreal. This was a bid for the organization of the 25th anniversary congress in 2020.

## Congress Peripetia

We were celebrating our victory in 2014 having no idea what we really had. This appeared clear only in 2020. The preparation started well, immediately after the 24th congress in Hyderabad in 2017. In 2017-18, the International Program Committee (IPC) was formed with 35 members, mostly representing IUCRr commissions. The IPC meeting was held from 14 to 16 May 2019 in Prague. This meeting related to some kind of workshop called 'Current Trends and Future of Crystallography', where representatives of all commissions presented current problems, trends, and highlights of their fields. During the subsequent two-day meeting that was very effective, the whole programme scheme was agreed on consisting of 3 plenary lectures, 35 keynote lectures, more than 100 standard scientific microsymposia, and several special sessions. In the following months, the basic programme was finalized. For all the sessions, two cochairs were asked to invite two speakers to their sessions for 30 minutes talsk assuming that four more speakers will be selected from contributed abstracts. In February 2020 this basic programme was more or less complete. However, this was also the time of the beginning of the pandemic. In the middle of March, an extraordinary meeting of IUCr EC (the first its online meeting) decided to postpone the congress to summer 2021 since it was clear that the organization of classical congress in August 2020 is not very realistic. In the full calendar of the Prague Congress Center one week after August 13 was possible. The prepared programme was fixed, and we could only watch the situation with the pandemic in the world. Unfortunately, this was not good at all. In January 2021, after a short discussion, we concluded that there was no room for further postponing of the congress for several reasons. The possibility of a classical congress remained unrealistic, and the simplest way was to change it to a pure online form. However, we were not bidding for such a congress, ad moreover, a significant number of people really looked forward to the congress in Prague. The only possibility was to leave the hybrid form open, i.e. the combination of real and virtual participation. At the beginning of February, we had a chance to see a demonstration of presentation system g Con developed by Prague group T.R.I. that is basically independent on the locations of chairpersons and speakers. We were convinced that hybrid congress should be possible depending on the overall situation, and final decision on the form can be made at relatively short time before the congress. This, of course, would require the maximum flexibility of all involved. It was clear that before about June we would not be able to make this decision simply because earlier anyone would know anything. Then we started communication with all cochairs and invited speakers, that is, with nearly 500 persons asking them to confirm their participation in any form. Any participation cancelled less than 10% of them. We open the registration for virtual participation with a possibility of upgrading to real one, and we were watching Covid numbers. In the second half of May the situation looked quite optimistic and, moreover, conditions for organization of events in summer were published. According to polls among preregistered people, it seemed that we could expect 700-800 people in Prague. During June, the program of sessions was optimized and completed. Real registration was open. However, Coronavirus did not seem to give up, transformed to the so-called delta form, and destroyed our hopes to the full extent. However, there was no way back. The last weeks before the congress were very hectic. Basically, what is usually prepared 3-4 months before the congress we had to do in about 3-4 weeks. The exhibitors were asking about the number of real participants on site. This was something we also wanted to know. The colors of the counts on the Covid maps changed often. The virus seemed to be able to distinguish citizenship since different conditions were defined for EU citizens living in UK than UK citizens. The latter were simply not allowed to come to Prague regardless of vaccination. However, even worse appeared to be the bans on travel put on travel by institutions. I think this was idealistic in the situation where people could travel easier and visit a risky environment in their cities. The uncertainty was enormous.

## Hybrid Congress

After all, the congress was realized basically as planned in the last monts as hybrid and in very nice atmosphere also for online participants as it follows form e-mails received after the congress. A very good quality programme could be prepared. In this aspect, the possibility of online presentation is very positive because for invited speakers this can be quite simple and much cheaper. Only a few approached speakers refused. We have more than 2500 preregistered people, and the total number of final registrations reached

nearly 1700. Less than one-third were able to come to Prague, quite often for a shorter time; they watched the rest online. With respect to restrictions, we had most real participants from Poland and Germany, but others arrived from France, Spain, Sweden, Denmark, Finland, Croatia, Italy, USA and other countries.

**Programme**

The programme consisted of three plenary lectures, five lectures connected with prizes, 35 keynote lectures, 103 standard sessions, 7 special sessions, Software Fayre – always 9 sesssions in parallel, 55 poster sessions and several commercial presentations. In total, 624 lectures and over 550 posters in different forms were presented at the congress.

In this year, two sessions were devoted to the structural biology of coronaviruses and to new methods to combat the pandemic. In biocrystallography, the highest number of abstracts reached the session on the structural biology of enzymes and also on bioinformatics. New W.H. and W. Bragg Prize lectures were also related to biocrystallography – Structure-guided design of nex-generation malaria vaccine (Jean-Philippe Julien, Kanada), Targeting COVID-19 viral enzymes in an evolving landscape of publishing and peer review (James Fraser, USA) - as well as one plenary lecture by David Eisenberg The Expanding Amyloid Family: Structure, stability, function, and pathogenesis related, for example, to Alzheimer's disease. The main Ewald prize and one plenary lecture were related to crystallographic data and databasis. The Ewald prize was awarded to Olga Kennard (UK) for the development of Cambridge structure database, and a plenary lecture by Helen Berman (USA) was devoted to protein database PDB. Several sessions and pre-congress school were devoted to electron crystallography (structural studies by electron diffraction). The school was mostly online, but the last day in hybrid form. There were nearly 200 registered participants. In this branch, the Gjonnes medals are awarded. The prize went to Sven Hovmöller (Sweden) and Ute Kolb (Germany). Another significant topic of the congress was quantum crystallography. For both the above topics, relatively many experts were able to come to Prague. Among materials, the highest attention attracted materials for energy conversion and storage, often studied in situ (also plenary lecture by Clare Grey on In situ and ex situ studies of battery materials with magnetic resonance and diffraction methods), nanomaterials, and magnetic materials. The highest number of abstracts was in the session - Complex structure of minerals and inorganic compounds, and in the session of phase transitions in complex materials. Especially interest was also expressed for the session of disordered materials. Despite low advertising of the congress among chemical crystallographers, the highest number of registered people were just from this area, materials important for the pharmaceutical industry, metal-organic frameworks (MOFs), and catalysis. Two sessions were dedicated to application of crystallography in art and many sessions to individual techniques as neutron scattering, small-angle scattering, synchrotron radiation, XAFS etc.

**How the Hybrid Congress Was Working**

All presentations were run from local servers in Prague (for details see also https://www.tri.cz ) and speakers were asked to upload their presentations (pptx, pdf) in advance, which was not accepted by all and caused stressful situations to technical staff, in particular at the beginning of the congress. Files underwent technical control before approval for smooth presentation. If the speakers were online then they had full control of presentation by arrows and mouse motion was mapped and shown (pointer). Remote participants could write questions into tab „Questions ". These questions were visible to all, and cochairs could select them for live discussion. The questions could be answered later by speakers in the 'Discussion.' As a new feature, the possibility of live entrance by additional participants was included by request "Raise hand". The cochairs allowed entry and for remote participants, a quick test of their microphone and camera was included before they were connected.

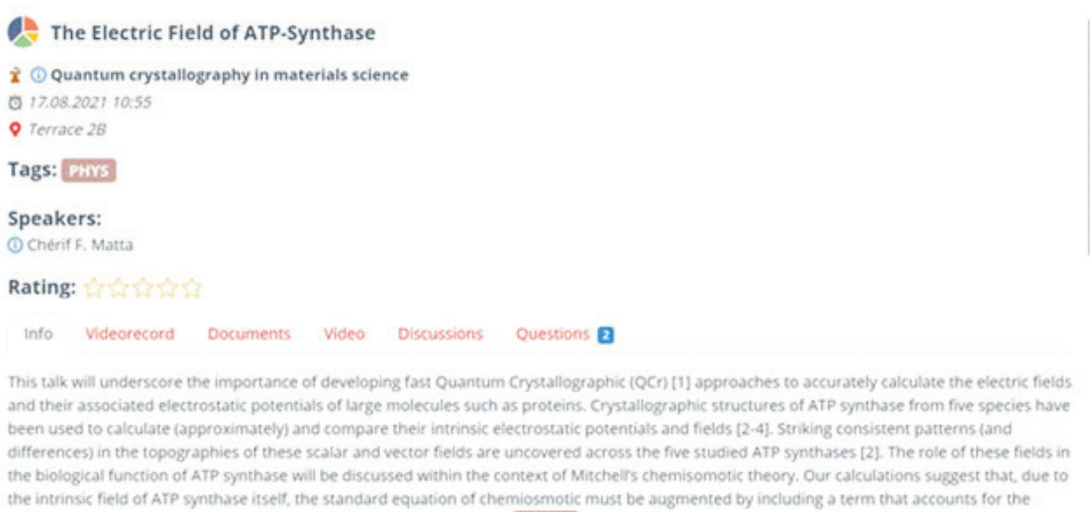


**Figure 1.** gCon page of one lecture – Info: abstract, Videorecord – recording of the lecture, Documents – documents for download, Video – video provided by the author for download, Discussions – active all the time, Questions – active only during the lecture and immediate discusssion but visible all the time.

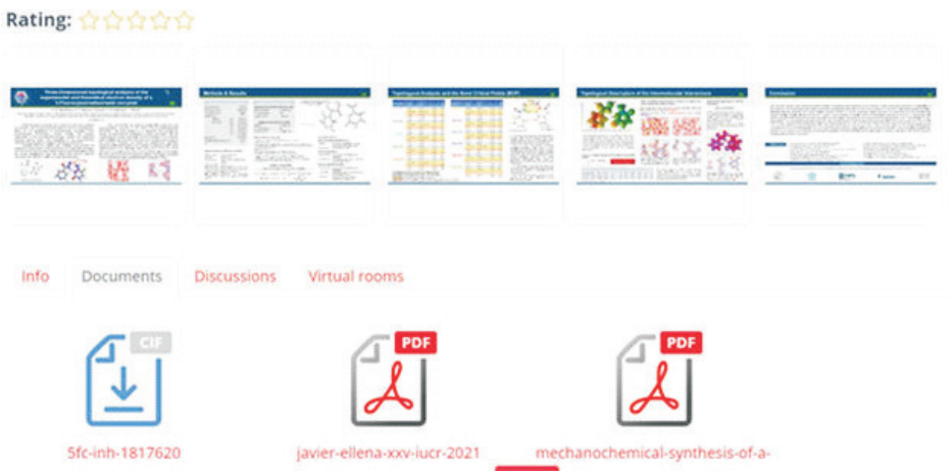


**Figure 2.** gConpage of a poster – the author uploaded more pages and in addition some documents. Virtual room was active only during corresponding virtual session.

Some speakers decided to upload the full lecture as an MP4 video. Especially in case of inconvenient time differences (such as west coast of the USA or Australia). Quite often, they were available live for discussion. The presentation files are not accessible by anyone, but each author could upload files without format restrictions to the tab 'Documents' and these files are available for download for registered participants. During congress, we met all possible combinations of locations of speakers, two cochairs and asking participants, and always everything worked well.

All poster files were available for viewing and download (unlike recordings). It was possible to upload not only posters, pdf but also pptx presentations or MP4 videos according to the needs of the authors. In time of poster sessions for each poster virtual room could be entered. The limit of one room was 25 visitors and the rooms were working for live meeting similarly to, e.g., Zoom with possibility of screen sharing. Of course, in hybrid mode it was necessary to separate virtual rooms from real poster sessions. In addition to usual poster panels, electronic panels were available too allowing easy search and zooming of details.

All responses of local and remote participants show that the congress was successful in most aspects and was better than expected when a number of people were sceptical to the hybrid form. Perhaps, it can be taken as an example for hybrid congresses. Credits should be given to all those involved in the organization. For the good impression of online participants, probably the greatest credit goes to T.R.I., their system gCon and very professional approach. Namely, the way of streaming and design with views of lecturers, chair persons, asking people, hall that made the congress really live. Online participants also appreciated the streamed concerts. They were simply attracted directly to the action of the congress. Below, there are screens captured from recordings.


**Figure 3.** Typical screen of live lecture in the stream


**Figure 4.** Remote speaker local listeners.


**Figure 6.** Remote chair persons, speaker, local listeners.

**Figure 8.** Concert in stream, watched by about 100 online participants.

The relatively long absence of real events was reflected in positive acceptance by the onsite participants, the work of the staff of the Prague Congress Center and the catering company Zátiší. All were doing their best to ensure the success of the conference. Of course, organizers should be mentioned first: colleagues from the Faculty of Mathematics and Physics - Milan Dopita and other colleagues and students, people from Institute of Organic Chemistry and Biochemistry CAS (Pavlna Řezáčová, chair of local organizing committe), Faculty of Science, University of South Bohemia in České Budějovice (Ivana Kutá Smatanová, chair of international programme committee), from the Institute of Biotechnology (CAS) and very important group Auletris (headed by Martin Haloun) www.auletris.com . We were very satisfied with the Conftool registration system (https://www.conftool.net ) and also presentation system gCon by T.R.I.


**Figure 5.** Remote chair, speaker, local listeners


**Figure 7.** Remote speaker, two local co-chairs

In addition to scientific programme, the Social programme was organized – boat trips on the Vltava River, conference dinner with a Brand new band concert at the National House and a train trip to Pilsen brewery. For more information, see https://www.iucr25.org .

Different conference statistics are available at https://iucr25.org/hybrid-conference-statistics/

Photos and short video clips https://www.xray.cz/iucr/photo/default.htm.

Finally, the gcon website with all the conference materials was open till the end of March 2022 and during all the time people were watching the materials. About 300 of registered participants never connected to the gcon system but over different 700 people have been watching something since the end of the congress. Most of the days during these 7 months at least one person opened something on the gcon website. The histogram of unique views (i.e. by different persons) can be seen in Figure 9.

The most viewed keynote lectures were by Dyan Jayatilaka on quantum crystallography (277), Lukáš Palatinus on electron crystallography on molecular crystals (246) and Andrew Goodwin on functional materials (227). The five most popular sessions were: Automation in bio-crystallography: tools, perspectives and applications (210 unique views), Crystal structures of pharmaceutical and organic compounds from electron diffraction (208), Total scattering (199), Structural biology against coronavirus/covid-1 (192) and Machine learning in biological and structural sciences (191)

The most on-line visited poster sessions were Powder diffraction (average views – i.e. per poster – 181), Drug design (133), Crystal structure prediction (127), General interest (103) and Structural bioinformatics (94). The most popular posters had over 200 visits while the least number of visits was 12 that is still not that bad.

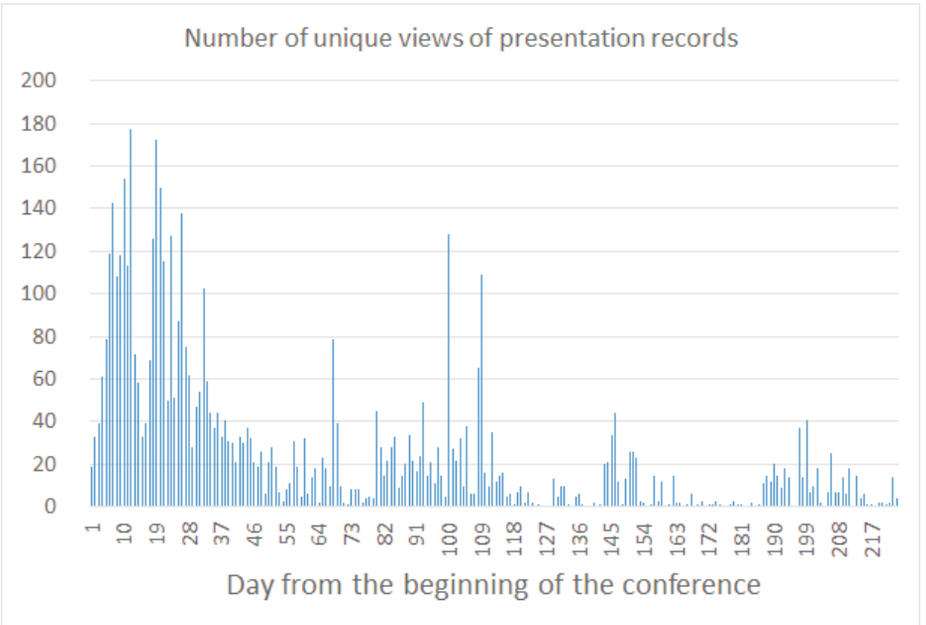


**Figure 9.** Number of unique views of presentation records

Such a kind of statistics has never been available and hopefully it will help also to organization of next congresses.

**Figure 10.** Last participants and organizers after closing ceremony (photo by Petr Pachl)

# STRUKTURA 2022 - PROGRAMME

## Monday, June 20

11:00–13:00 Registration

13:00 Struktura 2022 - Opening

13:15–15:45 Session I

*J. Drahokoupil, J. Maixner*

---

13:15
L1 81
**František Laufek**
*(Czech geological survey, Prague)*
Prvních padesát let práškové difrakce: Od Scherrera k Rietveldovi
First fifty years of powder diffraction: From Scherrer to Rietveld

13:45
L2
**Michal Hušák** 82
(*Institute of Chemical Technology, Praha)*
Predikce krystalové struktury - zkušenosti s účastí v CSP 7 slepém testu
Crystal structure prediction - experience with participation at CSP 7 blind test

14:15
L3 83
**Miroslav Pospíšil**
(*Fac. of Mathematics and Physics, Charles University, Praha*)
Struktura halloysitu s irinotecanem řešená molekulárními simulacemi
Structure of halloysite with irinotecan solved by molecular simulations

14:40
L4
**Jiří Hybler** 84
(*Institute of Physics, Czech Academy of Sciences, Praha)*
Vláknitá textura cronstedtitu
Fiber texture of cronstedtite

15:05
L5
**Jaromír Kopeček** 86
((*Institute of Physics, Czech Academy of Sciences, Praha)*
"Přírodní slitiny" z hlubokomořských konkrecí

15:30
L6 87
**Esther de Prado**
(*Institute of Physics, Czech Academy of Sciences, Praha)*
Structure and microstructure in (111) and (111)+(001) ScN/MgO thin films

15:55 *Coffee break*

16:20–18:50 Session II

*L. Horák, D. Šimek*

---

16:20
L7
**Gergely Farkas** 88
*(Institute of Nuclear Physics, Czech Academy of Sciences, Řež)*
Line profile and rocking curve analysis of 3D diffraction data

16:50
L8
**Petr Mikulík** 89
(*Faculty of Science, Masaryk University, Brno*)
Laboratory and synchrotron rocking curve imaging for crystal lattice misorientation mapping

17:15
L9
**Mojmír Meduňa** 90
(*Faculty of Science, Masaryk University, Brno*)
Radonova transformace v reciprokém prostoru
Radon transformation in reciprocal space

17:40
L10
**Zdeněk Matěj** 91
(*MAX IV Lund, Sweden)*
Image corrections for powder diffraction with thick sensor detectors

18:05
L11 144
**Radomír Kužel**
(*Fac. of Mathematics and Physics, Charles University, Praha*)
25. kongres IUCr v Praze, historie, zkušenosti, statistiky
25th IUCr congress in Prague, hitory, experience, statistics

---

19:00 Dinner

---

20:00–21:00
Discussions

## Tuesday, June 21

7:00–8:30 Breakfast

8:30–10:00 Session III - **Neutron scattering**
chair: *P. Javorský, P. Beran*

---

8:30
L12 93
**Mark Johnson**
(*ILL, Grenoble, France)*
Opportunities and perspectives at the Institut Laue Langevin: the Endurance upgrade programme

9:05
L13 93
**Thomas Hansen**
(*ILL, Grenoble, France)*
Neutron diffraction to study the structure of mate

9:40
L14 94
**Leonardo Chiappisi**
(*ILL, Grenoble, France)*
Soft matter seen by Small-angle Neutron Scattering, Neutron Reflectometry, and complementary techniques

10:15
L15 94
**Paul Steffens**
(*ILL, Grenoble, France)*
Inelastic neutron scattering - from structure to dynamics of functional materials

10:50 *Coffee break*

11:20-12:45 Session IV - **Neutron scattering**
chair: *J. Kulda, P. Javorský*

---

11:20
L16 95
**Andreas Schreyer**
(*ESS, Lund, Sweden)*
First science on the ESS instrument suite

12:05
L17 95
**Jan Šaroun**
(*Institute of Nuclear Physics, Czech Academy of Sciences, Rez)*
European Spallation Source - contribution of the Czech Republic

12:15
**Přemysl Beran**
L18 96
(*ESS, Lund, Sweden)*
BEER - science case and status

13:00 Lunch

8:30–10:00 Session V - **Neutron scattering**
chair: *J. Šaroun, P. Javorský*

---

14:30
L19 97
**Pavel Strunz**
(*Institute of Nuclear Physics, Czech Academy of Sciences, Rez)*
SANS investigation of microstructre evolution in single crystal Ti-15Mo metastable -Ti alloy at elevated temperatures

14:55
L20 99
**Vasyl Ryukhtin**
(*Institute of Nuclear Physics, Czech Academy of Sciences, Rez)*
Studies of precipitation in engineering materials using small-angle neutron scattering

15:20
L21 100
**Petr Čermák**
(*Fac. of Mathematics and Physics, Charles University, Praha*)
ALSA - Automatic Laue Sample Aligner

15:45
L22 100
**Gergely Nemeth**
(*Institute of Nuclear Physics, Czech Academy of Sciences, Rez)*
Neutron Diffraction Study of Residual Stresses in Engineering Components formed via Additive Manufacturing

16:05
L23 102
**Jiří Kulda**
(*ILL, Grenoble, France)*
Efficient modeling of single crystal diffuse scattering

---

16:35 *Coffee break*

17:00–18:50 Session VI - **Synchrotron radiation**
*Z. Šourek, P. Mikulík*

---

17:00
L24 102
**Rajmund Mokso**
(*Max IV Laboratory, Lund, Sweden)*
X-ray imaging at synchrotron facilities

17:35
L25 103
**Patrik Vagovič**
(*XFEL, Hamburg, Germany)*
MHz X-ray microscopy at European XFEL

18:10
L26 104
**Jozef Bednarčík**
*(Institute of experimental physics, Slovak Academy of Sciences, Košice)*
Strain mapping using high-energy X-ray diffraction

18:45
**Peter Oberta**
(*Institute of Physics, Czech Academy of Sciences, Praha)*
Information on ESRF, Czech membership

18:50
**Petr Mikulík**
(*Faculty of Science, Masaryk University, Brno)*
Information on European Synchrotron User Organization and WayForLight portal

---

19:15 Dinner

20:30 Meeting of the CSCA board

20:30 Meeting of users of neutron and synchrotron radiation

---

## Wednesday, June 22

7:00–8:30 Breakfast

8:30–10:00 Session VII
chair: *Z. Šourek, R. Kužel*

---

8:30
**Radomír Kužel**
(*Fac. of Mathematics and Physics, Charles University, Praha*)
Vzpomínka na Václava Janovce
Obituary - Václav Janovec

8:40
**Pavlína Řezáčová**
(*Institute of Organic Chemistry and Biochemistry, Czech Academy of Sciences Praha*)
Vzpomínka na Juraje Sedláčka
Obituary - Juraj Sedláček

8:50
**Petr Marvan**
(*Panalytical*)
Panalytical 2022

9:10
**Boris Míč**
(*MTM*)
Bruker 2022

10:30 *Coffee break*

10:00–12:00 Student session I
chair: *M. Pospíšil, Z. Matěj*

---

10:00
SL1
**Tereza Košutová** 112
(*Fac. of Mathematics and Physics, Charles University, Praha*)
Microstructure of thin layers of gold and gold nanoparticles

10:20
SL2
**Martin Podhorský** 112
(*Faculty of Science, Masaryk University, Brno)*
Strukturní chyby v mikrokrystalickém materiálu SiC
Structural defects in microcrystalline SiC

10:40
SL3
**Marianna Gerina** 114
(*Faculty of Science, Masaryk University, Brno)*
Size dependence of Surface Spin Disorder in Ferrite Nanoparticles

11:00
SL4
**Ruslan Barannikov** 115
(*Institute of Inorganic Chemistry, Czech Academy of Sciences, Řež)*
Metal carboxylates in paintings – the study of their structure and behaviour

11:20
SL5
**Suhaas Gupta** 116
(*Fac. of Mathematics and Physics, Charles University, Praha*)
Temporal evolution of optical absorption and emission spectra of thiol capped CdTe quantum dots

11:40
SL6
**Ubaid Ahmed** 118
(*Institute of Physics, Czech Academy of Sciences, Praha)*
In-situ loading on defect containing material observed under high-resolution tomograph

---

12:15 Lunch

13:40–14:40 Student session II
chair: *D. Šimek, J. Kopeček*

---

13:40
SL7
**Petr Machovec** 119
(*Fac. of Mathematics and Physics, Charles University, Praha*)
Mikrostruktura hexagonálních epitaxních vrstev $LuFeO_3$
Microstructure of Hexagonal $LuFeO_3$ Thin Epitaxial Layers

14:00
SL8
**Karel Trojan** 120
(*Fac. of Nuclear Engineering, Czech Technical Univ., Praha*)
Mikrostrukturální parametry, zbytková napětí a přednostní orientace laserem navařené nástrojové oceli
Microstructural parameters, residual stresses and preferred orientation of laser-welded steel

14:20
SL9
**Petr Veřtát** 121
(*Fac. of Nuclear Engineering, Czech Technical Univ., Praha*)
Tepelně indukované změny v modulované struktuře 10M $Ni_{50}Mn_{27}Ga_{22}Fe_1$ martenzitu
Challenging martensites in Ni-Mn-Ga-based alloys: Can minor changes in structural modulation affect physical properties?

---

14:50–16:30 Student session III
chair: *P. Řezáčová, P. Kolenko*

---

14:50
SL10
**Martina Poncarová** 122
*(Fac. of Science, Univ. of South Bohemia, České Budějovice)*
Photochemical degradation of selected pharmaceuticals under light conditions relevant to natural waters and study of toxicity of photoproducts

15:10
SL11
**Libor Hejduk** 123
*(Fac. of Science, Univ. of South Bohemia, České Budějovice)*
Decorin binding proteins from European Borrelia – do structural differences influence ligand binding?

15:30
SL12
**Tereza Kozelková** 124
*(Fac. of Science, Univ. of South Bohemia, České Budějovice)*
Lipolytic system in the hard tick *Ixodes ricinus*

15:50
SL13
**Daria Peremotova** 126
*(Fac. of Science, Univ. of South Bohemia, České Budějovice)*
Structural studies of Si3 endolysin mutants

16:10
SL14
**Anna Koutská** 127
*(Fac. of Science, Univ. of South Bohemia, České Budějovice)*
Molecular-biochemical and structural characterization of secreted ferritin II from Ixodes ricinus

---

16:30 *Coffee break*

17:00–19:00 Student session IV
chair: *J. Hašek, I. Kutá Smatanová*

---

17:00
SL15
**Jakub Hrubý** 128
(*Fac. of Nuclear Engineering, Czech Technical Univ., Praha*)
Záměna kovových iontů v aktivním místě nukleasy S1
Exchange of metallic ions in active site of S1 nuclease

17:20
SL16
**Martin Malý** 129
(*Fac. of Nuclear Engineering, Czech Technical Univ., Praha*)
Integrative structural analysis of antibiotic-inactivating enzyme from *Stenotrophomonas maltophilia*

17:40
SL17
**Stefan Djukic** 130
(*Institute of Organic Chemistry and Biochemistry, Czech Academy of Sciences Praha*)
Structural studies of human purine nucleoside phosphorylase and cyclin-dependent kinase 2 inhibitors

18:00
SL18 131
**Barbora Kaščáková**
*(Fac. of Science, Univ. of South Bohemia, České Budějovice)*
Structural insight into the salivary serpins of *Ixodes ricinus*

18:20
SL19 132
**Petra Havlíčková**
*(Fac. of Science, Univ. of South Bohemia, České Budějovice)*
TBEV and DENV RNA-dependent RNA polymerases - structure and interactions

18:40
SL20 133
**Milan Kočí**
(*Fac. of Nuclear Engineering, Czech Technical Univ., Praha*)
Investigation of the Rwp factor of paracetamol crystal structure

---

19.15 CSCA Assembly

20:00 Dinner

## Thursday, June 23

7:00–8:30 Breakfast

8:30–10:10 Session VII

chair: *J. Brynda*

---

8:30
L27 105
**Petr Kolenko**
(*Fac. of Nuclear Engineering, Czech Technical Univ., Praha*)
Paired refinement and crystal anisotropy

8:55
L28 105
**Jindřich Hašek**
(*Institute of Biotechnology, Czech Academy of Sciences, BIOCEV, Vestec*)
Structure database of organic polymers and their interactions with biomacromolecules

9:20
L29 106
**Ľubica Urbániková**
(*Insitute of Molecular Biology, Slovak Academy of Sciences, Bratislava*)
Unique structure of the cell wall binding domain of phage endolysin

---

9:45 *Coffee break*

10:15–12:45 Session VIII

chair: *M. Dopita, N. Ganev*

---

10:15
L30 107
**Silvia Švarcová**
(*Institute of Inorganic Chemistry, Czech Academy of Sciences, Řež*)
Studium maleb práškovou difrakcí
XRPD in the study of painted artworks

10:40
L31 107
**Pavla Roupcová**
*(Institute of Physics of Materials, Czech Acad. of Sciences, Brno)*
Determination of structure of small particles

11:05
L32 108
**Jan Drahokoupil**
(*Institute of Physics, Czech Academy of Sciences, Praha)*
Rtg tomografie - první zkušenosti
X-ray tomography - first experience

11:30
L33 109
**Petr Doležal**
(*Fac. of Mathematics and Physics, Charles University, Praha*)
Fázové transformace v titanových slitinách
Phase transformations in Ti alloys

11:55
L34 110
**František Lukáč**
(*Institute of Plasma Physicscs and Physics, Czech Academy of Sciences, Prague*)
Metastabilní aluminy v plasmových nástřicích
Metastable alumines in plasma sprayings

12:20
L35 111
**Petr Cejpek**
(*Fac. of Mathematics and Physics, Charles University, Praha*)
In-situ rtg difrakce tahové deformace nestechiometrického monokrystalu $Ni_2MnGa$
In-situ X-ray diffraction during tension on off-stoichiometric $Ni_2MnGa$ single crystal

---

12:45 **Student prizes**

13.15 Lunch

# Posters

P1 135
**Navid Assi**
*(Faculty of Science, Charles University, Prague)*
Hydrothermal conversion of Cerium Oxalate into CeO2.nH2O oxide

P2 137
**Malgorzata Cabaj**
(*Institute of Physics, Czech Academy of Sciences, Praha)*
The influence of energy-filtering on kinematical and dynamical structure refinement from 3D ED data

P3 138
**Margarida Henriques**
(*Institute of Physics, Czech Academy of Sciences, Praha)*
Solution of crystal and magnetic structures in Jana2020

P4 138
**Charles Hervoches**
(*Institute of Nuclear Physics, Czech Academy of Sciences, Rez)*
Crystal and magnetic structures in the $Nd_{1-x}Sr_xFeO_3$ ($0.1 \leq x \leq 0.9$) solid solution

P5 139
**Kshitij Gurung**
(*Institute of Physics, Czech Academy of Sciences, Praha)*
Crystal Structure Study of Xenon Compounds Using 3D Electron Diffraction

P6 140
**Petra Pullmanová**
(*Faculty of Pharmacy in Hradec Králové)*
X-ray diffraction and neutron diffraction of the skin barrier model

# Author Index

# Contents




**Materials Structure** **Bulletin Krystalografické společnosti**
Vydává a rozšiřuje Krystalografická společnost. Tiskne Karel Hájek designhhstudio.
S podporou Akademie věd ČR.
Adresa sekretariátu redakce: R. Kužel, MFF UK, Ke Karlovu 5, 121 16 Praha 2
Technická redakce: I. Kutá Smatanová, R. Kužel
**ISSN 1211 – 5894** díl **28** (2022), číslo 2 CSCA

NEW

# DECTRIS EIGER2X FEATURE UPGRADE

## Faster and cleaner experiments with four new acquisition features

- 8-Bit Readouts
- Double-Gating Mode
- Lines-ROI Mode
- STREAM2


Read more about these new features and watch our online launch event here.

dectris.com

European Conference on Residual Stresses

# ECRS 11

Praha 2024


www.rigaku.com


www.malvernpanalytical.com

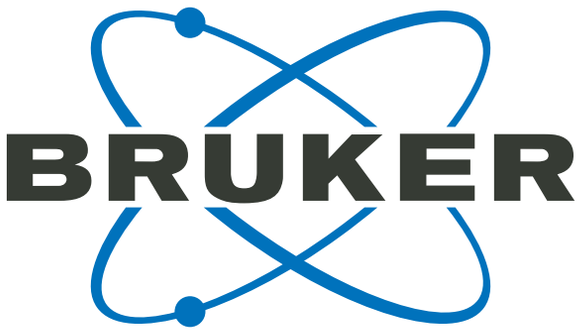


www.bruker.com


www.dectris.com


www.anton-paar.com